CHARACTERISATION AND MODELLING OF DYNAMIC BEHAVIOUR OF WIRE ROPE ISOLATORS

A THESIS SUBMITTED TO
THE GRADUATE SCHOOL OF NATURAL AND APPLIED SCIENCES
OF
MIDDLE EAST TECHNICAL UNIVERSITY

BY

KENAN GÜRSES

IN PARTIAL FULFILLMENT OF THE REQUIREMENTS
FOR
THE DEGREE OF DOCTOR OF PHILOSOPHY
IN
MECHANICAL ENGINEERING

JULY 2023

Approval of the thesis:

CHARACTERISATION AND MODELLING OF DYNAMIC BEHAVIOUR OF WIRE ROPE ISOLATORS

submitted by **KENAN GÜRSES** in partial fulfillment of the requirements for the degree of **Doctor of Philosophy in Mechanical Engineering, Middle East Technical University** by,

Prof. Dr. Halil Kalıpçılar
Dean, Graduate School of **Natural and Applied Sciences** ________________

Prof. Dr. M. A. Sahir Arıkan
Head of the Department, **Mechanical Engineering** ________________

Assist. Prof. Dr. Gökhan Osman Özgen
Supervisor, **Mechanical Engineering, METU** ________________

Examining Committee Members:

Prof. Dr. Yiğit Yazıcıoğlu
Mechanical Engineering, METU ________________

Assist. Prof. Dr. Gökhan Osman Özgen
Mechanical Engineering, METU ________________

Assoc. Prof. Dr. Mehmet Bülent Özer
Mechanical Engineering, METU ________________

Assoc. Prof. Dr. Can Ulaş Doğruer
Mechanical Engineering, Hacettepe University ________________

Assist. Prof. Dr. Kutluk Bilge Arıkan
Mechanical Engineering, TED University ________________

Date: 13.07.2023

I hereby declare that all information in this document has been obtained and presented in accordance with academic rules and ethical conduct. I also declare that, as required by these rules and conduct, I have fully cited and referenced all material and results that are not original to this work.

Name Last name: Kenan Gürses

Signature:

ABSTRACT

CHARACTERISATION AND MODELLING OF DYNAMIC BEHAVIOUR OF WIRE ROPE ISOLATORS

Gürses, Kenan
Doctor of Philosophy, Mechanical Engineering
Supervisor: Assist. Prof. Dr. Gökhan Osman Özgen

July 2023, 154 pages

When the effects of dynamic loading (shock and vibration) on the structures become intolerable, structural damage or failure may appear. The Wire Rope Isolator (WRI), one of the passive shock and vibration isolation elements, can effectively isolate the structure from disturbing loadings. WRIs are extensively used in the industry for vibration and shock isolation. WRI is a relatively newly developed, highly non-linear passive isolation element. Understanding the dynamic characteristics of "Wire Rope Isolators" and establishing the necessary theoretical background is challenging. Our motivation in this thesis is to fully characterize the highly non-linear dynamic behaviour of helical WRIs by presenting necessary theoretical models and verifying these theoretical models with various experimental measurements.

Keywords: Wire Rope Isolator, Characterisation and Modelling, Amplitude-Dependent, Finite Element Analysis, ABAQUS

ÖZ

ÇELİK SARMAL HALAT TİPİ SÖNÜMLEME ELEMANLARININ DİNAMİK DAVRANIŞININ KARAKTERİZASYONU VE MODELLENMESİ

Gürses, Kenan
Doktora, Makina Mühendisliği
Tez Danışmanı: Dr. Öğr. Üyesi Gökhan O. Özgen

Temmuz 2023, 154 sayfa

Dinamik yüklemenin (şok ve titreşim) yapılar üzerindeki etkileri dayanılmaz hale geldiğinde, yapısal hasar ortaya çıkabilemektedir. Pasif şok ve titreşim izolasyon elemanlarından biri olan Çelik Sarmal Halat Tipi Sönümleme Elemanı (WRI), ilgili yapıyı çevresindeki dinamik yüklerden etkili bir şekilde izole edebilmektedir. WRI'lar, endüstride titreşim ve şok izolasyonu için yaygın olarak kullanılmaktadır. WRI nispeten yeni geliştirilmiş ve oldukça doğrusal olmayan bir pasif izolasyon elemanıdır. WRI'ların dinamik davranışını karakterize etmek ve modellemek oldukça uğraşı gerektiren bir konudur. Bu tezdeki motivasyonumuz, gerekli teorik modelleri sunarak ve bu teorik modelleri çeşitli deneysel ölçümlerle doğrulayarak sarmal WRI'ların oldukça doğrusal olmayan dinamik davranışını tam olarak karakterize etmektir.

Anahtar Kelimeler: Çelik Sarmal Halat Tipi Sönümleme Elemanı, Karakterizasyon ve Modelleme, Genliğe Bağlı, Sonlu Elemanlar Analizi, ABAQUS

To my Mother, Father, Brother and to the
Memory of my Grandfather

ACKNOWLEDGMENTS

This thesis study was supported by the Defence Industry Agency (SSB) under the division of The Researcher Training Program for Defense Industry (SAYP).

The author wishes to express his deepest gratitude to his supervisor Assist. Prof. Dr. Gökhan Özgen for his guidance, advice, criticism, encouragement, and insight throughout the research.

The author would like to state his deepest gratitude to his brother Ahmet Gürses for his valuable suggestions on the mechanical design process of characterisation test fixtures and for providing the manufacturing of all fixtures used in all experimental setups.

The author would also like to thank the personnel of the *Material Characterisation Unit* as a part of the *Chemical Material Technologies Department*, operating within the Roketsan Inc., for enabling the sample-level characterisation tests of the Wire Rope Isolators to be performed via the "dynamic test instrument" found in the material characterisation laboratory.

Finally, the author declares his thanks to Roketsan Inc., which supported the realisation of this thesis study.

TABLE OF CONTENTS

LIST OF TABLES

TABLES

LIST OF FIGURES

FIGURES

LIST OF ABBREVIATIONS

ABBREVIATIONS

ACC	:	Accelerometer transducer
CAD	:	Computer-Aided Design
FE	:	Finite Element
FEA	:	Finite Element Analysis
FRF	:	Frequency Response Function
LPT	:	Displacement transducer
MAC	:	Modal Assurance Criterion
T/C	:	Tension-Comppression
WRI	:	Wire Rope Isolator

CHAPTER 1

INTRODUCTION

Vibrations and shocks are studied by utilizing different analysis techniques to predict their detrimental effects on the structures. When the effects of vibrations and shocks on the structures become intolerable, it may result in structural damage or failure. Therefore, adding a discrete isolation system between vibration/shock source and equipment is necessary. A general isolation system has two major components, namely, stiffness and damping. Firstly, the stiffness of the isolation system controls the static deflection required for different levels of isolation. Secondly, the damping component of isolator enables the energy dissipation of the external excitation to suppress it. The Wire Rope Isolator (WRI), which is one of the passive vibration isolation elements, can be used to effectively isolate the structure from disturbing vibrations. WRIs are extensively used in industry for vibration and shock isolation.

1.1 Types of Wire Rope Isolators

Wire rope isolators consist of wire rope strands held between two metal retainer bars in the form of helix shape or polycal shape (Figure 1.1). As the name implies, wire rope isolators use metal wire rope made up of individual wire strands that are in frictional contact with each other [36].

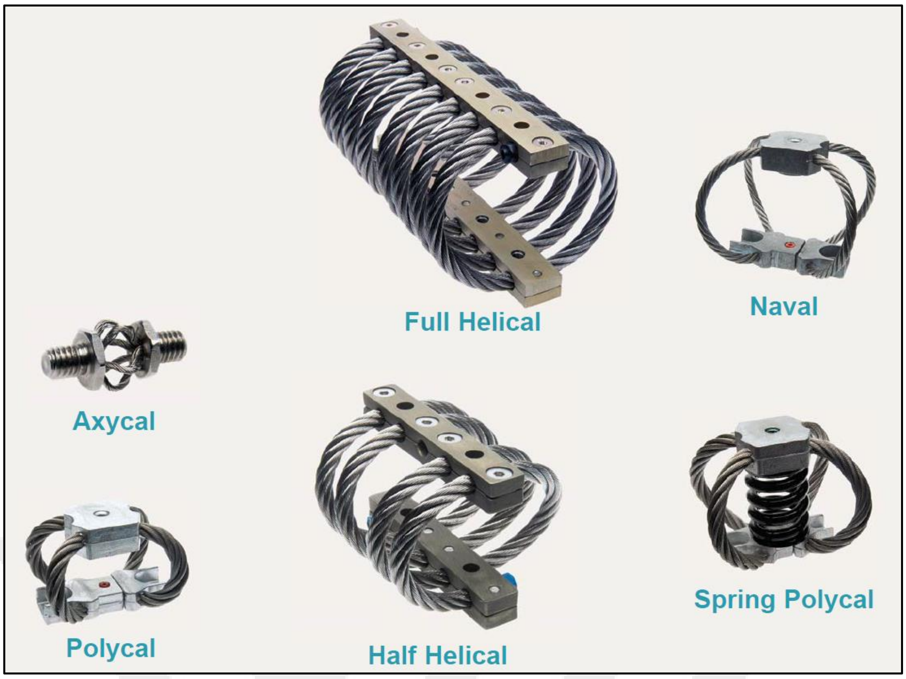

Figure 1.1 Wire Rope Isolator types supplied by vendors [33].

1.2 Application Fields of Wire Rope Isolators

A vibration and shock isolator has two components which are a spring to support the load and a damping element to dissipate the input energy. Wire rope isolators possess both of these properties and they are suitable for broad range of industrial and military applications as shown in Figure 1.2 and Figure 1.3.

Additionally, helical WRI have been used in numerous space applications. For example, helical WRI have been utilized on all shuttle flights to protect devices that control the passege of fluid to the rocket engines. WRI’s are also used in the shuttle launch facility to protect pipelines from shock and vibration [39]. The consideration of use of wire rope isolators on the Hubble space telescope is discusssed in reference [40].

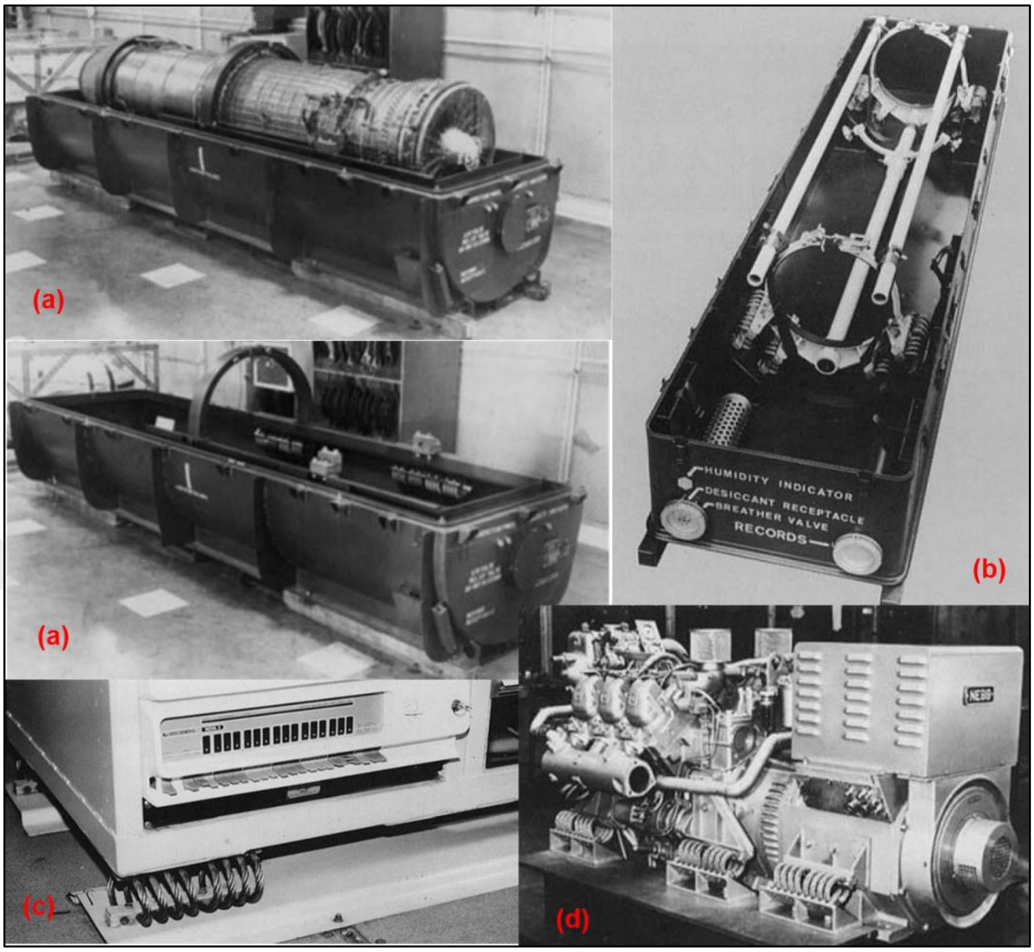

Figure 1.2 (a). Shipping container for military jet engines, (b). Shock-proof reusable container cradles missiles, (c). Electronics and computer systems, (d). Shipboard diesel generator [37].

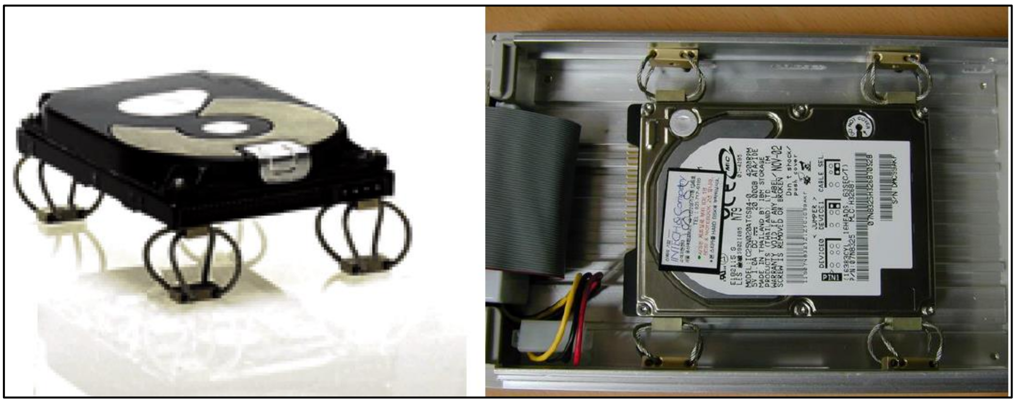

Figure 1.3 Mounting delicate hard disk drives [42].

1.3 Main Properties of Helical Wire Rope Isolators

A helical wire rope isolator or cable typically consists of several strands of wire wrapped around a metallic or fibrous core, by winding the cable in the form of a helix and fastening it with clamps to maintain the shape, helical wire rope isolators are consructed. Two different assembly process of helical WRI are shown in Figure 1.4.

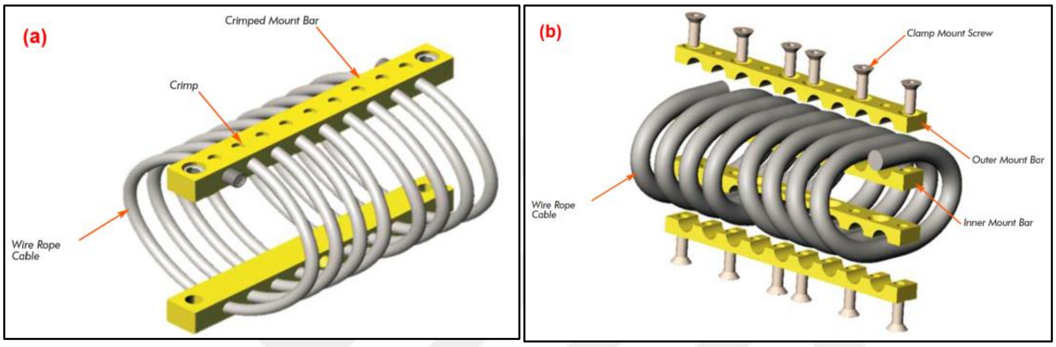

Figure 1.4 Crimped (a) and Clamped (b) Helical WRI [38].

WRIs are popular for reasons of high damping effectiveness, surviving hostile environements (corrosive, chemicals, abrasives, very low and high temperatures), relatively low cost, maintenance free, thermal insensitivity, no aging and multi axis vibration and shock isolation capability.

For helical WRIs, vendors recommend the following deformation modes, loading axes and orientations (Figure 1.5). The cross-coupling effect between main loading axes is always neglected for modelling and testing.

The dynamic behaviour of WRIs mainly depends on the following three parameters:

i. geometric parameters of WRI (Figure 1.6, Figure 1.7),
ii. static preload, and
iii. dynamic displacement amplitude.

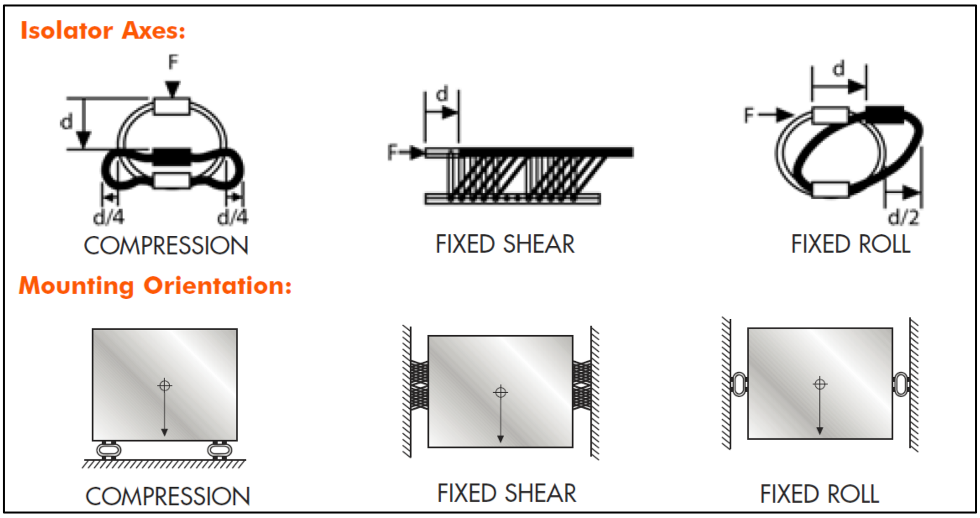

Figure 1.5 Helical WRI main loading modes and mounting orientations [38].

Since the Coulomb damping is relatively independent of excitation frequency, therefore the dynamic behaviour of WRI can be reasonably assumed as rate independent.

The main principle by which they WRI systems are designed and by which they work are inherent interfacial damping or sliding friction and adjacent wires move relative to each other, friction causes part of kinematic energy of the wires to be converted into heat, thereby dissipating vibrational energy. Quantitatively, the damping characteristics of helical WRI's depend on the following factors [4]:

a) the cable diameter R_c, R_h (Figure 1.6)
b) number of strands (Figure 1.6)
c) number of loops per isolator (Figure 1.7)
d) lay angle of the strands α (Figure 1.6)
e) the overall dimensions of isolator (Figure 1.7)

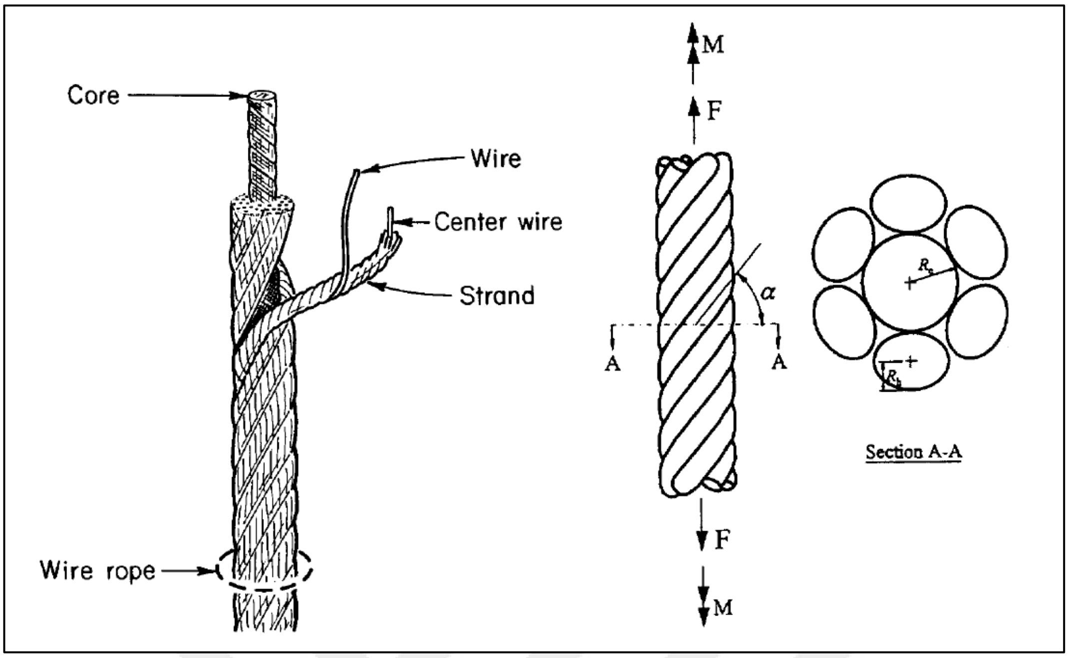

Figure 1.6 Structural elements in a typical wire rope [42].

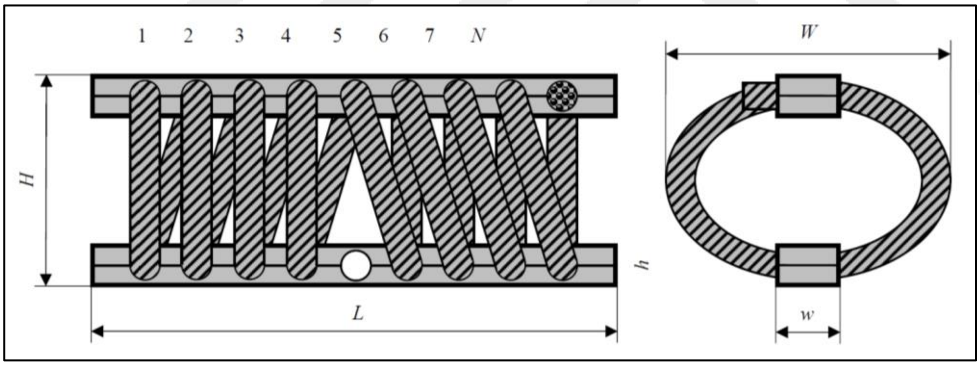

Figure 1.7 Helical WRI with its dimension variables [22].

1.4 Motivation of the Thesis

The damping and stiffness characteristics of helical WRIs are not well understood from a theoretical standpoint. Consequently, designing structures or systems involving WRIs is accomplished by using more or less some trial-and-error testing approaches, which are quite expensive and time-consuming since repeated physical prototype testing is needed. Therefore, developing realistic theoretical models of helical WRIs matching experimental results is highly significant and helpful for the design process.

Compared with the linear isolator devices, WRIs are relatively newly developed, strongly non-linear behaving passive isolation devices. Since the published literature on WRIs is relatively rare and primarily confidential, a comprehensive study on this area needs to be done.

Our motivation in this thesis is to fully understand the highly non-linear dynamic behaviour of helical WRIs by developing necessary theoretical models and verifying these theoretical models with various experimental measurements.

1.5 Objective of the Thesis

In the available open-source literature, there is not any recipe or test protocol for characterising the dynamic behaviour of WRI samples. Therefore, it is aimed to conduct characterisation test studies to understand the effect of various parameters (preload, excitation frequency, pre-cycling) on the dynamic behaviour of WRIs. The realisation of this aim requires that specimen-level tests be performed, preferably using an advanced dynamic (fatigue) test instrument.

Outputs of the WRI specimen-level characterisation tests are used to identify and calibrate the coefficients of the proposed theoretical model representing the dynamic behaviour of WRIs.

It is also aimed that the identified and calibrated data of the theoretical model representing the dynamic behaviour of WRIs be able to embed into the Abaqus Finite Element Analysis (FEA) software. Thus, large and complex three-dimensional mechanical systems having WRIs can be modelled and analysed by using Abaqus FEA software in a very realistic manner. The realisation of this aim requires system-level tests to be performed to validate the proposed theoretical model, which is also equivalent to the validation of the Abaqus FEA model.

In the end, it is aimed that to fully understand the highly nonlinear dynamic behaviour of helical WRIs by developing the necessary theoretical model and verifying these theoretical models with various experimental measurements.

CHAPTER 2

LITERATURE REVIEW

In this section, studies made by various authors on modelling hysteresis behaviour, which is found in multiple engineering fields, are mentioned elaborately in many different aspects.

2.1 Literature Survey

In this paper, Iwan [1] points that hysteresis phenomenon can be observed in many different physical systems such as due to considerable amount of material damping on a structure, discrete damping elements or plastic yielding of some portion of the structure. Although the bilinear model is the most basic model of studying hysteresis phenomenon nevertheless the very few of real systems show bilinear hysteresis behaviour. A general hysteretic system –representing the plastic yielding of continuous material– can be considered as consisting large number of ideal elastoplastic elements each having different yield levels. The model proposed consists of N number of Jenkin's (elastoplastic) elements parallelly connected. The stiffness of each element is k/N while the maximum allowable force of each Coulomb element is f_i/N. Naturally, suggested hysteresis model satisfies the Masing's hypothesis.

Transmissibility curves of a Coulomb (dry) friction-based isolation system comprising of a mass supported by a parallel combination of a linear stiffness and a non-linear dry-friction damping element is studied by Ruzicka [2]. Also, parameters effecting transmissibility curves are studied comparatively. For the case of harmonic vibration excitation of the support structure, the equation for absolute displacement transmissibility is presented. Investigations show that as the level of Coulomb damping is increased, the resonant transmissibility goes through a minimum and the resonant frequency varies between ω_0 and ω_∞. Passing through a minimum indicates that there is an optimum degree of damping for which the transmissibility at resonance is a minimum. Thus, under operating conditions, designing a dry friction isolation system close to this optimum point is important. Depending on the parameters chosen, resonance frequency of system is settled down somewhere between ω_0 (full slipping) and ω_∞ (full sticking). It must be noted that, "equivalent viscous damping" $\left(c_e = \frac{4\mu\, F_n}{\pi U \omega}\right)$ assumption is utilized for the derivation of transmissibility curves of Coulomb friction damped system. For this assumption, the transmissibility curves generated are approximate and should be treated as such. Although, they certainly give much information about the characteristics of the Coulomb damped system, but do not embody the non-linear characteristics.

First investigations made on Wire Rope Isolators (WRIs) are presented by Cutchins [3] in a technical report. In this report, parameters effecting the effective bending modulus of rigidity (E_{eff}) and torsional rigidity (G_{eff}) of a simple straight metallic wire rope for different end conditions are analyzed to obtain static response. Utilizing Nastran FE software, static behavior of simple straight and single loop wire rope models with different complexities are also captured. A wire rope isolation system having four identical isolator and a mass is devised for base excitation shaker experiments. Wire rope isolators in the system are oriented so that only shear direction mode is tested both statically and dynamically. It is shown that, 1-D simple mathematical models established with Coulomb damping is future promising, especially when compared to base excitation shaker test (based on transmissibility curve) results. Also, hysteresis loops for different excitation frequencies are obtained by solving proposed 1-D simple mathematical models.

In Tinker's [4] dissertation, main effort is spent to develop 1-D simple mathematical model that complies with base excitation shaker test results in terms of hysteresis, phase trajectory and frequency response curves. To this end, various damping models including (a). a model with cubic stiffness and linear viscous damping, (b).

a model with cubic stiffness and constant Coulomb friction damping, (c). a semi-empirical model with cubic stiffness, n^{th} power velocity damping and variable (function of relative amplitude) Coulomb friction damping are investigated respectively to find best fit with experiments. It is observed that wire rope vibration isolation system behaves nonlinearly due to the variations in friction forces between wires found within strands of wire. Experimentally obtained frequency response curves demonstrate a reduction in resonance frequency as base excitation amplitude is increased which is a diagnosis of Payne or Fletcher-Gent effect. Additionally, shape of experimental hysteresis curves – especially sharp pointed ends – indicate that damping in the wire rope isolation system is due to stick-slip friction between individual wires.

The use of wire rope isolators to provide seismic base isolation for the equipment located within the buildings are studied by Demetriades [5] both analytically and experimentally. Experimental studies implemented can be classified in two sections that is component level and the product (equipment) level. Product level and component level experiments are carried out on a shake table device and on a hydraulic actuator test bench corresponding to different loading orientations, respectively. Static and dynamic tests of wire rope isolators are conducted by a hydraulic actuator operating in a displacement-controlled mode for low frequencies ranging from 0.1 to 5.0 (Hz) and various displacement amplitudes. Especially in tension/compression loading mode, sinusoidal cyclic motion is also superimposed on a given preload during component level tests. Wire rope isolators in roll and shear mode loading tests exhibit symmetrical hysteresis loops whereas in tension-compression mode loading tests exhibit asymmetrical hysteresis loops and, in both case, loops are independent to excitation frequency. Restoring force generated by isolator is modeled using smooth bilinear hysteretic Bouc-Wen model which is usually represented by a first order non-linear ODE. The same Bouc-Wen model is also used for defining asymmetrical hysteresis loops after few modifications. Constant parameters used to represent Bouc-Wen model are obtained by calibration of analytical results with experiments. Assumptions made for analytical modeling can be given as: no coupling between loading axes which means each axis of isolator is modeled independent hysteretic elements, rotational stiffness of isolator around each axis is negligible, and equipment located on isolators is rigid. By integrating the DAEs in time domain, response to seismic excitation is obtained and verified by shake table experiments. Since energy dissipation in WRI is modeled by means of hysteresis loop, it is found that hysteretic damping decreases with increasing displacement amplitude.

Ottl [6] has described the hysteresis phenomenon and some of the important properties of hysteretic systems. The Greek word means “lagging behind” and indicates effects that occur in hysteretic systems. Hysteresis is a well-known phenomenon in many fields of science (e.g., magnetic, optical, mechanical hysteresis etc.) and is unveiled by very different processes.

If a known input $u(t)$ acts on a system or object, this input can cause an output $f(t)$ that remains or continues to run, even though the input has long since ceased. The current state of the system under consideration depends on the previous states. In short: the system has a memory. Therefore, they are called systems with memory.

It is possible to model mechanical systems with memory by means of additional state variables (inner variables). They are called internal state variables or internal variables because you cannot measure them directly. However, they clearly influence the output variable $f(t)$ because they cause the phenomenon of hysteresis. If the frequency has no influence on hysteresis mechanism, then it is called as static hysteresis.

The hysteresis is accompanied by energy dissipation, which results from different physical processes and may cause considerable heating. This can overheat a material or component and eventually destroy it.

In dissertation of Kolsch [7], the phenomenon of static hysteresis found in mechanical systems is elaborately surveyed from theoretical point of view, including real life examples. The Masing’s hypothesis (also known as Masing’s rules), Masing model, Valanis model, Bouc-Wen model, models of plasticity theory are described in this study. Main requirements – for the mathematical models to be used for the representation of static hysteresis – are given as: (a). be physically justified, (b). apply to any time course of the inputs, (c). easy to integrate in standards methods of vibration calculation, and (d). can be easily adapted by a user to his special needs.

The proposed theoretical model is a variant of Masing model which is come up with the introduction of additional amplitude dependencies to the model parameters.

The model equations are solved for any time course of the inputs in the time domain. The numerical integration and the calculation of periodic solutions using shooting methods and a modified collocation are used as solution techniques. The parameters of the calculation models are identified from hysteresis in the force-deformation plane. Several optimization methods determine the model parameters satisfactorily. Parameter identification using a multi-target method has proven to be particularly suitable due to its good convergence and short computing time.

Kolsch [8] also emphasizes that the characterization measurements should be planned in two separate parts: one for the parameter identification purpose and other for the proving the validity of the model with identified parameters.

An approach for modelling the random response behavior of WRI is proposed by Rassaian [9]. Essentially, WRI shows non-linear behavior with respect to operational conditions (amplitude dependent) so it does not lend itself to the frequency domain based linear analyses such as random response, and shock response spectrum. The basic approach proposed here consists of two separate steps.

First step involves assuming a non-linear WRI model which is a combination of discrete spring, dashpot, and dry friction elements. Static tests are implemented on a standard universal test machine. Following, dynamic tests are performed in vertical direction by attaching two isolators on shaker table with a dummy payload mounted above. Measured transmissibility plots clearly show that evolution of resonance frequency and damping as constant-g amplitude of slow sine sweep 5-160 (Hz) excitation is increased. Validation of assumed WRI model is done by utilizing both static and dynamic test.

Second step describes the approach used for derivation of equivalent stiffness and damping corresponding to the interested input PSD. For this purpose, acceleration PSD input is converted to an acceleration time input, then applying this forcing to corresponding SDOF of MDOF model acceleration time response is obtained. Acceleration time response converted into PSD response, so that the transmissibility can be obtained by dividing the response PSD to the excitation PSD. It should not be forgotten that calculated transmissibility curve is unique to given excitation PSD level.

Briefly, implementing a time domain analysis on a small MDOF or SDOF system, transmissibility curve is obtained. Following a linearized stiffness and damping can be obtained by processing transmissibility curve which corresponds to that unique input PSD. In the end, linearized stiffness and damping values can be plug into a large FE model ready for linear PSD analysis. In application, the two-step approach proposed in this study seems to be error-prone and open to misinterpretation, especially the first step.

An approach for modelling the steady-state response of turbine blade relying on Coulomb friction damping is developed by Sanliturk [10]. Aforementioned approach can be applicable to any hysteretic behaviour especially that can be characterized by its initial loading or backbone curve. This initial monotonic loading curve can be represented by a series of macro-slip elements which compose of a micro-slip element. The stiffness and maximum stiction force limit of each macro-slip element can be assessed from this initial loading curve. Then amplitude dependent complex stiffness representation of micro-slip element is calculated. In other words, friction forces are treated as external stiffness modifications to the system equations instead of applying them as external excitations.

It should be emphasized that the present HBM formulation is somewhat different from the conventional HBM approach such that here the aim is to determine a linearized amplitude dependent complex stiffness rather than simply calculating the first harmonic component of a non-linear friction force. Allowing the friction forces to be considered as external stiffness modifications, this approach is found to be particularly useful for frequency-domain analysis.

Austrell [11] states that carbon black filled rubbers show amplitude dependent behavior in contrast to unfilled rubbers whose behavior is mostly rate dependent. Hysteresis loops obtained by testing of filled rubbers demonstrate a distortion from perfect ellipse path which is a manifestation of the existence of non-linear behavior. It means that, response of the rubber isolator when a single sine frequency input is applied contains multiple frequencies (higher harmonics). Similar to filled rubbers, wire rope isolators also exhibit distorted hysteresis loop (nearly parallelogram-shaped). Having compared filled rubbers and WRIs, it can be said that both show amplitude dependent behavior (Payne effect), although filled rubbers also shows strong rate (frequency) dependent behavior with respect to WRIs. Therefore, modeling approach used to capture the amplitude dependency of filled rubbers can be generalized to WRIs.

In this study, a simple frictional solid model including one elastic and one elastoplastic member connected in a parallel way is suggested for modeling amplitude dependent and rate independent behavior. Since the simple 1-D rheological model shows fully rate independent behavior, it does not make any difference whether sinusoidal or triangular input is applied to the isolator. In either way the same hysteresis loop is obtained.

For simple frictional solid model, dynamic stiffness and loss factor as function of amplitude is derived and amplitude dependency is clearly observed. Furthermore, adding more elastoplastic (frictional) elements to simple frictional model leads to generalized frictional solid model also known as Masing’s model. Generalized frictional model including arbitrary number of frictional (Jenkin’s) elements can be fitted to experimental results which can be given either in terms of hysteresis loops or amplitude dependent dynamic stiffness / loss factor. Moreover, asymmetric hysteresis loop can be obtained replacing the linear spring with a non-linear hyperelastic spring.

Van Aanhold's [12] study focuses on developing a simple two parameter damping model (is also referred as Dahl's model) for representing small amplitude vibration damping behavior of a polycal type wire rope isolator. Since the relation between restoring force and deflection is non-linear, therefore an equivalent linear SDOF system for frequency domain analysis is developed. Suggested model includes enhancement over bilinear conventional Coulomb friction model, so that for small vibration amplitudes hysteresis loop can be formed. Thus, an enhanced dry friction model is obtained and can be easily plugged into equation of motion. This enhanced dry friction model is very convenient for time domain analyses. However, to be able to use this enhanced dry friction model in frequency analysis, an equivalent linear model with amplitude dependent stiffness and damping is developed. Preloading the three polycal WRI with a mass in vertical direction, shaker table sine sweep tests are implemented which correspond to different velocity amplitudes within a 2-30 (Hz) range. As a conclusion, proposed enhanced model matches very well with quasi-static experiment results. However, for sine sweep shaker test a serious mismatch exists and to compensate this mismatch two damping parameters (friction sliding force and exponential decay) need to be updated.

Detailed experimental and theoretical studies on WRIs are implement by Ni et al [13]. Generally, experimental and theoretical studies made on WRIs focus on relatively small deformation region where the WRIs demonstrates symmetrical softening hysteresis loops in the shear or roll modes. This symmetrical softening hysteresis behaviour is a nominee for the application of classical Bouc-Wen equation provided that deflections are relatively small. However, when the small deflection assumption is violated, then the use of classical Bouc-Wen model is also limited. For this reason, a theoretical model promising to capture both small and large deformation is developed in this study.

It is experimentally confirmed that hysteretic behaviour of Coulomb friction-based dampers involving WRIs are rate-independent which is in harmony with the mathematical definition of hysteresis. By excluding the inertial effects from the characterization measurements, nearly rate-independent hysteresis loops can be obtained. Therefore, utilizing this fact, dynamic cyclic tests can be replaced with quasi-static cyclic tests to determine the hysteretic behaviour of WRIs.

A special hanged measurement setup is developed for the implementation of cyclic tests. Test setup consists of two rigid plates which are hanged parallel to each other and these plates are guided such that they can only move only in the excitation direction. The WRI to be tested for each of three different modes (tension-compression, shear and roll) is attached sequentially between those rigid plates. Cyclic displacement loading is applied over the lower plate. In the test setup, rigid plates do not apply any preload on the WRIs thus WRIs are tested for no preload condition. Before starting quasi-static cyclic loading test, continuous monotonic static loading test is conducted. Cyclic tests are implemented specifically only for given displacement amplitude one at a time. And for each cyclic test a number of steady cycles are captured. By this way, a number of cyclic tests are carried out by increasing the displacement amplitude, sequentially. The author also points that, a memory-removing (also known as demagnetizing) process is implemented upon completion of each cyclic test.

Experimental results show that the tension-compression mode promises larger energy dissipation when compared with the roll or shear mode.

In theoretical side, the classical Bouc-Wen equation is utilized for modelling hysteresis behaviour observed in measurements. However, it is found that this model is insufficient especially when it comes to modelling asymmetric hysteresis behaviour and the hardening overlapping envelope (backbone curve in tension region) behaviour. Therefore, an improved version of the Bouc-Wen equation is proposed so that these two behaviours can be included in modelling. Improved version of Bouc-Wen equation contains nine constant parameters that must be determined by the identification process.

In this study, an approach for the identification of parameters of improved Bouc-Wen model is proposed by Ni et al [14]. To this end, a computationally efficient frequency-time domain alternating scheme is introduced. Firstly, the measured (quasi-static cycle test) restoring force and relative displacement data is modulated in time domain so the both have a period of 2π. Moreover, the experimental data to be modulated does not have to be exactly periodic, they can be any time data whose peaks alternating between specified amplitudes.

Knowing that input displacement signal is a sinusoidal signal hereafter, output force signal can be represented with multiple harmonics by means of Fourier series. Minimization of error function for identification process is implemented by continuously switching between time and frequency domains with the aid of FFT and IFFT routines. Additionally, a weight function that is inversely proportional to the square root of cyclic displacement amplitude is introduced for the evaluation of error function.

After the identification process, steady-state response of the proposed Bouc-Wen model is calculated iteratively in frequency domain by utilizing the multi harmonic balance method. Frequency response curves obtained from steady-state response analysis exhibit super-harmonic resonances due to the strong nonlinearity involved in WRI.

Leenen [15] conducted a research on the modelling and identification of hysteretic behavior of a WRI for both statically and dynamically. To this end, a differential model, known as a modified version of the original Bouc-Wen model, is proposed. This non-linear differential model includes the time-history-dependent nature of the hysteretic force, known as the memory effect. It is also shown that the proposed Bouc-Wen model can be used to represent Dahl friction model, and Preisach type of hysteresis model. Hysteretic behaviour of WRI is recorded by applying quasi-static cyclic triangular excitation profiles on a tension/compression test bench. Moreover, quasi-static cyclic tests are also repeated for different operating points other than no-preload condition. To this end, one cyclic test under tension preload, and the other cyclic test under compression preload are implemented, however the hysteresis loops obtained from the cyclic tests are only examined in qualitatively without searching the effects of the preload on the other amplitude dependent parameters.

Utilizing quasi-static measurements, parameters of the proposed Bouc-Wen model are identified by applying a relevant optimization method. The dynamic response behavior of a wire rope isolation system is evaluated using numerical time domain integration technique. In order to obtain frequency response to base excitation input, slow frequency sweeping approach (at constant amplitude) is used to approximate the steady-state frequency response of the non-linear hysteretic system. Additionally, the importance of removing the memory effect, before beginning a new quasi-static measurement is highly underlined and an approach is recommended for the "de-memorization" process.

In this study, a test set-up is presented by Juntunen [16] as a benchmark to implement dynamic measurements of WRIs when random or sinusoidal base excitations are applied. The proposed structure includes helical WRIs that are mounted between the base mass of an electrodynamic shaker and a load mass. Vibrations tests are performed using sine and random excitations corresponding to different amplitude levels. Total force at the bottom, base mass acceleration, top mass acceleration, and relative displacement between masses are recorded simultaneously during measurements. As expected, measurement results exhibit non-linear behavior of WRIs which are typically change of dynamic stiffness and damping depending on amplitude.

Modeling the dynamic characteristics of wire cable which is a restoring force generating member of Stockbridge damper is taken into consideration by Sauter [17]. It is intended to find dynamic behavior of wire cable by only measuring the quasi-static properties of it. This wire cable is also known as messenger cable. Obviously, the source of hysteretic damping is due to Coulomb (dry) friction between the individual wires of the cable (inter-strand friction) undergoing bending deformation. To this end, arranging elastic springs in conjunction with dry friction elements, a phenomenological rate independent model referred as Masing model is proposed. In this model, several Jenkin elements are connected in parallel with a linear spring, and each Jenkin element consisting of a linear spring and a Coulomb friction element. The identification of the model parameters from the experimentally obtained data was done numerically in the time domain.

In thesis of Schwanen [18], experimental and theoretical researches based on modified version of Bouc-Wen model are implemented. Only tension-compression mode hysteretic behaviour of a polycal type WRI is studied. Characterization of hysteresis behaviour of WRIs are conducted through the cyclic quasi-static loading measurements on a 10 kN test bench. Quasi-static cyclic triangular excitation profiles are used for the characterization tests. In addition to characterization tests, system level sine-sweep shaker table and shock table tests representing the tension-compression mode of WRI are conducted. It is noteworthy that frequency response curve obtained from sine-sweep results include multi peaks. The reason for this is strongly due to the unequal and poorly designed mass distribution over the shaker table.

Three steps identification procedure is adopted to assess parameters of the modified Bouc-Wen model. In the first step, non-linear stiffness behaviour is examined and related parameters describing the non-linear stiffness are fixed for use in the next step. In the second step, parameters effecting the shape of hysteresis are determined. In the third step, fine tuning is achieved by allowing all parameters to be changed within a certain range. Results obtained from the identified modified Bouc-Wen model show a good consistency for relatively for the large deflections. However, the same is not true for the small deflection region of the WRI.

Damping behaviour of a relatively large WRI is examined by Foss [19] using two different experimental approaches. Additionally, the effect of some parameters such as frequency, preload on damping estimates are investigated. In first approach, a test frame consisting of hydraulic cylinder, load cell, and displacement transducer is used to implement amplitude (displacement) sweep measurements at constant frequencies 0.1, 0.5, 2.5, and 5.0 (Hz). Plotting force vs displacement, hysteresis curves are obtained, and damping estimation is done by calculation of the area within the hysteresis cycle which is simply the ratio of the energy dissipated to the max. strain energy stored for a given hysteresis cycle. Using this hysteresis area approach, variation of equivalent viscous damping vs displacement amplitude is generated as a plot and later it is used as a comparison metric.

Tests performed at discrete sine frequencies of 0.1, 0.5, 2.5, and 5.0 (Hz) by sweeping amplitude show that damping has a very small dependency to excitation frequency. Similarly, test performed with a preload of 60% of maximum static load of WRI (Socitec, CB1800-17) appears to be little or no effect on damping.

In second approach, a test setup fixed one end of isolator to ground and loading other end of isolator with a weighting mass (under preload condition) is utilized. Sine sweep excitation is introduced with a shaker which is descended from top of the mass. Following, point FRFs (not transmissibility) in units of g/N are measured for a given constant displacement P-P amplitudes 0.058, …, 2.014 (mm) but this time sweeping frequency. In order to find equivalent viscous damping estimates, FRF curves corresponding to a variety of displacement amplitudes are fitted with a rational fraction polynomial curve method. As expected, FRF peak shifts to lower frequencies as the amplitude of sine sweep (load input) is increased.

As a result, comparing the damping vs displacement plot estimates from two approaches shows a considerable variation. Additionally, two important comments on damping and hysteresis cycle are given in this study.

First is the deformation of WRI results in a combination of frictional (Coulomb) and viscous damping between wires within the strands. At very small vibration amplitudes, the wires stick together, and little sliding occurs, so damping is very low, and the behaviour is viscous dominant. As displacements get higher, Coulomb damping starts dominating and large amounts of energy is absorbed due to slip-stick friction cycle. And at very large displacements viscous effects dominate again over, frictional effects.

Second is the hysteresis cycle consists of upper and lower backbone curves representing the limits of cycle. At very small amplitudes, cycles turn around origin without reaching backbone curve which results in small (viscous) dominated damping and very high dynamic stiffness. However, at amplitudes where the cycles start joining backbone curves the damping (loss factor) reaches its maximum.

Olsson [20] focused on modelling the rate and amplitude dependent effects of rubber materials, using the finite element method. For simple shear loading of rubber material, the amplitude and rate dependence can be modelled with simple 1-D models. Parameters from 1-D mathematical models can be easily transferred to finite element models. 1-D mathematical model proposed consists of three parallel connected branches which are an elastic or hyperelastic branch, a rate dependent viscoelastic branch, and an amplitude dependent elastoplastic branch. According to experimental researches made with rubber, amplitude dependent and rate dependent behaviour can be considered as independently among themselves so that principle of superposition can be applied. Overlay method proposed in this study relies on this superposition idea, which states that the stress tensor stems from each branch can be overlaid in terms of finite element mesh. Using this approach, a model representing both rate and amplitude dependent behaviour can be created in a commercial finite element code such as Abaqus/Standard. Otherwise, derivation of elaborate constitutive equations and coding them into special user defined material (UMAT) or user defined element (UEL) is unavoidably needed. As a result, the idea proposed in this study can be implemented for modelling dynamic behaviour of WRIs.

In this study, frequency response of a non-linear hysteretic SDOF system is modelled by Li [21] utilizing the Bouc-Wen model which is a widely used model for describing the non-linear hysteretic behaving systems in engineering field. Basically, Bouc-Wen model introduces an extra mapping variable to estimate corresponding restoring force. To this end, numerical analysis of the hysteretic system is implemented using the Runge-Kutta time integration. Frequency responses show that Bouc-Wen model for different set of parameters can exhibit the hardening or softening behaviour.

An indirect method targeting the audible frequency range for estimating dynamic stiffness of the WRI is experimentally investigated by Kari [22]. A special designed test set-up is utilized for stepped sine excitation 100, 110, …, 1000 (Hz) measurements. It is found that, dynamic stiffness exhibit rate dependency after some frequency, in contrary to low frequency range where dynamic stiffness shows rate independent behavior. Measurements are repeated for three different amplitude and preload levels to reveal their effects on dynamic stiffness. Since, amplitude levels for measurements are so small (order of µm) dynamic stiffness shows amplitude independent behavior as expected. However, increasing static preload results in a decrease in dynamic stiffness up to certain frequency which is about 300 (Hz).

In this study, no comment is made about the local peaks appeared on dynamic stiffness curve. It is thought that they are probably stem from the internal resonances of WRI though it is not proved.

As a part of a seismic protection system WRIs are characterized using quasi-static measurements, identification of proposed model with respect to measurements is done and time domain solutions for seismic base excitations is obtained by Paolacci [23], respectively. Some of important findings for quasi-static measurement are worth mentioning. During quasi-static measurements implemented at constant amplitude and frequency, an unstable behavior in the form of hysteresis cycle is observed by diagnosing the constantly increasing stiffness. To remove this effect, implementing a *pretest* at relevant preloading is recommended before commencing a real measurement. Another experimental finding is that as compressive preload on the tension/compression axis of a WRI increased, the roll and shear stiffness exhibit a gradual decrease which appears itself in the slope of hysteresis cycles. *However, necessary importance to this preload effect has not been attributed in this study*. During quasi-static measurements of WRI another phenomenon known as preload relaxation is also observed. Since the preload is applied as a constant displacement, after for a while preload force asymptotically is decreased to a lower value. For this reason, pretest of WRI is highly recommended.

Preload and amplitude dependent (Payne effect) dynamic behaviour (transmissibility) of elastomer using a commercial FE code (Abaqus) is presented by Petitjean et al. [24]. Basic assumption made by all commercial FE codes is the separability between frequency (rate) dependency and amplitude dependency, so that a simple form of equations can be written. However, there are some materials that do not fit this assumption. For example, expectedly dynamic modulus and preload show an inverse proportional relationship, nevertheless -after some point- further increase in preload may result in a direct proportional relationship. To this end, it is necessary to update dynamic modulus corresponding to the actual static strain value to capture preload effect on dynamic modulus. Amplitude dependency is another important non-linear effect needs to be taken into consideration for vibration analyses. Unless modeling this effect, prediction of resonance frequency of a vibration isolation system is practically impossible. For this purpose, an iterative approach needs to be applied due to the fact that resonant frequency and amplitude of transmissibility at resonance depend on the dynamic stiffness and loss factor, respectively. However dynamic stiffness and loss factor depend on dynamic amplitude, so updating iteratively these two parameters and running analyses are needed until a converged solution for a given tolerance is obtained.

Application of this iterative approach is carried out using Python language (wrapper program) and Abaqus FE software (Core FE package).

A procedure describing how to calibrate the parameters of Dahl model using a quasi-static measurement (sweeping amplitude at constant frequency) results is described by Mangin et al [25]. Proposed Dahl friction model is used for modelling hysteresis cycle of WRI. To describe the shape of hysteresis cycle, Dahl friction model contains two physical parameters which are maximum friction force and contact stiffness, respectively. Quasi-static tests are performed using a DMA instrument. First step in the procedure is to implement constant frequency tests at different displacement amplitudes. Following it goes on with a curve fitting of the largest hysteresis cycle to estimate amplitude dependent variable stiffness. Afterwards, friction damping force, again as a function of amplitude is calculated by using a graphical method. Lastly, contact stiffness parameter is found by iteration.

At the end, validity of the model is verified by implementing a product level base excitation shaker testing. Verification is done by applying a small constant displacement sine sweep base excitation, so that relative displacement generated by WRI is about 0.0015mm.

Ülker-Kaustell [26] utilized the Bouc-Wen model for representing the hysteretic energy dissipation through the bearings supporting railway bridges in his dissertation. In order to implement Bouc-Wen model in Abaqus FE code, a user element (UEL) is developed using FORTRAN language. Abaqus FE results are also benchmarked with MATLAB using a single and two degree of freedom systems. Additionally, some important details about time domain implementation of UEL in Abaqus FE code is mentioned.

Wang [27] conducted periodic loading tests of a new O-type WRIs to investigate the impact of the loading frequency, loading amplitude on the dynamic characteristics of O-type WRI. The WRIs are tested on a "MTS 831 Elastomer Test System" corresponding to shear, roll, and tension-compression mode loadings. For the testing of roll and shear mode configurations, two isolators are bolted symmetrically to test fixture to avoid unbalanced load. Synchronous force and displacement data are acquired at a rate of 512 samples per cycle, according to the loading frequency. Before proceeding into identification process, it is also suggested that filtering the measured raw data by a low-pass filter, in case of its corrupted by noisy effects.

A modified Bouc-Wen model that can capture "the hardening overlapping loading envelope" is adopted to model the dynamic behaviour of the O-type WRI and the model parameters are identified using a two-stage identification procedure from experimental data. Steady-state response analysis results reveals that the isolator is more effective for isolating vibration in the tension-compression mode rather than in shear or roll mode. Also, no trace is found for the multi-valued responses in the steady-state analysis results. Experimental results demonstrate that hysteresis loops are almost independent of the excitation frequency whereas completely dependent on excitation amplitude.

Dynamic behaviour of a hybrid damper consisting of a viscoelastic rubber part and a helical WRI part which are serially connected is investigated by Tax [28]. For this purpose, both WRI and rubber isolator separately tested, modelled, identified and verified. Symmetric and asymmetric hysteresis behaviour of WRI are established by using n-th order Iwan (Masing) model instead of using famous Bouc-Wen model. Each parallel branch in the Iwan model comprises of a spring and a Coulomb friction element connected in serial. Modelling of the asymmetry in the hysteresis loops is accomplished by introducing a non-linear spring which is described by the addition of linear, quadratic, and cubic terms, respectively. Due to the replacement of single parallel linear spring with a non-linear one, the model proposed is named as modified Iwan model. Equations of motion of proposed model are solved in time domain for both harmonic base and shock excitations. Frequency response of the model is also inspected in time domain by applying a single harmonic recursively for a frequency range which takes too much effort. Two types of quasi-static "measurements are implemented with WRI including one for small and the other for large deflection range. For a n-th order modified Iwan model there are 2n+3 parameters need to be identified. To identify these parameters, a three steps optimization method is suggested. Response for a given input PSD to WRI is also analyzed in time domain which necessitates the conversion of input acceleration PSD into a time domain signal. Following the time domain solution, time response is converted back into response acceleration PSD so that transmissibility can be found.

In this study, to be able to isolate a large diesel generator for seismic excitation WRI's are utilized by Tartary [29]. WRI's are mounted in pairs at angle of 45° inclination with respect to its major tension/compression axis. This inclined mounting makes it possible to increase the allowable travel in the suspensions and to obtain identical stiffness characteristics in the 45° inclined planes with respect to major tension/compression axis which involves both tension/compression mode and roll mode deflections of the WRI.

In this study, the Dahl model is proposed to capture the non-linear stiffness and dry friction behaviour by determining the model parameters from experimental characterization data. Due to its simplicity and robustness the Dahl model (continuous first order non-linear differential equation) is often used since the model relies on only two parameters. Restoring force calculated by model is decomposed into an elastic and a dissipative force component which is a function of relative displacement of WRI.

The elastic component is extracted from the hysteresis cycles of the WRI by means of an identification process adapted, more or less to the median curve of hysteresis cycle. Fairly accurate characteristics of dynamic stiffness and loss factor of WRI is also represented by this model. Random response simulations are carried out using transient analysis and PSD estimates are obtained by processing transient responses.

A study to provide earthquake protection for an inverter used in a nuclear power plant is implemented by Smetryns [30]. For the proposed WRI isolation system, choice of WRIs is justified by calculations and characterization measurements.

These WRIs make it possible to strongly filter the earthquakes and to limit the accelerations transmitted to less than 1 or 2 (g), thus guaranteeing the functionality of these equipments after the earthquake.

The sine sweep excitation in the 1-55 (Hz) band and constant amplitude equal to 0.2 (g) for the complete equipment is performed at a laboratory. Simulations representing the sine sweep excitation is performed in time domain, by performing a transient calculation for each frequency studied by means of SYMOS software (in house software of SOCITEC company).

2.2 Hysteresis Phenomenon

The Greek word means "lagging behind" and indicates effects that occur in hysteretic systems [6]. If a known input *u(t)* acts on a system or object, this input can cause an output *f(t)* that remains or continues to run, even though the input has long since ceased. The current state of the system under consideration depends on the previous states. In short: the system has a memory. Therefore, they are called systems with memory [6].

It is possible to model mechanical systems with memory by means of additional state variables (inner variables). They are called internal state variables or internal variables because you cannot measure them directly. However, they clearly influence the output variable *f(t)* because they cause the phenomenon of hysteresis. If the frequency has no influence oh hysteresis mechanism, then it is called as static hysteresis [6].

As an illustration, force-deflection hysteresis curves belonging to various spring-viscous-Columb damper combinations is given in Figure 2.1.

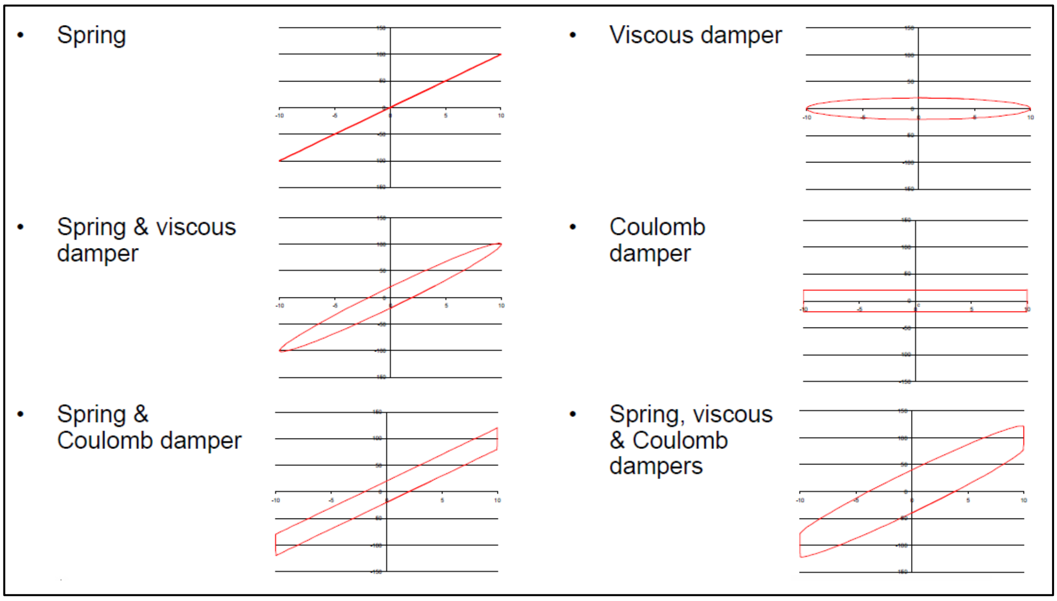

Figure 2.1 Force-deflection characteristics for various sping and damper combinations [42].

WRI’s show both compliant and frictional behavior. The bending of the wire strands results in compliant behavior. The rubbing between the strands results in friction forces. Both phenomena characterize the force-displacement relation. The damping properties are determined from the resulting so-called *hysteretic behavior.*

Experiments with the WRI have indicated that, returning position after a single compression (loading and unloading) test differs from its starting position. This history dependent behavior is what is called a memory effect [15]. Dry friction between wire strands is the main reason of this memory effect. Also remembering the fact that Coulomb friction is rate-independent.

It is experimentally confirmed that hysteretic behaviour of Coulomb friction-based dampers involving WRIs are rate-independent which is in harmony with the mathematical definition of hysteresis. By excluding the inertial effects from the characterization measurements, nearly rate-independent hysteresis loops can be obtained. Therefore, utilizing this fact, dynamic cyclic tests can be replaced with quasi-static cyclic tests to determine the hysteretic behaviour of WRIs [13].

Figure 2.2-(a), -(b) and -(c) show the measured steady state hysteresis loops in shear, roll and tension-compression respectively with the displacement amplitudes ranging from 0.5 to 4.0 (mm). It is observed that the loops in shear mode Figure 2.2-(a) resembles to those in the roll mode Figure 2.2-(b). The tested isolators displays symmetric hysteresis loops in both the shear and the roll modes owing to its symmetric configuration in these directions. This conclusion holds only when no static pre-loading or pre-deflection is applied to the isolator [13]. Figure 2.2-(c) indicates that the isolator exhibits *asymmetric* hysteresis loops in the tension-compression mode, and the asymmetry is increasingly apparent when the loading amplitude is increased. The helical WRI possesses hardening stiffness in tension and softening stiffness in compression.

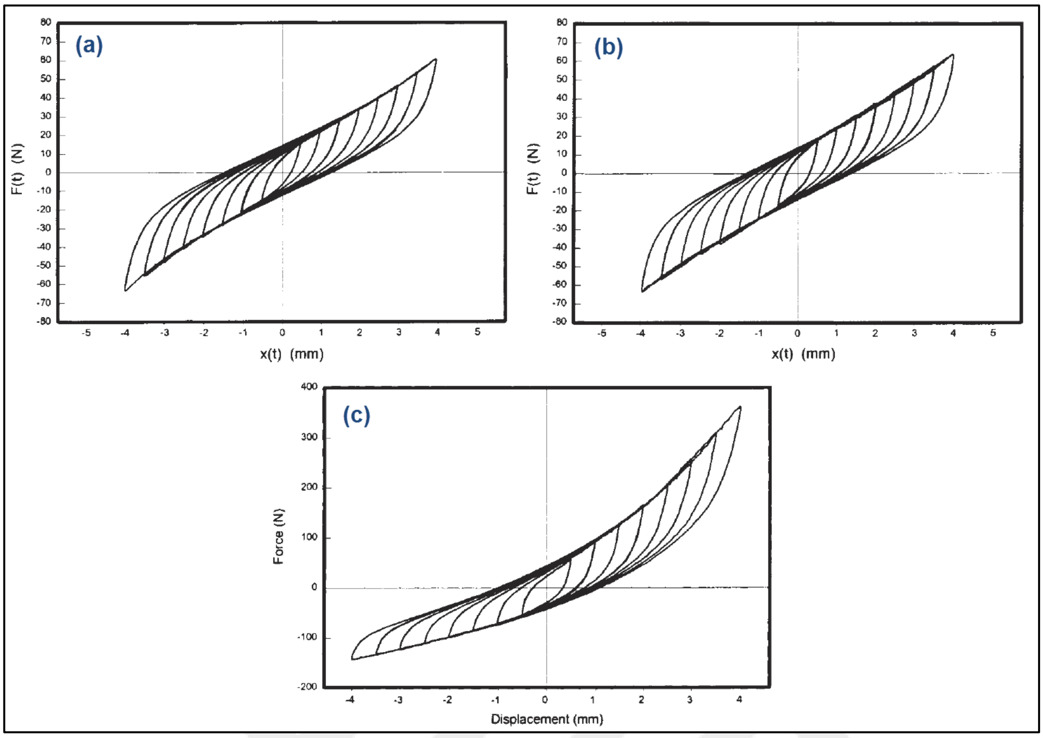

Figure 2.2 Measured hysteresis loops from quasi-static cyclic loading tests, (a) shear mode, (b) roll mode, (c) tension-compression mode [13].

The softening is due to the decrease in the contact points between the wire strands under compression load. The hardening in the tension is due to the increase in the contact points under tension load, which results in increased friction between the wire strands [36].

Figure 2.3-(a) and -(b) illustrate the effective stiffness (dynamic stiffness) and the hysteresis loop area of the tested WRI respectively [13]. The effective stiffness, K_e is defined as,

$$K_e = \frac{F_{\max} - F_{\min}}{x_{\max} - x_{\min}} \tag{2.1}$$

For the same displacement amplitude, the effective stiffness in the tension-compression mode is much greater than that in the shear or the roll mode (Figure 2.3-(a)). The hysteresis loop area implying the energy dissipated per cycle in the tension-compression mode offers much larger energy dissipation than the shear and the roll modes (Figure 2.3-(b)).

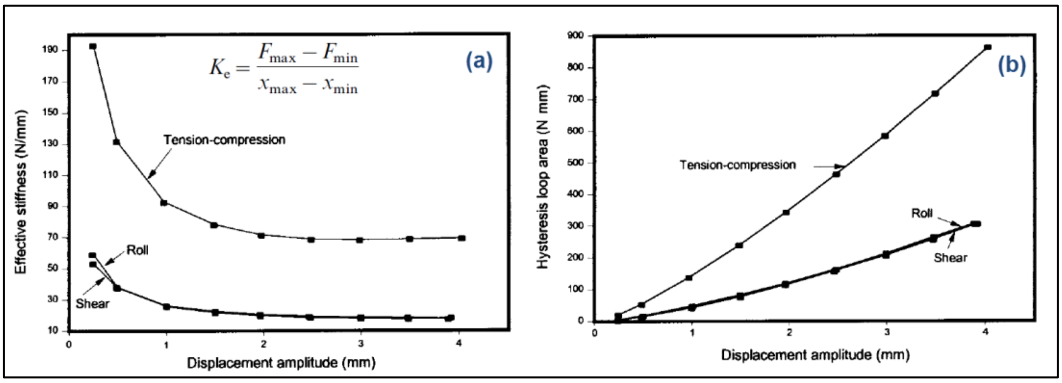

Figure 2.3 (a) Effective stiffness vs displacement amplitude, (b) Hysteresis loop area vs displacement amplitude [13].

The hysteresis is accompanied by energy dissipation, which results from different physical processes and may cause considerable heating. This can overheat a material or component and eventually destroy it [6].

Additionally, the importance of removing the memory effect, (also known as demagnetizing) before beginning a new quasi-static measurement is highly underlined and an approach is recommended for the “de-memorization” process [13], [15].

2.3 Comparison of Wire Rope and Elastomeric Isolators

Since WRI’s are made of stainless steel stranded wire, they have significant advantages over conventional rubber or elastomeric isolators for the severe operational environments of mechanical systems. For example, they perform well through a wider temperature range (– 240°C to 370°C) and are less susceptible to wear and deterioration than elastomers and are able to provide isolation in all directions. Dynamic behavior of WRI’s depends on geometric properties of isolator, amount of applied preload on it, input amplitude. In addition to these three parameters -unfortunately- dynamic behavior of elastomeric isolators depends highly on forcing frequency and temperature.

From theoretical point of view, a better way to represent the WRIs is by the elastically connected Coulomb damper model, and a better way to represent the elastomers is by the elastically connected viscous damper model [33], both of which are shown in Figure 2.4.

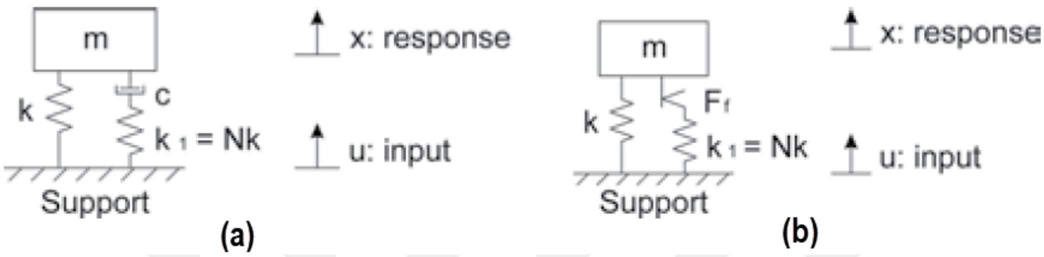

Figure 2.4 Basic theoretical models for (a) Rubber isolator and (b) Wire rope isolator [33].

2.4 Transient Response Analysis

Restoring force generated by isolator is modeled using smooth bilinear hysteretic Bouc-Wen model which is usually represented by a first order nonlinear ODE. The same Bouc-Wen model is also used for defining asymmetrical hysteresis loops after few modifications. Constant parameters used to represent Bouc-Wen model are obtained by calibration of analytical results with experiments. Assumptions made for analytical modeling can be given as: no coupling between loading axes which means each axis of isolator is modeled independent hysteretic elements, rotational stiffness of isolator around each axis is negligible, and equipment located on isolators is rigid. By integrating the DAEs in time domain, response to seismic excitation is obtained and verified by shake table experiments [5].

Kolsch [7] proposed a theoretical model a variant of Masing model which is come up with the introduction of additional amplitude dependencies to the model parameters. After re-arranging the equations of motion as first order ODE set, they are solved for any time course of the inputs in the time domain. The numerical integration and the calculation of periodic solutions using shooting methods and a modified collocation are used as solution techniques [7].

Van Aanhold [12] used the Dahl's model, whose parameters identified from the results of quasi-static measurement, to capture the transient response of polycal type of WRI for the periodic base excitation.

Olsson [20] focused on modelling the rate and amplitude dependent effects of rubber materials, using the finite element method. According to experimental researches made with rubber, amplitude dependent and rate dependent behaviour can be considered as independently among themselves so that principle of superposition can be applied. *Overlay method* proposed in this study relies on this superposition idea, which states that the stress tensor stems from each branch can be overlaid in terms of finite element mesh. Using this approach, a model representing both rate and amplitude dependent behaviour can be created in a commercial finite element code such as Abaqus/Standard. Otherwise, derivation of elaborate constitutive equations and coding them into special user defined material (UMAT) or user defined element (UEL) is unavoidably needed. *As a result, the idea proposed in this study can be implemented for modelling dynamic behaviour of WRIs.*

Ülker-Kaustell [26] utilized the Bouc-Wen model for representing the hysteretic energy dissipation through the bearings supporting railway bridges in his dissertation. In order to implement Bouc-Wen model in Abaqus FE code, a user element (UEL) is developed using FORTRAN language. Abaqus FE results are also benchmarked with MATLAB using a single and two degree of freedom systems.

2.5 Steady-State Response Analysis

2.5.1 Frequency Domain Approaches:

Transmissibility curves of a Coulomb (dry) friction-based isolation system comprising of a mass supported by a parallel combination of a linear stiffness and a nonlinear dry-friction damping element is studied by Ruzicka [2]. Also, parameters effecting transmissibility curves are studied comparatively. For the case of harmonic vibration excitation of the support structure, the equation for absolute displacement transmissibility is presented. Investigations show that as the level of Coulomb damping is increased, the resonant transmissibility goes through a minimum and the resonant frequency varies between ω_0 and ω_∞. It must be noted that, "equivalent viscous damping" $\left(c_e = \frac{4\mu\, F_n}{\pi U \omega}\right)$ assumption is utilized for the derivation of transmissibility curves of Coulomb friction damped system. For this assumption, the transmissibility curves generated are approximate and should be treated as such. Although, they certainly give much information about the characteristics of the Coulomb damped system, but do not embody the nonlinear characteristics [2].

In Tinker's [4] dissertation, main effort is spent to develop 1-D simple mathematical model that complies with base excitation shaker test results in terms of hysteresis, phase trajectory and frequency response curves. To this end, various damping models including: (a). A model with cubic stiffness and linear viscous damping, (b). A model with cubic stiffness and constant Coulomb friction damping, and (c). A semi-empirical model with cubic stiffness, n^{th} power velocity damping and variable (function of relative amplitude) Coulomb friction damping are investigated respectively to find best fit with experiments. Experimentally obtained frequency response curves demonstrate a reduction in resonance frequency as base excitation amplitude is increased which is a diagnosis of Payne or Fletcher-Gent effect. Additionally, shape of experimental hysteresis curves –especially sharp pointed ends– indicate that damping in the wire rope isolation system is due to stick-slip friction between individual wires [4].

A variant of Masing's model proposed by Kolsch [7] comes up with the introduction of additional amplitude dependencies to the model parameters. The model equations are solved for any time course of the inputs in the time domain. The numerical integration and the calculation of periodic solutions using *multiple shooting* and *modified collocation method* are used as solution techniques [7].

An approach for modelling the steady-state response of turbine blade relying on Coulomb friction damping is developed by Sanliturk [10]. This approach can be applicable to any hysteretic behaviour especially that can be characterized by its initial loading or backbone curve. This initial monotonic loading curve can be represented by a series of macro-slip elements which compose of a micro-slip element. The stiffness and maximum stiction force limit of each macro-slip element can be assessed from this initial loading curve. Then amplitude dependent complex stiffness representation of micro-slip element is calculated. It should be emphasized that the present HBM formulation is somewhat different from the conventional HBM approach such that here the aim is to determine a linearized amplitude dependent complex stiffness rather than simply calculating the first harmonic component of a nonlinear friction force. Allowing the friction forces to be considered as external stiffness modifications, this approach is found to be particularly useful for frequency-domain analysis [10].

Austrell [11], gives various algorithms to be used for (a). The calculation of Masing's model parameters from the initial loading (backbone) curve, (b). The calculation of initial loading (backbone) curve from the Masing's model parameters, and (c). The calculation of dynamic stiffness and loss factor (which is identical to "*amplitude dependent complex stiffness"*) from the initial loading (backbone) curve. In this way, any transition between these Masing's model parameters, initial loading (backbone) curve and amplitude dependent complex stiffness can be implemented easily.

Van Aanhold [12] used the Dahl's model –whose parameters first identified from the results of quasi-static measurement and then estimating "approximate equivalent" amplitude-dependent stiffness and damping coefficients– to capture the steady-state response of polycal type of WRI for the periodic base excitation. However, steady-state response does not match well with the sine-sweep shaker measurement results.

Having identified the nine parameters of *improved version of Bouc-Wen model*, Ni et al. [14] calculated steady-state response of the this model utilizing <u>*multi harmonic balance method*</u> iteratively in frequency domain. This *improved version of Bouc-*

Wen model is capable of representing the *asymmetric hysteresis loops* and *hardening overlapping loading envelope* behaviour of WRI in tension-compression mode. Frequency response curves obtained from steady-state response analysis exhibit super-harmonic resonances due to the strong nonlinearity involved in WRI [14].

Schwanen [18] used the shooting method in combination with the path following continuation technique to obtain frequency domain steady-state response of modified Bouc-Wen model.

Petitjean et al. [24] developed an iterative approach for modelling the amplitude dependent effect (Payne effect) for the three dimensional continuum rubber components. For this purpose, an iterative approach needs to be applied due to the fact that resonant frequency and amplitude of transmissibility at resonance depend on the dynamic stiffness and loss factor, respectively. However dynamic stiffness and loss factor depend on dynamic amplitude, so updating iteratively these two parameters and running analyses are needed until a converged solution for a given tolerance is obtained. Application of this iterative approach is carried out using Python language (wrapper program) and Abaqus FE software (Core FE package).

2.5.2 Time Domain Approaches:

By means of modified Bouc-Wen model, Leenen [15] investigated the dynamic response of a WRI system using numerical time domain integration technique. In order to obtain frequency response to base excitation input, slow frequency sweeping approach (at constant amplitude) is used to approximate the steady-state frequency response of the nonlinear hysteretic system. The approach needs filtering time domain results carefully. In order to make sure that steady-state response is not multi-valued, it needs implementing two transient analyses which are sweeping frequency up and down.

A study to provide earthquake protection for an inverter used in a nuclear power plant is implemented by Smetryns [30]. For the proposed WRI isolation system, choice of WRIs is justified by calculations and characterization measurements utilizing Dahl’s model. The sine sweep excitation in the 1-55 (Hz) band and constant amplitude equal to 0.2 (g) for the complete equipment is performed at a laboratory. Simulations representing the sine sweep excitation is performed in time domain, by performing a transient calculation for each frequency studied by means of SYMOS software (in house code of SOCITEC company).

2.6 Random Response Analysis

An approach for modelling the random response behavior of WRI is proposed by Rassaian [9]. To this end, an acceleration PSD input is converted to an acceleration time input, then applying this forcing to corresponding SDOF of MDOF model acceleration time response is obtained. Acceleration time response converted into PSD response, so that the transmissibility can be obtained by dividing the response PSD to the excitation PSD. It should not be forgotten that calculated transmissibility curve is unique to given excitation PSD level.

Tax [28] also followed similar approach using n-th order Iwan (Masing) model. Modelling of the asymmetry in the hysteresis loops is accomplished by introducing a nonlinear spring which is described by the addition of linear, quadratic, and cubic terms, respectively. Response for a given input PSD to WRI is also analyzed in time domain which necessitates the conversion of input acceleration PSD into a time domain signal. Following the time domain solution, time response is converted back into response acceleration PSD so that transmissibility can be found.

Tartary [29] utilized the Dahl’s model to capture the nonlinear stiffness and dry friction behaviour by determining the model parameters from experimental characterization data. Due to its simplicity and robustness the Dahl’s model (continuous first order nonlinear differential equation) is used since the model relies on only two parameters.

For given WRIs by mapping the identified Dahl's model into a 3D multi body dynamics software SYMOS (in house code of SOCITEC company), random response simulations are carried out using transient analysis and PSD estimates are obtained by processing transient responses.

2.7 Properties Effecting the Dynamic Behavior of WRIs

Dynamic behavior of a WRI is frequently described by using dynamic stiffness and loss factor parameters. In some references, dynamic stiffness is also referred as equivalent stiffness, and it can be given as (Figure 2.5)

$$k_{eq} = k_{dyn} = \frac{\Delta F}{\Delta x} \tag{2.2}$$

Loss factor is given as the ratio of energy dissipated to the maximum elastic energy stored in that hystersis cycle

$$\eta = \frac{E_{diss}}{2\pi W} \tag{2.3}$$

where $W = \frac{1}{2} k_{dyn} \Delta x^2$ is the max elastic (strain) energy stored in hysteresis cycle, which is illustrated in Figure 2.6.

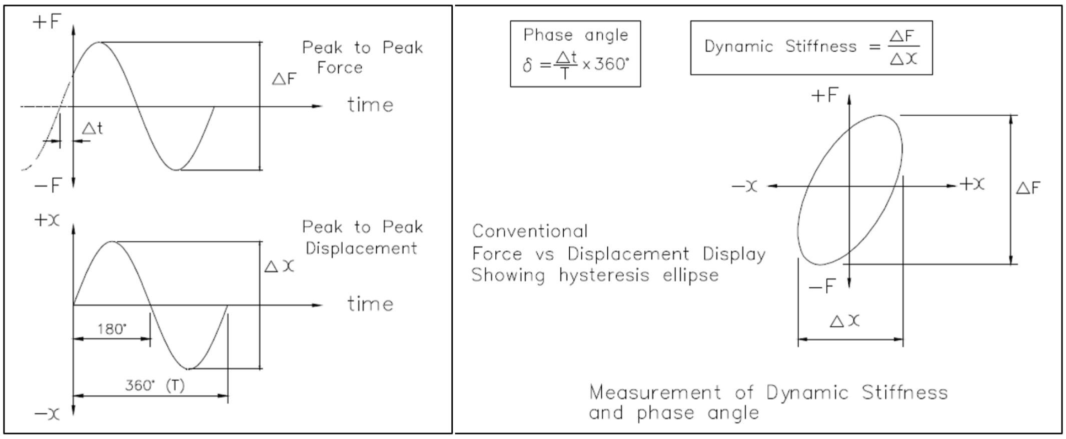

Figure 2.5 Definition of dynamic stiffness [34].

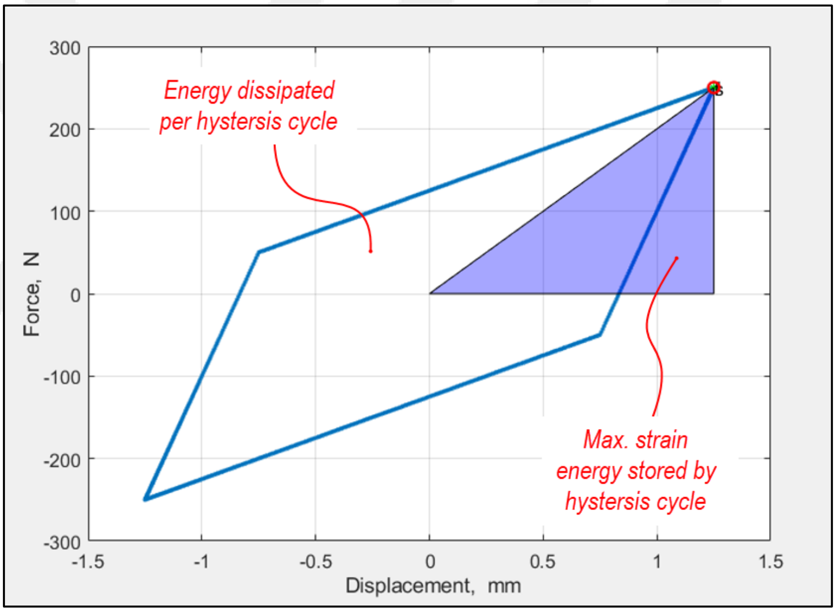

Figure 2.6 An example of simple bilinear hysteresis cycle

Input parameters effecting the dynamic behaviour of a WRI can be given as:

- *Dynamic relative displacement amplitude,*
- *Preload, and*
- *Frequency (very lightly)*

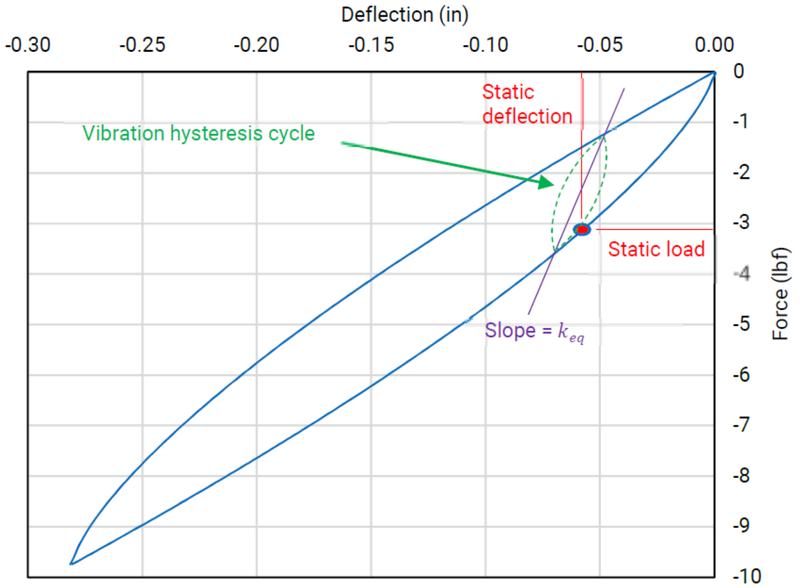

Figure 2.7 Hysteresis cycle of a typical WRI under compression preload [33].

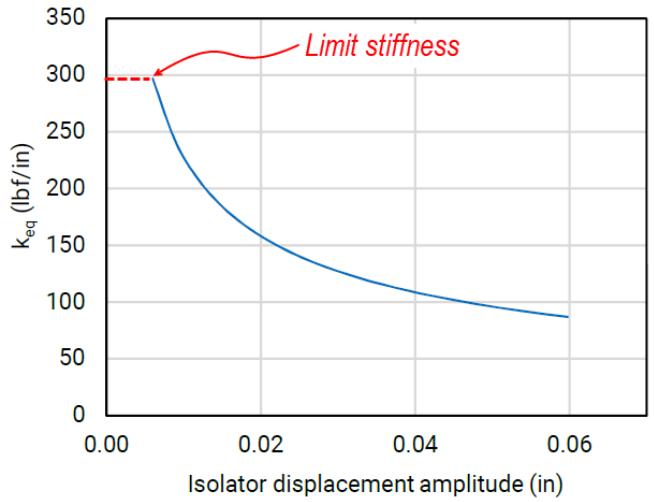

Figure 2.8 Dynamic stiffness as a function of dynamic displ. amplitude for a typical WRI [33].

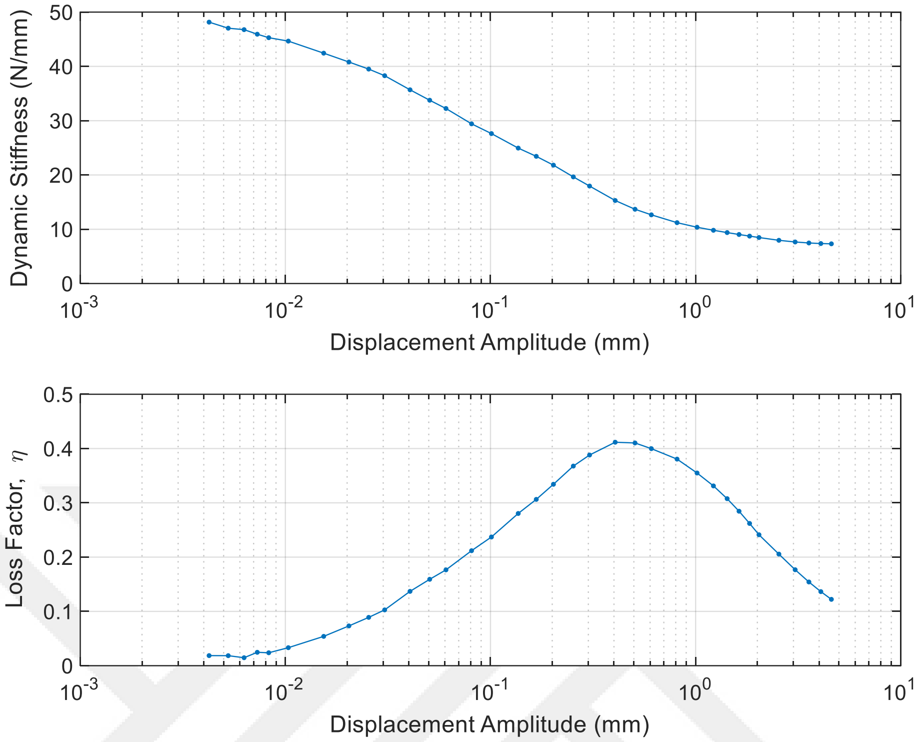

Figure 2.9 Dynamic test results of a typical WRI

The flexing of wire rope involves both Coulomb and viscous damping. At very low vibration levels, the wire strands stick together, and little sliding occurs. The damping is low, and the behavior is viscous. With higher displacements, Coulomb damping predominates as the wires break free and start to slide against each other, absorbing large amounts of energy. At large displacements the bending and stretching of the wire strands overshadows the sliding friction and viscous behavior again starts to show. Also, lubrication used in the manufacturing process wire rope cables may trigger the viscous effects specially at small vibration amplitudes.

It can be seen from Figure 2.9-(a) that, the dynamic stiffness is rate independent especially at medium and higher displacement amplitudes, while for small amplitudes it seems to be frequency dependent. The reason for this is the domination of viscous effects at smaller amplitudes; particularly where the end points of hysteresis cycles do not touch upper and lower backbone curves yet. However, in Figure 2.9-(a) at a constant (small) amplitude, with increasing frequency dynamic stiffness converges to a value which resembles the case shows up in rubber isolators (Figure 2.10).

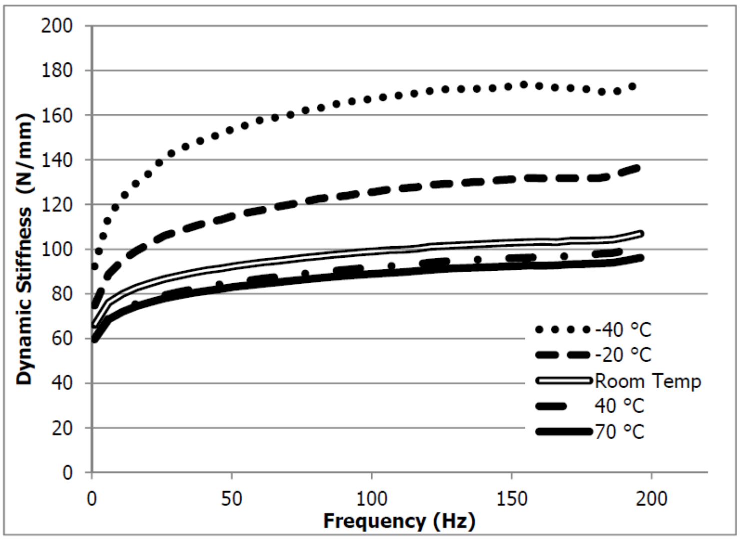

Figure 2.10 Frequency dependent radial dynamic stiffness of AM-005-2 isolator [35].

CHAPTER 3

THEORETICAL MODELS FOR MODELLING HYSTERESIS BEHAVIOUR

In this chapter, various theoretical models for modelling the dynamic behaviour of WRIs are described. Examining the theoretical models in the literature indicates that Masing's and modified Masing's models are the most suitable theoretical models in terms of modeling ease, compatibility with programming, and compliance with experimental data in modeling hysteresis curves exhibited by WRIs.

3.1 Basic Elements of Hysteresis Models

3.1.1 Jenkin's Element (Serial Connection)

This very basic hysteretic model is also known as: elastically connected dry (Coulomb) friction element, Prandtl element, elastoplastic element, Maxwell-slip element and macro-slip element.

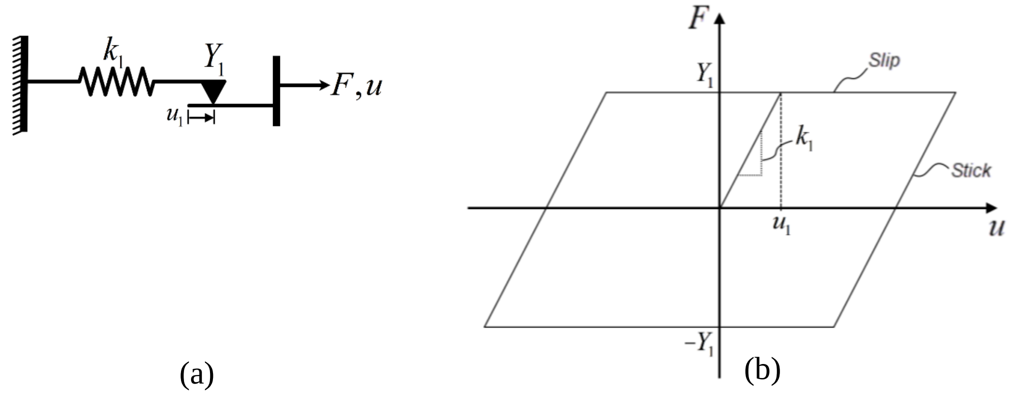

Figure 3.1 Jenkin's element model (a) and its corresponding hysteresis cycle (b).

Restoring force through the Jenkin's element is given as follows [31], [32]:

$$F(t)=\begin{cases} r_1(t), & abs(r_1(t))<Y_1 \\ Y_1\,\mathrm{sgn}(\dot{u}(t)), & else \end{cases} \tag{3.1}$$

where

$$r_1(t)=k_1\left(u(t)-u_{rev}\right)+Y_1\,\mathrm{sgn}\left(\dot{u}_{rev}\right) \tag{3.2}$$

u_{rev} is the displacement immediately prior to velocity reversal. $Y_1=\mu N_1$ is maximum friction force occurring on Coulomb friction element and It is assumed that static and kinetic coefficient of friction is equal to each other.

3.1.2 Dry Friction Model (Parallel Connection)

Dry friction model includes a spring and a Coulomb friction element connected in parallel. Restoring force through the bilinear model is:

$$F(t)=F_s+F_d \tag{3.3}$$

where

$$F_s = k_1 u \tag{3.4}$$

The stiffness term F_s can also be approximated well by a higher order polynomial curve, but here it is assumed approximately linear.

$$F_d = Y_1 sgn(\dot{u}) \tag{3.5}$$

where the term Y_1 is the maximum friction force.

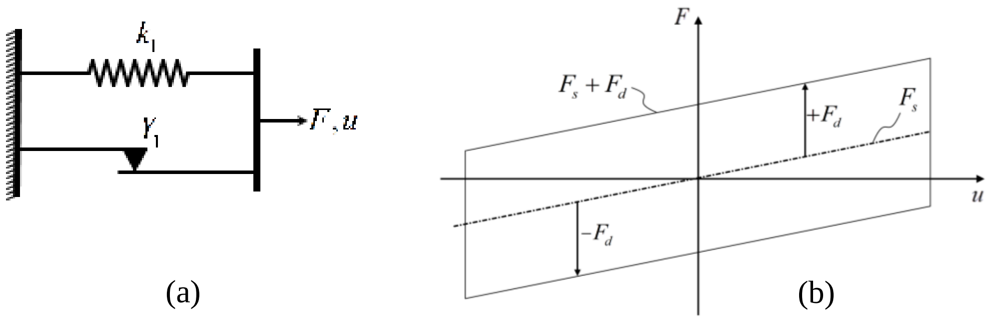

Figure 3.2 Dry friction model (a) and its corresponding hysteresis cycle (b)

.

3.2 Theoretical Models for Modelling Hysteresis Behaviour

Following theoretical/phenomenological models have been used for modeling the dynamic behaviour of WRIs in varios studies found in the literature. These theoretical models are Bilinear model, Dahl's model, Bouc-Wen model and Masing's model.

3.2.1 Bilinear Model

Bilinear model is also known as simple frictional solid model or elastically coupled Coulomb damper model.

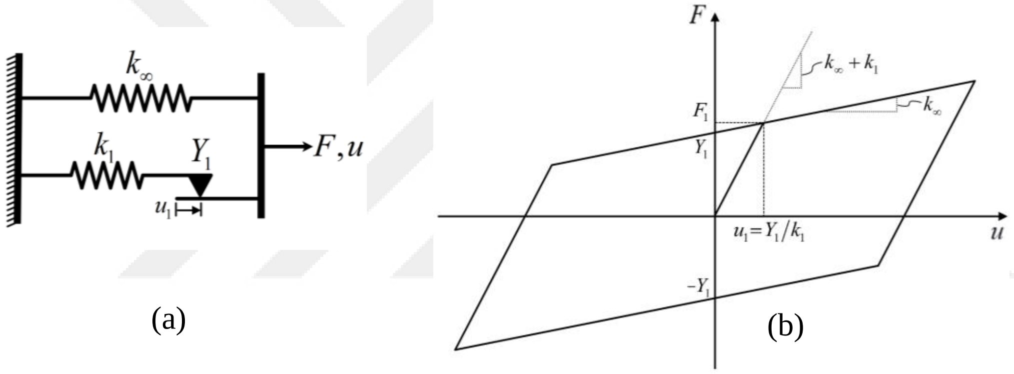

Figure 3.3 Bilinear model (a) and its corresponding hysteresis cycle (b).

Restoring force through the bilinear model is given as follows [31], [32]:

$$F(t) = k_\infty u(t) + \begin{cases} r_1(t), & abs(r_1(t)) < Y_1 \\ Y_1 \operatorname{sgn}(\dot{u}(t)), & else \end{cases} \tag{3.6}$$

where

$$r_1(t) = k_1(u(t) - u_{rev}) + Y_1 \operatorname{sgn}(\dot{u}_{rev}) \tag{3.7}$$

u_{rev} is the displacement immediately prior to velocity reversal. $Y_1 = \mu N_1$ is maximum friction force occurring on Coulomb friction element and It is assumed that static and kinetic coefficient of friction is equal to each other.

3.2.2 Dahl's Model

Due to the lack of modeling capability of bilinear Coulomb friction model for small amplitude vibrations, Van Aanhold [12] proposed the use of a more accurate Dahl's friction model.

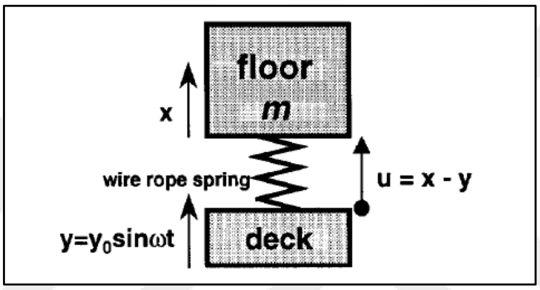

Figure 3.4 Vibration isolation for the vertical direction [12].

Restoring force through the bilinear model is given as follows:

$$F(t) = F_s + F_d \tag{3.8}$$

For spring force stiffness is approximated as linear:

$$F_s \approx k.u \tag{3.9}$$

Conventional Coulomb damping is given as:

$$F_d = d.\mathrm{sgn}(\dot{u}) \tag{3.10}$$

Such a dry friction model is sufficiently accurate for large deflections such as under shock conditions. The conventional dry friction model is however not suited for small amplitude vibrations. Traditional model fails to model the gradual load reversal after each velocity reversal correctly and will lock for small amplitudes where the spring force does not exceed d.

$$F_d = \left[d - u_c \frac{dF_d}{du} \right] . \mathrm{sgn}(\dot{u}) \qquad (3.11)$$

where u_c is a deflection constant which describes the exponential decay on load reversal. When $u_c = 0$ the standard dry friction model is obtained. So this *enhanced dry friction model* is well suited for use in time domain analysis.

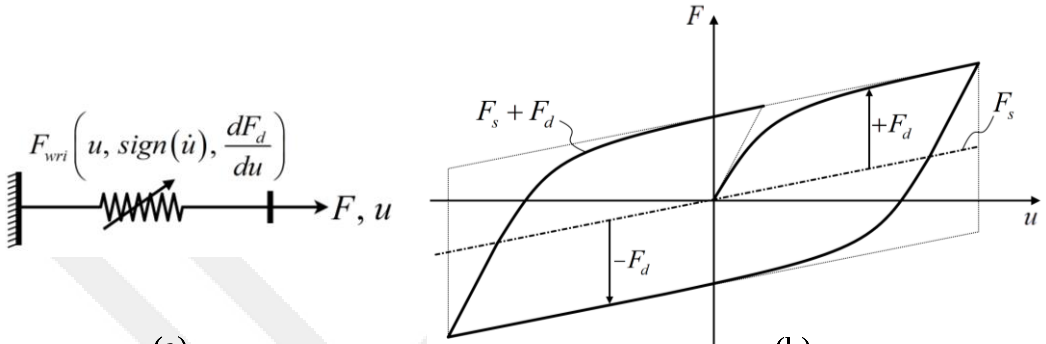

(a) (b)

Figure 3.5 Dahl’s (enhanced dry friction) model (a) and its corresponding hysteresis cycle (b).

3.2.3 Bouc-Wen Model

Hysteretic behaviour can be described by the Bouc-Wen model. This empirical model describes various hysteretic phenomena. A modified version to include the asymmetric behavior is already applied in several studies. The model parameters are not directly related to the physical behavior. The empirical Bouc-Wen model describes hysteretic behavior in general form [13], [14], and [18]. Restoring force through the Bouc-Wen model is given as follows:

$$F(t) = \underbrace{a \frac{F_y}{u_y} u(t)}_{elastic\ force} + \underbrace{(1-a) F_y\, z(t)}_{hysteretic\ \ force} \qquad (3.12)$$

where, the parameter "a" is the ratio of post-yield to pre-yield stiffness:

$$a = \frac{k_\infty}{k_0} < 1.0 \qquad (3.13)$$

$$\dot{z}(t) = \dot{u}(t)\,\frac{1}{u_y}\left[1 - |z(t)|^n \left\{\gamma + \beta \operatorname{sgn}\big(\dot{u}(t)z(t)\big)\right\}\right] \qquad [-] \tag{3.14}$$

where $z(t)$ is non-dimensional hysteresis parameter and β, γ, n are also non-dimensional quantities controlling the shape of hysteresis loop. For small values of n, smoother transition from pre- to post-yield is obtained, whereas for larger values of n, sharper transition is obtained resembling that of the bilinear model. Parameters β and γ control the size and the shape of hysteresis loop.

Another representation of Bouc-Wen model can be given as follows:

$$F(t) = F_1(t) + z(t) \tag{3.15}$$

where $F_1(t)$ is linear elastic force:

$$F_1(t) = k_\infty u(t) = ak_0 u(t) \tag{3.16}$$

and $z(t)$ is nonlinear hysteretic force:

$$\dot{z}(t) = \dot{u}(t)\left[\alpha - |z(t)|^n \left\{\gamma + \beta \operatorname{sgn}\big(\dot{u}(t)z(t)\big)\right\}\right] \qquad \left[\frac{N}{s}\right] \tag{3.17}$$

In this form, $z(t)$ is ***dimensional*** hysteresis parameter. Units of the Bouc-Wen model parameters are given in Table 3.1.

Table 3.1 Units of Bouc-Wen model parameters.

parameter	**unit**
z	[N]
n	[-]
α	$[N/m]$
β	$[N^{(1-n)}/m]$
γ	$[N^{(1-n)}/m]$

The model in this form, describes a symmetric hysteretic system without softening or hardening behavior. Symmetry is defined here as identical behavior in tension and compression.

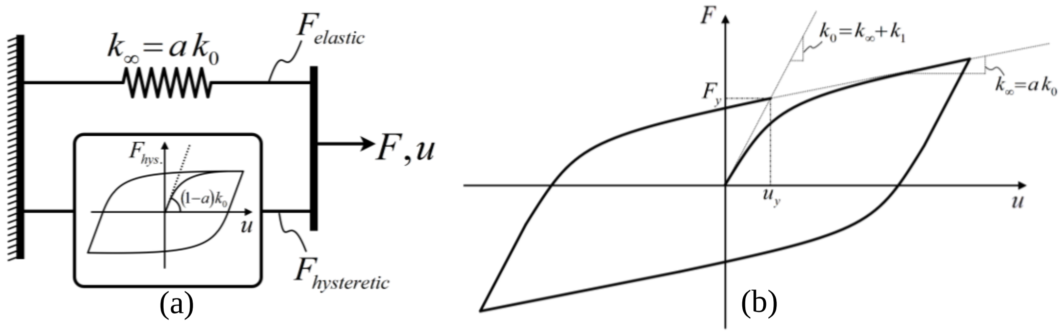

Figure 3.6 Bouc-Wen model (a) and its corresponding hysteresis cycle (b).

3.2.4 Modified Bouc-Wen Model

Restoring force through the modified Bouc-Wen model is given as follows [18], [28]:

$$F(t) = F_2(t)\left[F_1(t) + z(t)\right] \tag{3.18}$$

where $F_1(t)$ is nonlinear elastic force:

$$F_1(t) = g_1 u(t) + g_2 \operatorname{sgn}(u) u(t)^2 + g_3 u(t)^3 \tag{3.19}$$

and $F_2(t)$ is a kind of shaping function which assures the hardening overlapping loading envelope:

$$F_2(t) = b^{cu(t)} \tag{3.20}$$

and $z(t)$ is nonlinear hysteretic force to be modulated with $F_2(t)$:

$$\dot{z}(t) = \dot{u}(t)\left[\alpha - |z(t)|^n \left\{\gamma + \beta \operatorname{sgn}\left(\dot{u}(t) z(t)\right)\right\}\right] \qquad \left[\frac{N}{s}\right] \tag{3.21}$$

In this form, $z(t)$ is <u>*dimensional*</u> hysteresis parameter. Units of the modified Bouc-Wen model parameters are given in Table 3.2.

Table 3.2 Units of modified Bouc-Wen model parameters.

parameter	unit
z	$[N]$
n	$[-]$
α	$[Nm^{-1}]$
β	$[N^{1-n}m^{-1}]$
γ	$[N^{1-n}m^{-1}]$
b	$[-]$
c	$[m^{-1}]$
g_1	$[Nm^{-1}]$
g_2	$[Nm^{-2}]$
g_3	$[Nm^{-3}]$

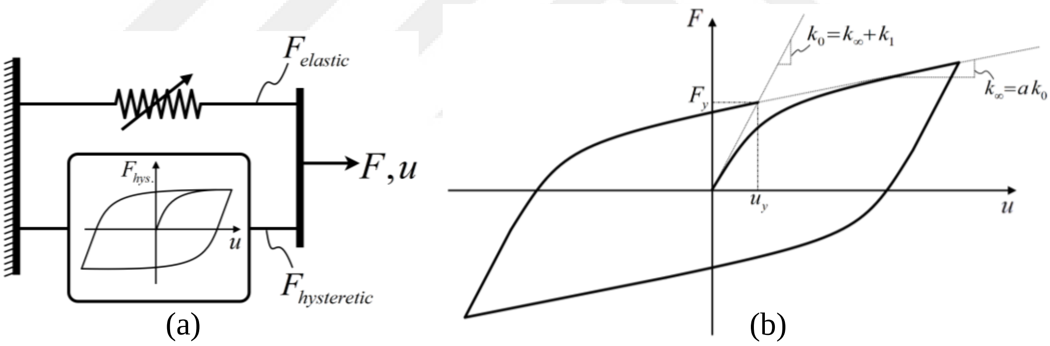

Figure 3.7 Modified Bouc-Wen model (a) and its corresponding hysteresis loop (b).

3.2.5 Masing Model

Restoring force through the Masing model is given as follows:

$$F(t) = \underbrace{k_\infty u(t)}_{\text{elastic force}} + \underbrace{\sum_{i=1}^{n} H_i(t)}_{\text{hysteretic force}} \tag{3.22}$$

writing the equation above more explicitly:

$$F(t) = k_\infty u(t) + \sum_{i=1}^{n} \begin{cases} r_i(t), & abs(r_i(t)) < Y_i \\ Y_i \,\mathrm{sgn}(\dot{u}(t)), & else \end{cases} \tag{3.23}$$

where,

$$r_i(t) = k_i\left(u(t) - u_{rev}\right) + Y_i \,\mathrm{sgn}\left(\dot{u}_{rev}\right) \tag{3.24}$$

and, u_{rev} is the displacement immediately prior to velocity reversal.

If the hysteretic force H_i through a single Jenkin element is expressed in terms of its time derivative $\dot{H}_i$, then only one equation is sufficient to describe the behavior of both spring and friction element. The evolution equation for a single Jenkin element is given as:

$$\dot{H}_i(t) = \frac{1}{2} k_i \,\dot{u}(t) \{ saturation + re\,activation \} \tag{3.25}$$

where,

$$saturation = 1 - \mathrm{sgn}\left[H_i(t)^2 - Y_i^2 \right] \tag{3.26}$$

$$re\,activation = -\mathrm{sgn}\left[\dot{u}(t) H_i(t) \right] . \left(1 + \mathrm{sgn}\left[H_i(t)^2 - Y_i^2 \right] \right) \tag{3.27}$$

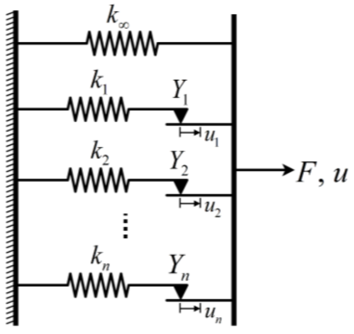

(a)

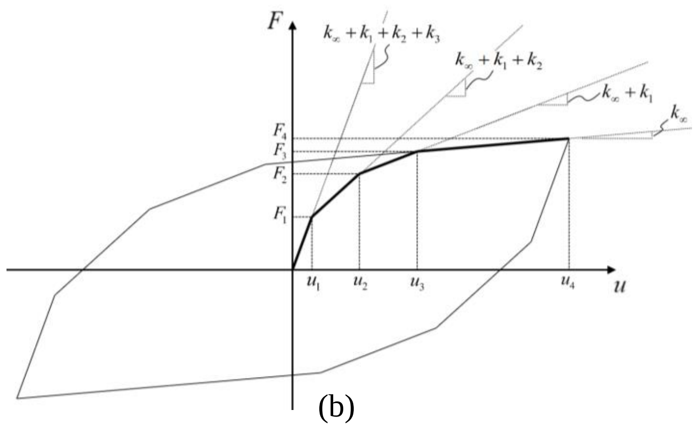

(b)

Figure 3.8 Masing model (a) and its corresponding hysteresis cycle (b).

Increasing the number of Jenkin elements (the order of the Masing model) result in smoother hysteresis characteristics. Since, the behavior in tension and compression is identical, this model is called as a symmetric model.

Hysteresis cycle of a 3rd order Iwan-Masing model is shown in Figure 3.8-(b) which includes n=3 Jenkin elements (or break points). The elements are assumed to yield in the order 1,2, …, n and a particular break point means that limit load has been reached in one element.

3.2.6 Modified Masing Model

To be able model asymmetric softening-hardening behavior in Masing model the single parallel spring is described in the following nonlinear form (linear, quadratic and cubic term): The quadratic term ensures the symmetry. Both quadratic and cubic term may result in softening and/or hardening behavior. All hysteresis and softening-hardening asymmetric behavior are defined by this *modified Masing model*. So the restoring force through the asymmetric hysteresis cycles of the modified Masing model is given by:

$$F(t) = g_1 u(t) + g_2 u(t)^2 + g_3 u(t)^3 + \sum_{i=1}^{n} H_i(t) \tag{3.28}$$

and,

$$\dot{H}_i(t) = \frac{1}{2} k_i \dot{u}(t) \{ saturation + re\,activation \} \tag{3.29}$$

where,

$$saturation = 1 - \text{sgn}\left[H_i(t)^2 - Y_i^2 \right] \tag{3.30}$$

$$re\,activation = -\text{sgn}\left[\dot{u}(t) H_i(t) \right] . \left(1 + \text{sgn}\left[H_i(t)^2 - Y_i^2 \right] \right) \tag{3.31}$$

3.3 Tranmissibility Function of Bilinear Dry-Friction Model

Transimissibility function of bilinear dry-friction model or elastically coupled Coulomb damper model shown in Figure 3.9. The methodology derived by Ruzicka [2] is an approximate solution, which relies on the basis of equilavelent viscously damped system.

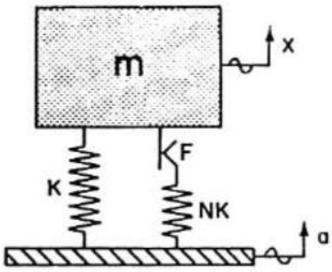

Figure 3.9 Bilinear dry-friction model [2].

For zero damping, the mass is supported solely by the isolator static stiffness K; therefore, the absolute transmissibility T_0 and the undamped natural frequency ω_0 are given by

$$T_0 = \frac{1}{1-\beta^2} \ , \qquad \omega_0 = \sqrt{\frac{K}{m}} \tag{3.32}$$

Infinite transmissibility will occur when the excitation frequency ω coincides with the undamped natural frequency ω_0. For infinite damping, the mass is supported by the stiffness $(N+1)K$; therefore, the absolute transmissibility T_∞ and the natural frequency ω_∞ are given by

$$T_\infty = \frac{(N+1)}{(N+1)-\beta^2} \ , \qquad \omega_\infty = \sqrt{\frac{(N+1)K}{m}} \tag{3.33}$$

For the case of harmonic vibration excitation of the support structure, the equation for absolute displacement transmissibility is given approximately by,

$$(T_A)_D = \sqrt{\frac{1 + \left(\frac{4}{\pi}\right)^2 \left[\frac{N+2}{N} - 2\left(\frac{N+1}{N}\right)/\beta^2\right]}{(1-\beta^2)^2}} \tag{3.34}$$

for values of the frequency ratio β which fall within the break-loose and lock-in frequency ratios defined by,

$$\beta_L = \sqrt{\frac{\left(\frac{4}{\pi}\Psi\right)(N+1)}{\left(\frac{4}{\pi}\Psi\right) \mp N}}, \qquad \Psi = \frac{F}{Ka_0} \tag{3.35}$$

where the plus sign corresponds to the break-loose frequency ratio and the minus sign corresponds to the lock-in frequency ratio. For frequency ratios not falling between the break-loose and lock-in frequency ratios, the absolute transmissibility is given by equation (2) since no relative motion exists across the Coulomb damping element and resistance to inertial forces is provided entirely by the stiffness $(N+1)K$. Dimensionless transmissibility curves calculated by using the Ruzicka's method is shown in Figure 3.10.

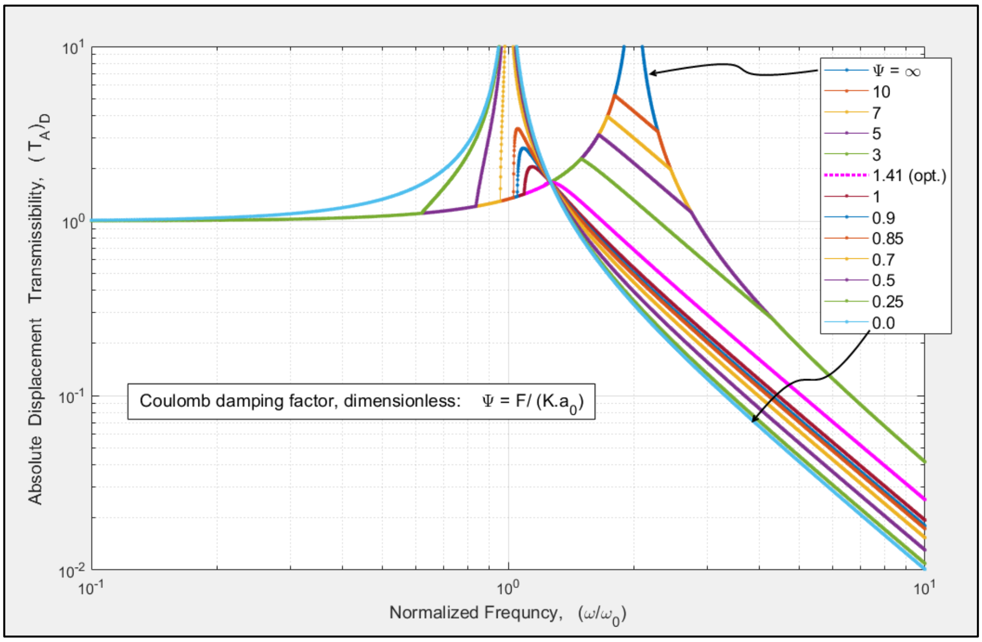

Figure 3.10 Absolute displacement transmissibility curves for vibration isolation system with elastically connected Coulomb damping

It must be noted that, “equivalent viscous damping” $\left(c_e = \frac{4\mu F_n}{\pi U \omega}\right)$ assumption is utilized for the derivation of transmissibility curves of Coulomb friction damped system. For this assumption, the transmissibility curves generated are approximate and should be treated as such. Although, they certainly give much information about the characteristics of the Coulomb damped system, but do not embody the nonlinear characteristics.

3.4 Iterative Nonlinear Harmonic Analysis

In this part, a methodology is derived for the implementation of frequency domain harmonic analysis of equivalent systems, which is shown in Figure 3.11.

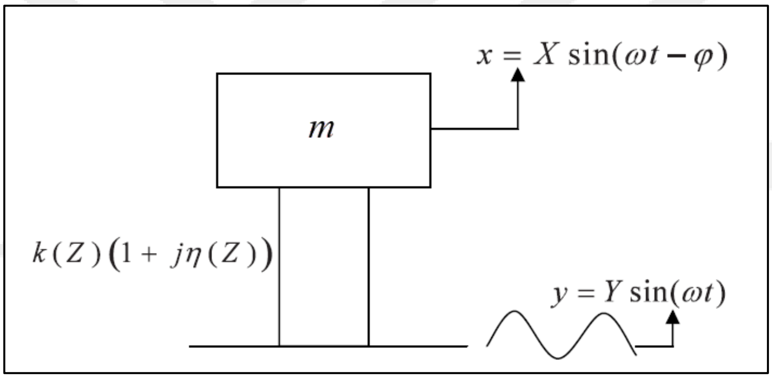

Figure 3.11 Equivalent amplitude-dependent system of WRI [69]

The steady-state response under harmonic excitation of the system shown in Figure 3.11 is

$$[-\omega^2 m + k(1 + j\eta)]X = [k(1 + j\eta)]Y \tag{3.36}$$

or

$$[-\omega^2 m + k(1 + j\eta)]Z = m\omega^2 Y \tag{3.37}$$

where $z = x - y$ is the relative displacement (where Z its amplitude) between the mass and the base, that is the deformation of the mount and ω is the excitation frequency. Note that the dependency of stiffness and damping to the amplitude Z is omitted for the sake of brevity.

The transmissibility is defined as the nondimensional quantity that at each frequency quatify how much disturbance has passed from the source to the receiver through the transmission path. The absolute transmissibility is

$$|T| = \left|\frac{X}{Y}\right| = \left|\frac{k(1+j\eta)}{k(1+j\eta)-\omega^2 m}\right| \tag{3.38}$$

The algorithm proposed for implementing harmonic analyses in the frequency domain is given in Table 3.3.

Table 3.3 Algorithm for the *Iterative Nonlinear Harmonic Analysis*

==

$i = 0$

$Make\ initial\ estimate\ for\ \left|Z^{(i)}\right|\ \ \rightarrow @\ each\ frequency$

$REPEAT$

$\quad \left[-\omega^2 m + k\left(\left|Z^{(i)}\right|\right) * \left(1 + j\eta\left(\left|Z^{(i)}\right|\right)\right)\right] Z^{\,(i+1)} = m\omega^2\, Y^{(i+1)}$

$\quad i = i + 1$

$\quad Update\ \left|Z^{(i)}\right|$

$\quad UNTIL\ Converged$

==

Here, it must be remembered that the dynamic stiffness $k(Z)$ and the loss factors $\eta(Z)$ parameters to be supplied into the algorithm given in Table 3.3 will be obtained from the characterization test implemented by the dynamic test instrument.

3.4.1 An Application of the Iterative Nonlinear Harmonic Analysis

In this section, a numerical case study is implemented using the inputs shown in Figure 3.12 and Figure 3.13.

Transmissibility results are shown in Figure 3.14. For comparison, one of the results for a specific base excitation amplitude ($u_0 = 0.075\ mm$) is plotted with Ruzicka's approximate solution shown in Figure 3.15. It can be said that a good agreement is obtained between two different approaches.

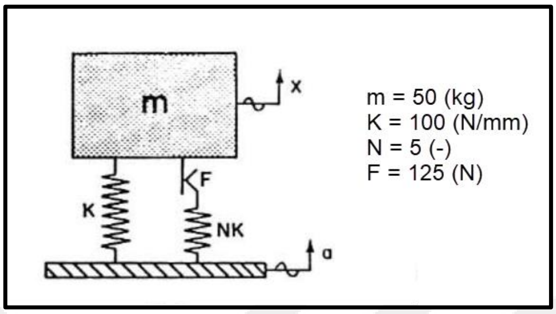

Figure 3.12 Bilinear dry-friction model with numerical values [2]

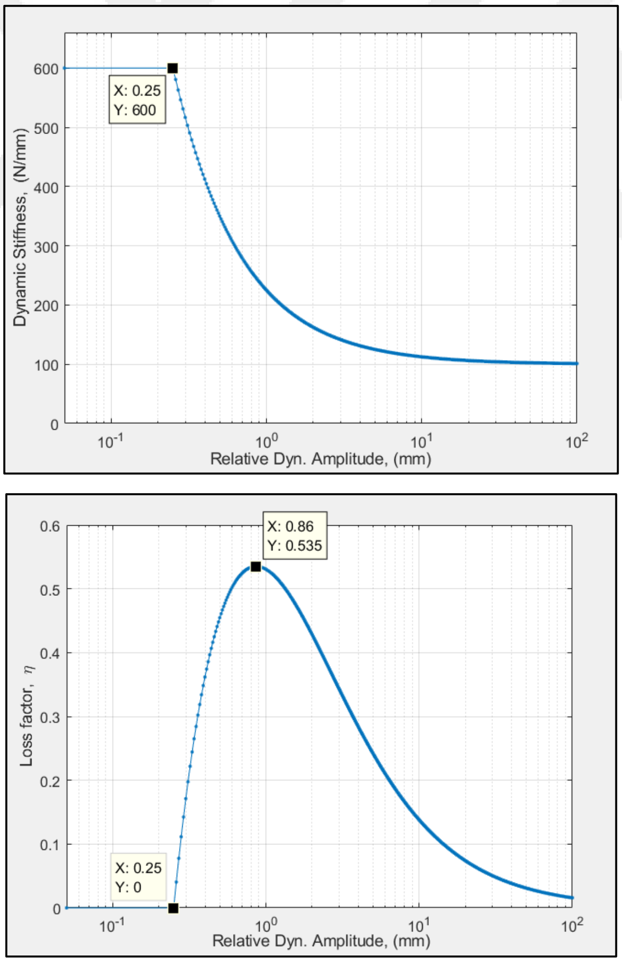

Figure 3.13 Amplitude-dependent dynamic stiffness and loss factor.

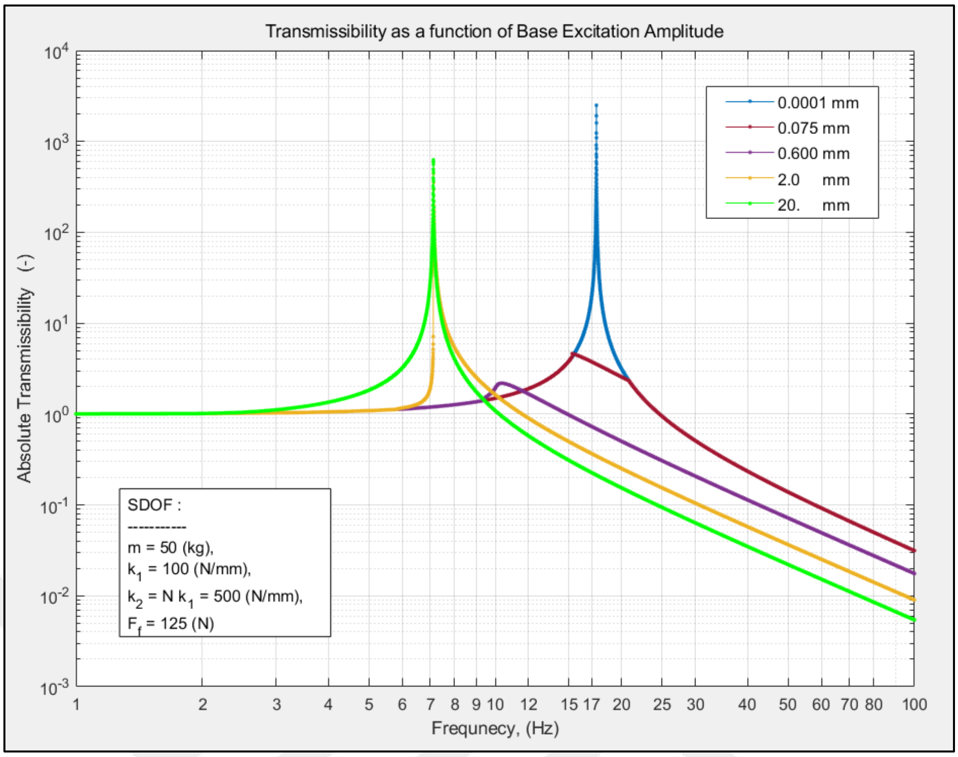

Figure 3.14 Steady-state response obtained with iterative method, for a given range of input amplitudes

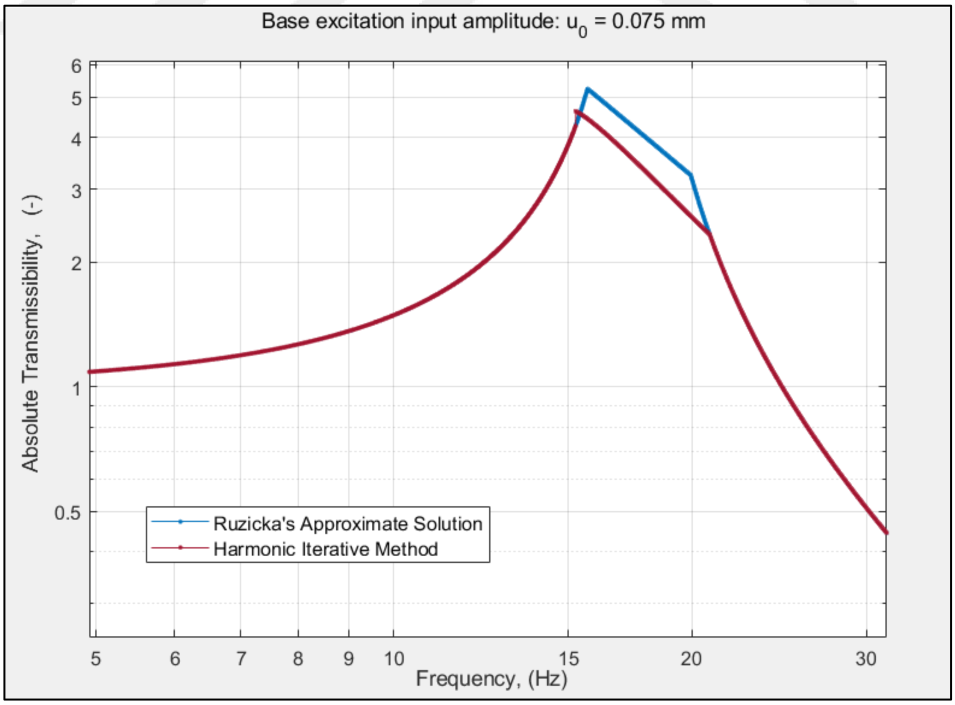

Figure 3.15 Comparison of Ruzicka’s [2] approximate solution and the proposed iterative solution method

CHAPTER 4

CHARACTERISATION TESTING OF WIRE ROPE ISOLATORS

Specimen-level characterization tests and the results obtained are mentioned in this section. The outcomes of characterisation testing of WRIs is also given in this chapter.

4.1 Methodology of the Characterisation Tests.

It is realized that there is a close similarity between the low cycle fatigue testing of metallic material samples and the cyclic testing of WRI's, because of the existance of Coulomb friciton related hysteresis behavior for both of them. Therefore, some testing concepts used for the low cycle fatigue testing of metallic materials can be utilized for the sample characterization testing of WRI's.

Basically, WRI sample characterization tests will be applied in two seperate stages, that is one for monotonic and the other is for cyclic loading.

4.1.1 Monotonic and Cyclic Loading

In this section, the terms Force-Displacement (F, x) and Stress-Strain (σ, ϵ) are used interchangeably to make a generalization for the hysteresis behavior of WRI's.

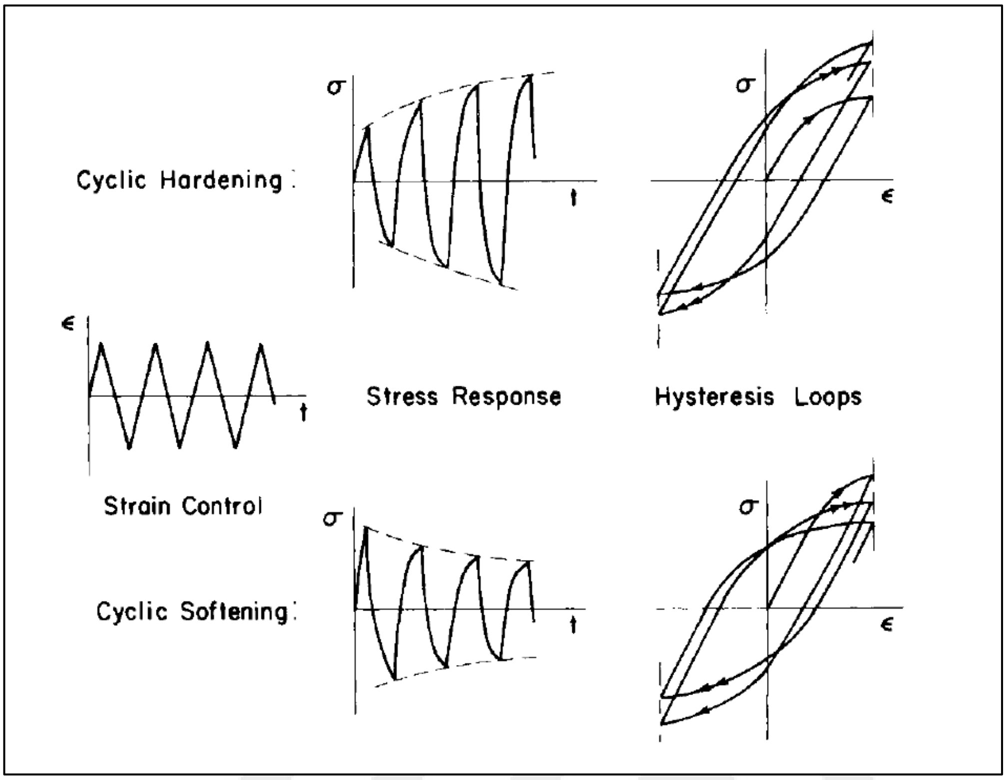

Figure 4.1 Completely reversed controlled strain test and two possible stress responses, cycle-dependent hardening and softening [44].

When transient effects (shown in Figure 4.1) die out, stress response seems to converge a constant value for both cyclic hardening and cyclic softening behavior. For this reason, in order to obtain stabilized (steady-state condition) hysteresis loops a pre-cycling test protocol is vital and it is a must.

In engineering metals, the cyclic hardening or softening is usually rapid at first, but the change from one cycle to the next decreases with increasing numbers of cycles. Often, the behavior becomes approximately stable in that further changes are small [44].

Based on the trial test results, it is also found that WRIs are prone to exhibit a kind of cyclic hardening behavior.

An important feature that can be observed from cyclic loading fatigue test of a metallic material is shown in Figure 4.2. Hysteresis loops from near half the fatigue life are conventionally used to represent the approximately stable behavior. Such loops from tests at several different strain amplitudes can be plotted on one set of axes, as shown in Figure 4.2. A line from the origin that passes through the tips of the loops, such as O-A-B-C, is called cyclic stress–strain curve (also known as skeleton or backbone curve). Where the branches in tension and compression do not differ greatly (which is often the case), their average is used. The cyclic stress–strain curve is thus the relationship between stress amplitude and strain amplitude for cyclic loading [44].

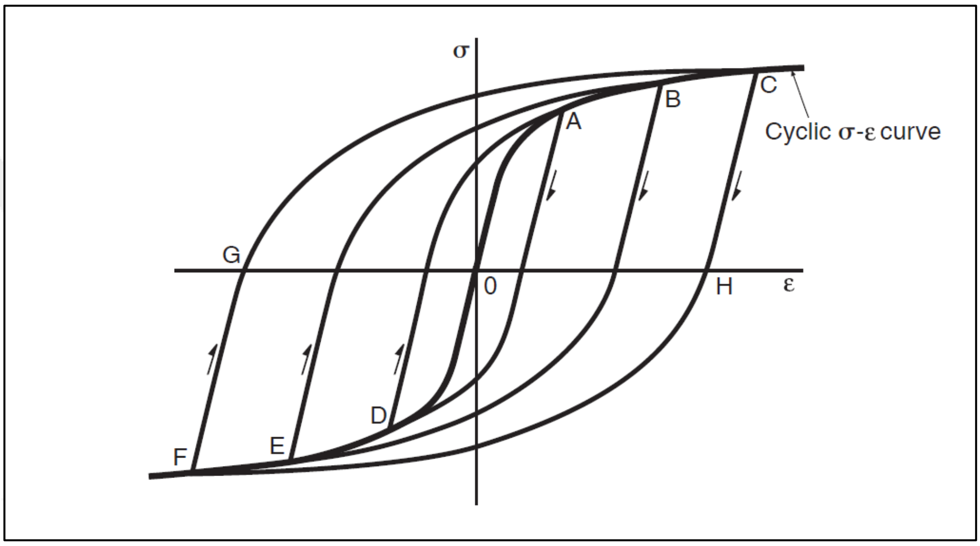

Figure 4.2 Cyclic stress–strain curve defined as the locus of tips of hysteresis loops. Three loops are shown, A-D, B-E, and C-F. The tensile branch of the cyclic stress–strain curve is O-A-B-C, and the compressive branch is O-D-E-F [44].

Cyclic stress–strain curves for several engineering metals are compared with monotonic tension curves in Figure 4.3. Where the cyclic curve is above the monotonic one, the material is one that cyclically hardens, and vice versa. A mixed behavior may also occur, with crossing of the curves indicating softening at some strain levels and hardening at others. The cyclic curves virtually always deviate smoothly from linearity, even for materials where the monotonic curve has a distinct yield point or even a yield drop [44].

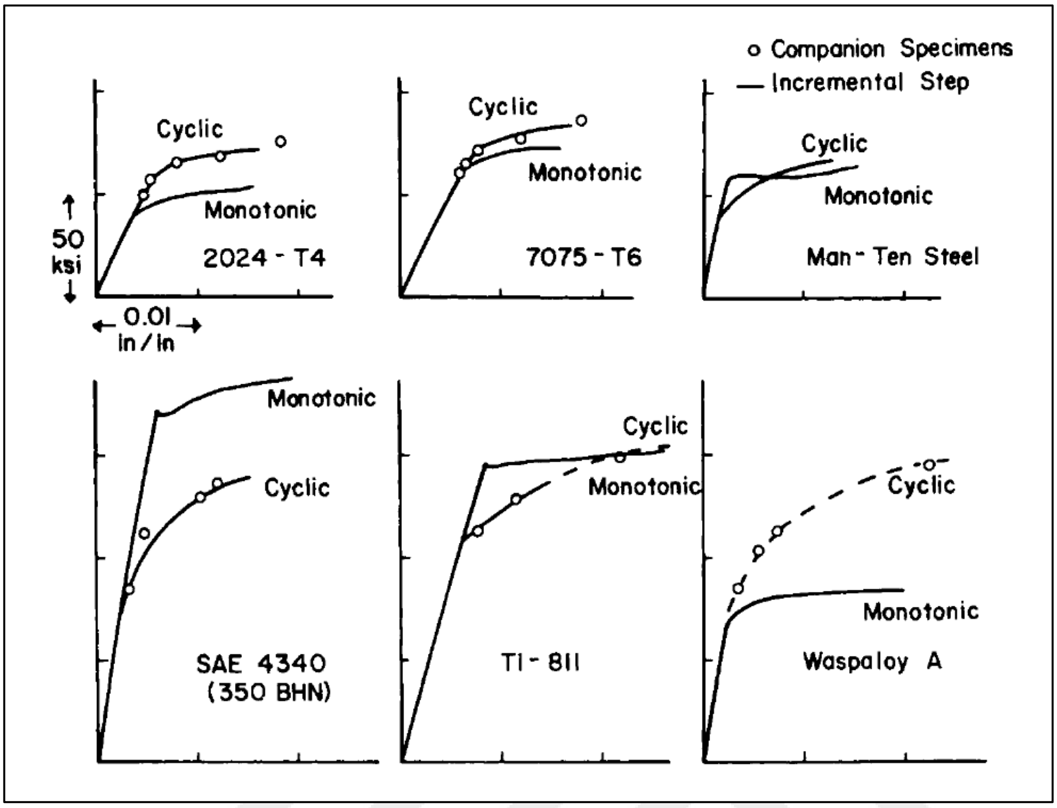

Figure 4.3 Cyclic and monotonic stress–strain curves for several engineering metals [44].

Stress- and strain-controlled fatigue represent extremes of fully unconstrained and fully constrained loading conditions. In real engineering components, there is usually some structural constraint of the material at fatigue-critical sites. It thus seems appropriate to characterize fatigue response of engineering materials on the basis of data obtained under strain-controlled fatigue rather than cyclic stress-controlled conditions [45].

Three commonly used strain-controlled test methods are indicated in Figure 4.4. In the constant amplitude test, the specimen is cycled within a constant plastic strain limit (until failure) to obtain a single stable hysteresis loop. Multiple test specimens are needed to determine the entire Cyclic Stress-Strain (CSS) curve using this method. In the multiple step method, a specimen is cycled between constant plastic strain limits until a saturation loop results. Then the plastic strain limits are incremented until another stable hysteresis loop is obtained. This process is continued until the entire CSS curve is measured from a single test specimen.

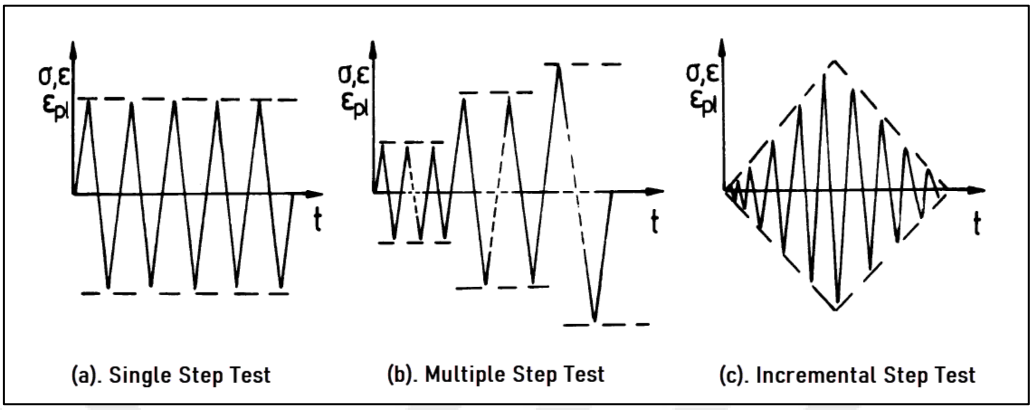

Figure 4.4 Comparison of the loading test profiles for (a). single step test, (b). multiple step test, and (c) incremental step test [46].

In the incremental step method, the specimen is subjected repeatedly to a strain pattern comprising linearly increasing and decreasing amplitudes, from zero to a certain maximum total strain. The resulting stable hysteresis loop provides the CSS plot. In some alloys exhibiting planar slip deformation, the incremental step method provides a CSS response which is different from the other direct methods because of the variations in the development of dislocation structures [45].

Of the three test methods mentioned above, the most suitable one for characterization of WRI behavior is *multiple step test* method which is also shown in Figure 4.4.

4.2 Dynamic Test Instrument

A new dynamic-fatigue testing instrument acquired by Roketsan Inc., shown in Figure 4.5, is to be used for the implementation of specimen-level characterisation tests of WRIs of a specific size and capacity.

The instrument is capable of carrying out fatigue test by controlling, force amplitude, displacement amplitude, excitation frequency or preload in terms of both software and hardware.

Figure 4.5 Instron® ElectroPuls® E10000 Linear-Torsion All-Electric Fatigue and Dynamic Test Instrument [47].

4.3 Characterisation Test Fixtures

Mechanical designing and manufacturing of necessary test fixtures allowing the WRI specimens to be able loaded in their main three axes that suits the attachment of high precision interfaces of dynamic test instrument have been realised. Fixtures designed and manufactured for tension/compression mode loading characterisation tests are shown in Figure 4.7, Figure 4.8, and Figure 4.8.

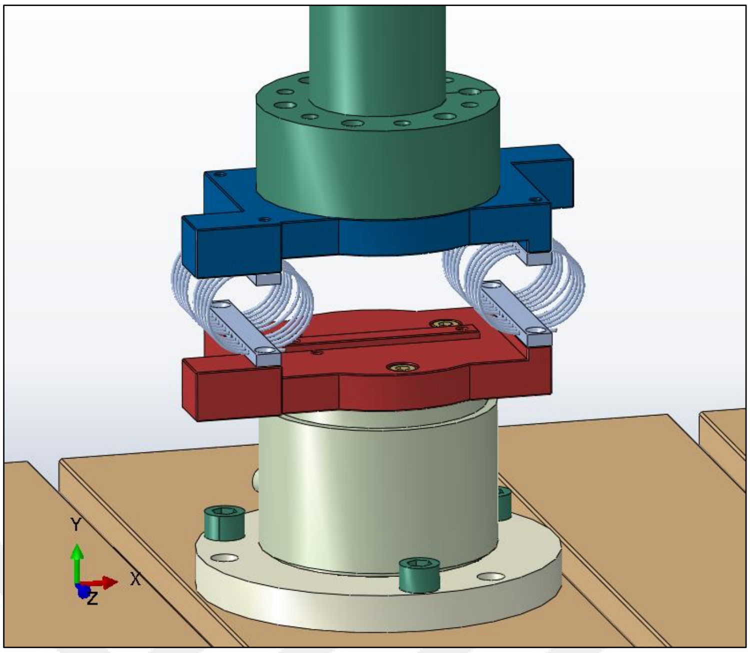

Figure 4.6 Designed CAD model for Tension/Compression mode loading fixture of the WRIs.for sample level characterisation tests

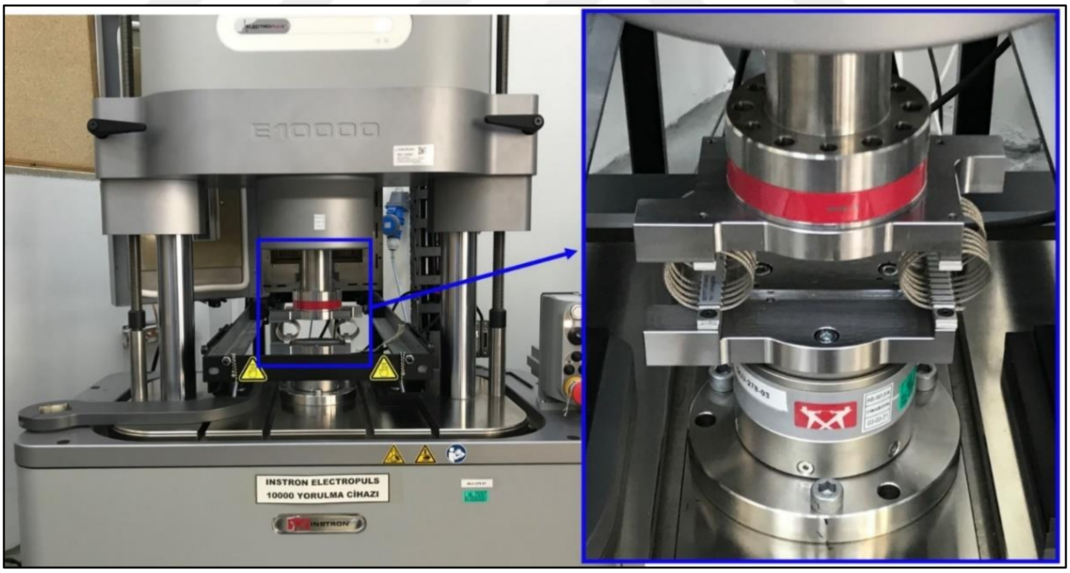

Figure 4.7 Tension/Compression mode loading fixture assembled to the test instrument.

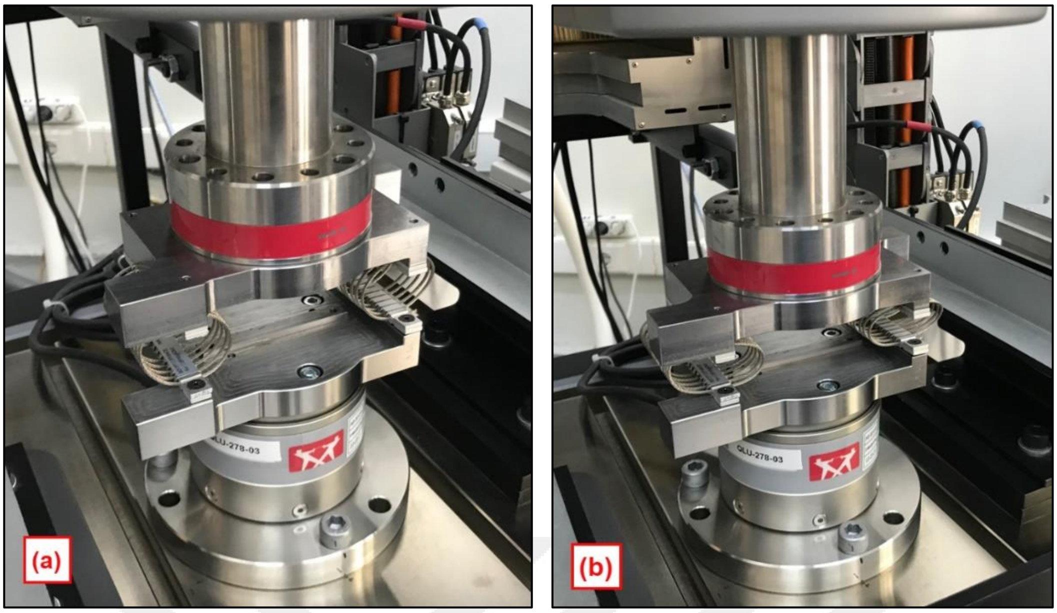

Figure 4.8 Tension/Compression mode loading fixture of the WRI with no preload (a) and with compression preload applied (b)

Fixtures designed and manufactured for shear/roll mode loading characterisation tests are shown in Figure 4.9, Figure 4.10, and Figure 4.11.

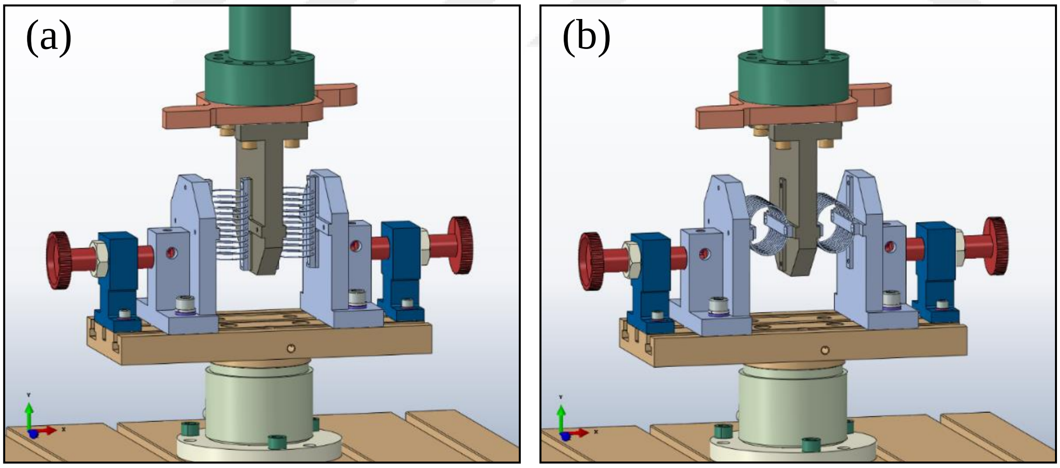

Figure 4.9 Designed CAD models for Shear mode (a) and Roll mode (b) loading fixture configuration of the WRIs for sample level characterisation tests

Both shear and roll mode loading specimen-level characterisation tests of WRIs can be done using the same fixture design shown in Figure 4.9.

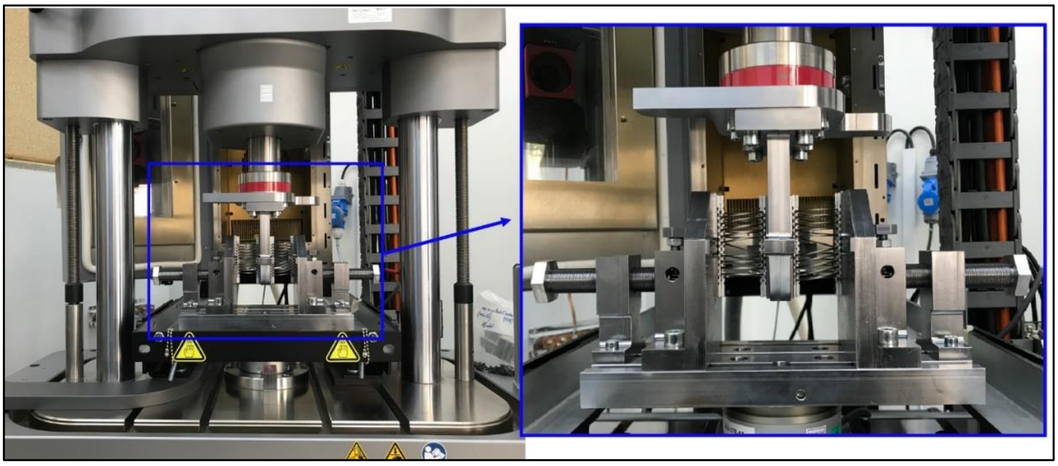

Figure 4.10 Shear/Roll mode loading fixture assembled to the test instrument.

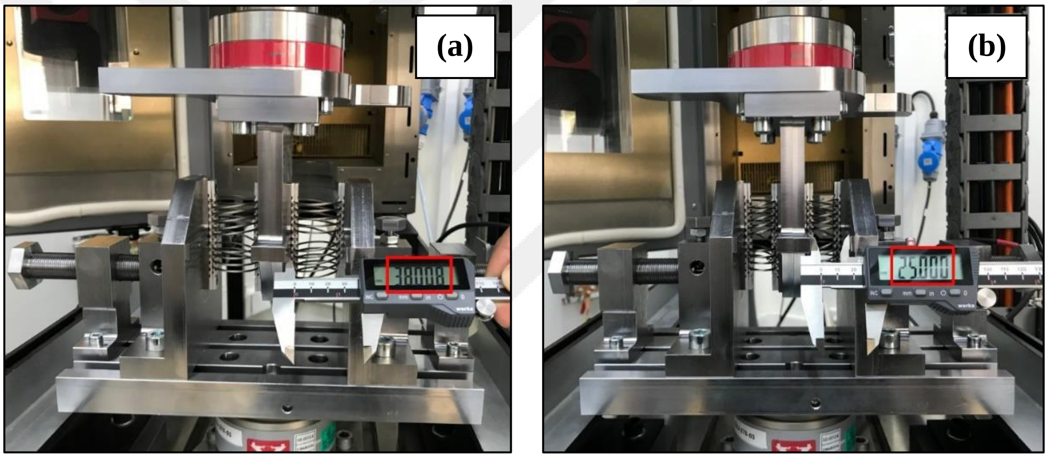

Figure 4.11 Shear/Roll mode loading fixture of the WRI with no preload (a) and with compression preload applied (b).

4.4 Methodology for Dynamic Characterisation Testing

Dynamic tests are carried out under displacement control. However, the sinus displacement amplitude with a fixed frequency is first gradually increased up to a certain value during the test, and then displacement amplitude is gradually decreased which is shown in Figure 4.12 and Figure 4.13.

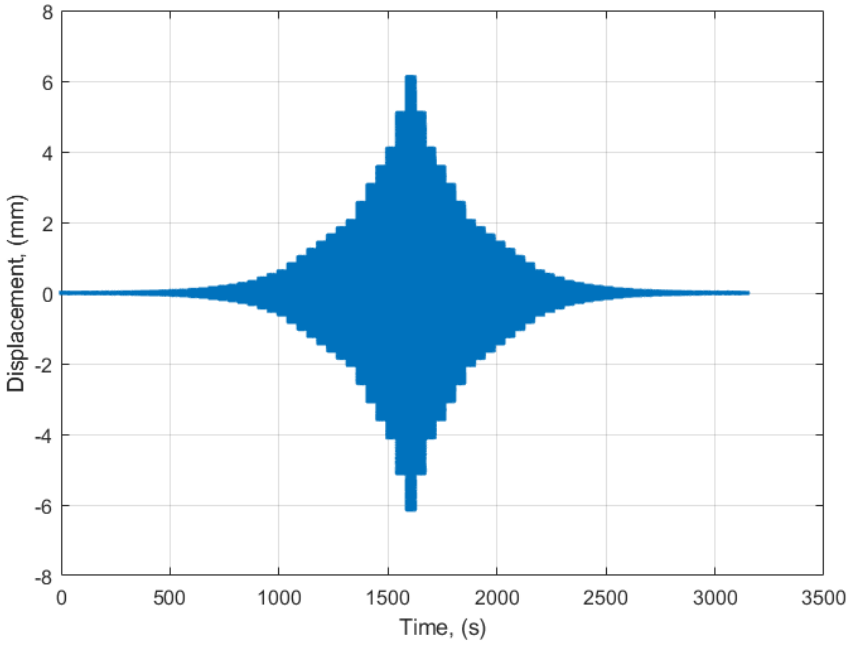

Figure 4.12: Displacement controlled sine testing (without preload)

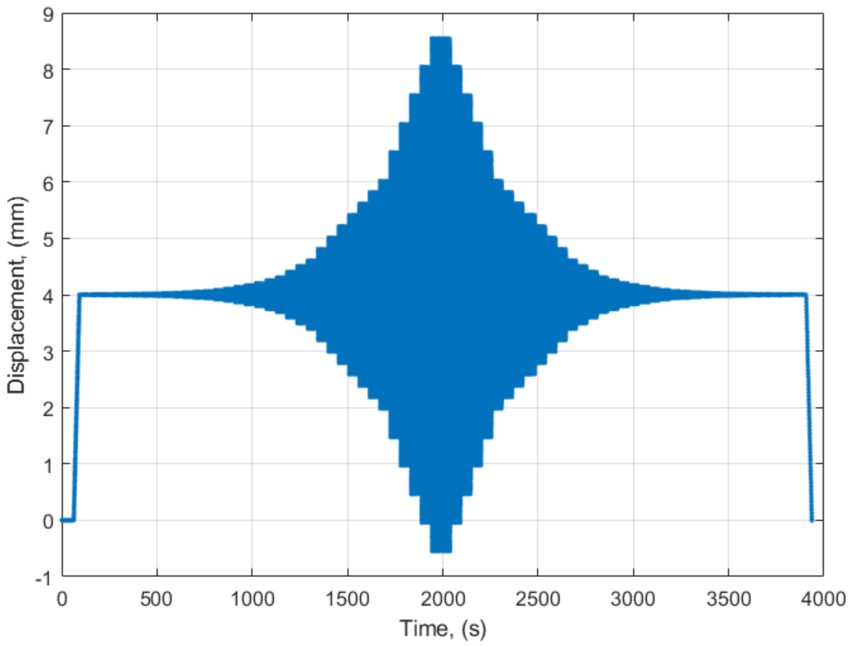

Figure 4.13: Displacement controlled sine testing (with preload)

4.5 Performed Characterization Tests of Wire Rope Isolators

The characterization tests performed in this section were carried out with relatively small size WRIs and it was aimed to examine the effects of preload and excitation frequency on dynamic stiffness and loss factor.

C2H-1010 and C2H-510 type Socitec brand insulators listed below tests have been carried out.

- C2H-1010 isolator is tested in T/C direction @1.0Hz with following preload values: 0.0mm compression, 2.0mm compression, 4.0mm compression, 6.0mm compression, 2.0mm tension, 4.0mm tension.
- C2H-1010 isolator is tested in T/C direction @0.1Hz with following preload values: 2.0mm compression.
- C2H-1010 isolator is tested in T/C direction @10Hz with following preload values: 2.0mm compression, 4.0mm compression, 2.0mm tension.
- C2H-1010 isolator is tested in T/C direction @20Hz with following preload values: 2.0mm compression, 4.0mm compression, 2.0mm tension.
- C2H-510 isolator is tested in T/C direction @1.0Hz with following preload values: 0.0mm compression, 1.0mm compression, 2.0mm compression, 3.0mm compression, 1.0mm tension, 2.0mm tension.
- C2H-510 isolator is tested in Shear direction @1.0Hz with following preload values: 2.0mm compression, 3.0mm compression,
- C2H-510 isolator is tested in Roll direction @1.0Hz with following preload values: 2.0mm compression, 3.0mm compression,

When the test results are examined, it is understood that the dynamic stiffness and damping ratio are almost independent of the excitation frequency. However, the same cannot be said for the preload.

The effect of the preload applied on the WRI in the T/C direction on the dynamic stiffness and damping ratio was investigated under 1.0(Hz) excitation frequency, and the results are given in Figure 4.14 and Figure 4.15.

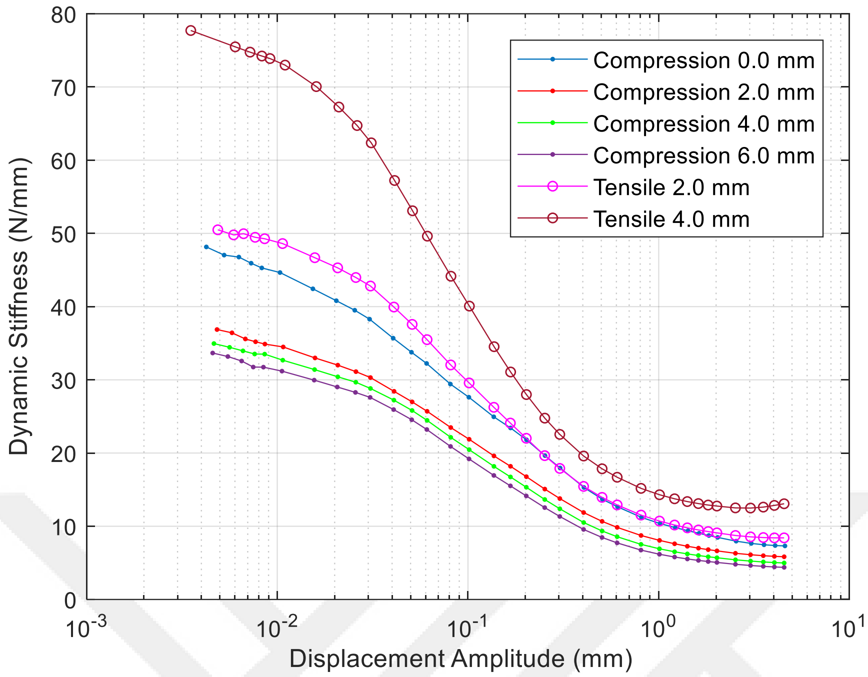

Figure 4.14: Dynamic stiffness of “C2H-1010” isolator in T/C loading

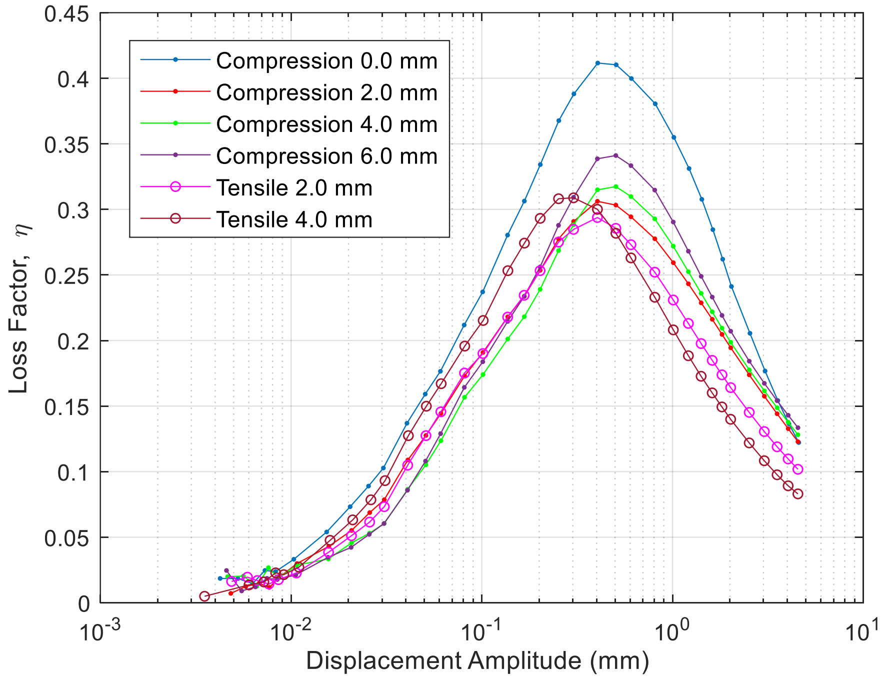

Figure 4.15: Loss factor of “C2H-1010” isolator in T/C loading

When the data in Figure 4.14 are examined, it can be said that the dynamic stiffness is more sensitive to the preload in the tensile direction, but the preload in the compression direction converges to a certain value. Similarly if the data in Figure 4.15 are examined, it can be said that the damping ratio has less dependence on the preload, in contrast to the dynamic stiffness.

4.6 Patent Application for an Adjustable Test Fixture for Characterisation Testing of WRIs

Within the scope of this thesis and The Researcher Training Program for Defense Industry (SAYP), the application for the patent titled “An adjustable test fixture for the characterisation testing of wire rope isolators” shown in Figure 4.16 with the application number TR 2023/004708 has been realized.

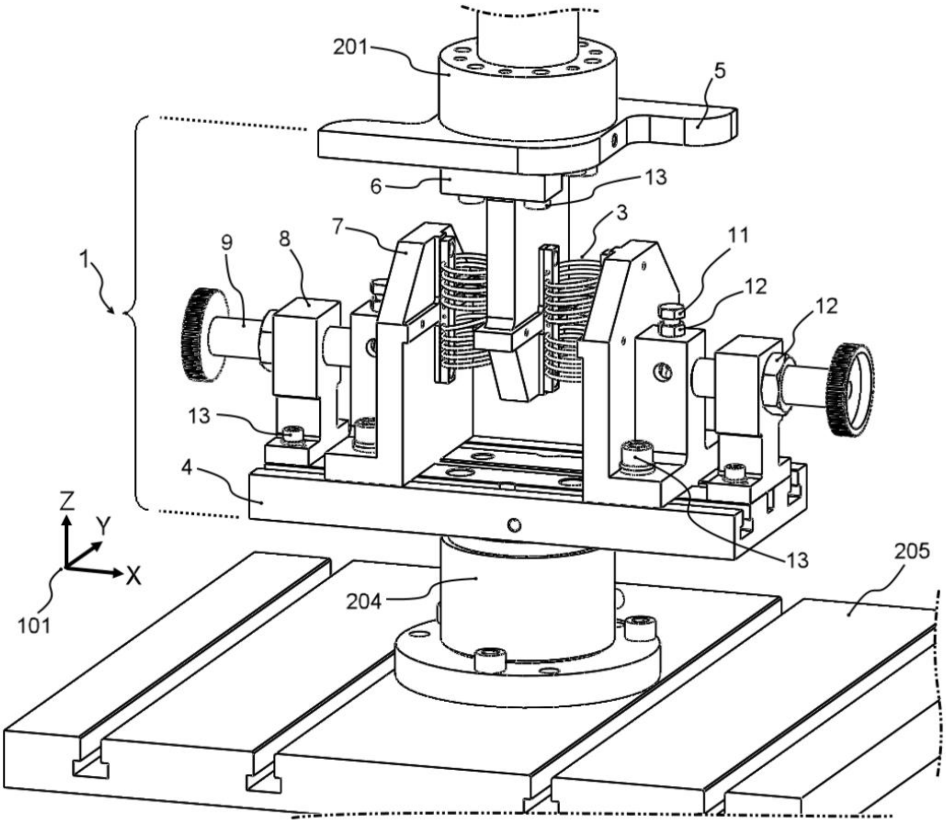

Figure 4.16: An adjustable test fixture for the characterisation testing of wire rope isolators [71]

Briefly, the invention relates to an adjustable test device developed to characterize the static and dynamic behavior of WRIs. In particular, the invention enables the characterization tests representing the static and dynamic behavior of the WRIs in the shear direction and rolling direction axes to be carried out, as well as the fact that it is adjustable, thanks to its adjustable feature, both perpendicular to the test execution axis in the shear direction and rolling direction of the WRIs. It relates to a test device that enables the preload to be applied in the tensile-compression direction axis as well as the execution of characterization tests of WRIs of different sizes which can regarded as a novely when available literature is taken into consideration.

CHAPTER 5

IDENTIFICATION OF THEORETICAL MODEL

The main aim of the identification process is to make the theoretical model parameters derived and calibrated by utilising the specimen-level characterisation test results. The application of the identification method mentioned in this section is given in section 7.3.

5.1 Identification Methodology

Austrell [11] gives various algorithms to be used for (a). the calculation of Masing's model parameters from the initial loading (skeleton or backbone) curve, (b). the calculation of initial loading (backbone) curve from the Masing's model parameters and, (c). the calculation of dynamic stiffness and loss factor (which is identical to "*amplitude dependent complex stiffness*") from the initial loading curve. In this way, any transition between these Masing's model parameters, initial loading curve and amplitude dependent complex stiffness can be implemented easily.

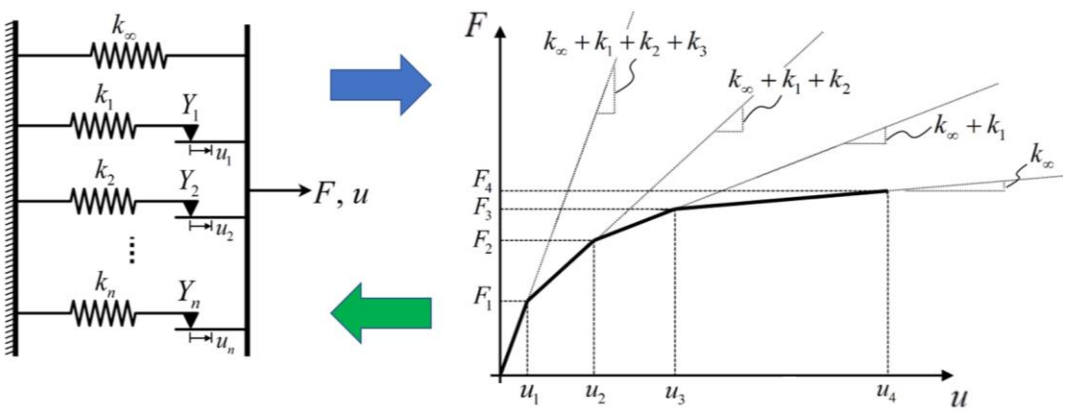

Figure 5.1 Masing's model and corresponding initial loading curve

The model parameters can be obtained from the initial loading curve. It is a piecewise linear curve according to Figure 5.1. The elements are assumed to yield in the order 1, 2, .., n with respect to Figure 5.1, and a particular break point means that limit load has been reached in one element. The parameters are determined directly from

$$k_i = \frac{F_i - F_{i-1}}{u_i - u_{i-1}} - \frac{F_{i+1} - F_i}{u_{i+1} - u_i} \qquad and \qquad Y_i = k_i u_i \tag{5.1}$$

The inverse relation, i.e. the break points obtained from the model parameters, is given by

$$u_i = \frac{Y_i}{k_i} \qquad and \qquad F_i = \sum_{p=1}^{i-1} k_p u_p + \left(k_\infty + \sum_{p=i}^{n} k_p \right) u_i \tag{5.2}$$

where it is assumed that the first sum vanishes if $i = 1$. The dynamic stiffness for the generalized model is also found directly from the loading curve. Values of the dynamic stiffness for amplitudes corresponding to the break point displacements are

$$k_{dyn}^{i} = \frac{F_i}{u_i} \tag{5.3}$$

Damping for displacement amplitudes corresponding to the break point displacements can be calculated by summing the enclosed areas for the frictional elements that have yielded at the particular displacement amplitude and using equation $k_{eq} = k_{dyn} = \frac{\Delta F}{\Delta x}$ and $\eta = \frac{E_{diss}}{2\pi W}$, where $W = \frac{1}{2} k_{dyn} \Delta x^2$ is the max elastic (strain) energy stored in hysteresis cycle.

As a result, if the initial loading curve (skeleton or backbone) is known, one can obtain parameters of the Masing model or vice versa. Similarly, one can calculate amplitude dependent dynamic stiffness and loss factor, if the initial loading curve (skeleton or backbone) is known or vice versa.

CHAPTER 6

EXPERIMENTAL INVESTIGATION OF AMPLITUDE-DEPENDENT BEHAVIOUR OF A WIRE ROPE ISOLATOR SYSTEM USING MODAL TESTING METHODS

In this chapter, it is clearly shown that a WRI isolation system exhibits an amplitude-dependent non-linear behaviour through the FRFs obtained by modal testing. More importantly, it has been experimentally proven which type of stiffness and value of stiffness of a WRI should be used when implementing the modal analysis of a WRI isolation system, which can be considered a novelty concerning the limited studies in the literature.

The approach typically practised in the past was to derive the stiffness value to be used in the modal analysis from the slope of the monotonic static loading curve of the WRI; that is, the resonance frequency was tried to be calculated by taking into account the static stiffness value. However, in this study, it has been experimentally proven which type of stiffness and value of stiffness of a WRI should be used when implementing the modal analysis of a WRI isolation system, which can be considered a novelty concerning the studies in the literature. As a result, the resonance frequency of a WRI isolation system can be calculated more realistically in a complex FEA model corresponding to the small loading amplitude.

6.1 Introduction

Wire Rope Isolators (WRIs) are extensively used in many fields of industry, such as defence and aerospace [48], especially where the absorption of shock and vibration loading exerted on sensitive equipment is a significant concern. Also, the ability to survive in harsh environments (corrosive, wear, extreme temperatures etc.) makes WRIs more attractive in passive shock and vibration isolation applications than rubber-based isolators. Basically, shock and vibration loading is attenuated through the Coulomb (dry) friction mechanism occurring between individual wires found within a wire strand [49], [50]. As a result of the complex friction mechanism, hysteresis behaviour appears when the isolation system is suddenly or cyclically loaded. Inevitably, the dissipation or damping mechanism of WRIs to the shock and vibration loading is closely related to the area enclosed by the hysteresis cycle and the maximum energy stored in that hysteresis cycle.

In literature, amplitude-dependent behaviour is also known as Payne [52] or Fletcher-Gent [53] effect. The Payne effect can be interpreted as the dependency of the dynamic stiffness on the dynamic amplitude, which is a harmonic loading amplitude. Besides, the Payne effect manifests itself as a shift in the resonance frequency of the isolation system depending on the loading amplitude, which can be diagnosed from the frequency response functions (FRFs). In addition to WRIs, especially filled rubbers [52], [53] exhibit this behaviour. Filled rubbers, contrary to the unfilled natural rubbers, reveal a significant effect of the vibration amplitude on the storage and loss moduli of the rubber; i.e., the vibration amplitude has a considerable effect on the stiffness and damping properties of the rubber [54].

In this study, a vibration isolation system setup consisting of four helical WRIs and one floating mass was investigated experimentally. The relevant experimental setup is designed in such a way that the lower part of the WRIs is connected to the fixed base while the upper part is to the floating mass, which is different from the experimental setup illustrated in the study made by Juntunen [55].

Since the presence of the amplitude-dependent behaviour can be easily observed in the frequency domain, then frequency response functions are measured by exciting the WRI system both using an impact hammer and modal shaker. To this end, LMS Test.Lab software [56], [57] is utilised. It is found that for relatively small excitation amplitudes, both impact hammer and modal shaker excite nearly identical resonance frequencies. On the other hand, for relatively larger amplitudes, modal shaker excitation generates more accurate resonance frequencies and the FRF data compared to impact hammer excitation. Besides system-level modal testing of the WRI system, sample-level dynamic characterisation testing of the WRI samples is accomplished by utilising a dynamic (fatigue) test instrument.

A theoretical model, referred to as the Masing model [58], relying on dry friction phenomena, is proposed for modelling the steady-state dynamic behaviour of the WRIs. Subsequently, identification of the basic parameters of the Masing model is given by utilising the modal testing and characterisation testing results. Moreover, the confidence level in the test results has increased by correlating the results of both the modal testing and characterisation testing.

In this study, it is clearly shown that a WRI isolation system exhibits an amplitude-dependent non-linear behaviour through the FRFs obtained by modal testing. More importantly, it has been experimentally proven which type of stiffness and value of stiffness of a WRI should be used when implementing the modal analysis of a WRI isolation system, which can be considered a novelty concerning the limited studies in the literature. Thus, this study which was mainly performed experimentally brings an innovative approach to the modelling and validation of WRI.

6.2 Modal Testing of the WRI System

6.2.1 Experimental Setup

The experimental setup to be investigated in this study is shown in Figure 6.1. The experimental setup consists of three main components: *base part*, *WRIs*, and *floating mass part* at the top. The base part using bolted connections is fixed to the T-slot table, whose mass is about one tonne. Once the base part is fixed, the four WRIs are bolted to the base part at one end, and similarly, they are bolted to the floating mass piece at the other end.

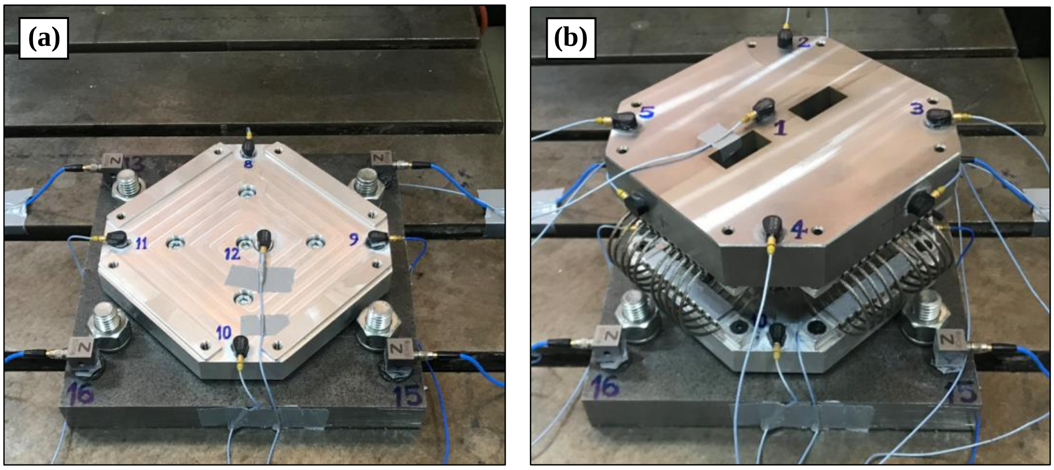

Figure 6.1: Components of the WRI system: base part (a) and floating mass part (= 2.59(kg)) (b).

Two different types of WRI are used in the experimental setup of the WRI system, whose properties are approximately given as follows:

- WRI type-A: length = 95 (mm), height = 25 (mm), wire diameter = 1.6 (mm), number of loops = 10.
- WRI type-B: length = 95 (mm), height = 40 (mm), wire diameter = 1.6 (mm), number of loops = 10.

Initially, three floating mass parts corresponding to three different masses (m = 1.14, 1.68, and 2.59 (kg)) are machined to be used in the experimental setup. However, the one with 2.59 (kg) is chosen to be used in the experimental setup, which can be seen in Figure 6.1-(b). Besides, the accelerometer instrumentation of the WRI system and its experimental mesh can also be seen in Figure 6.1.

6.2.2 Excitation Methods

To calculate the frequency response functions (FRFs) and thus resonance frequency of the WRI system, both impact hammers and electrodynamic shakers, shown in Figure 6.2, are utilised to excite the WRI system. In addition to the conventional size excitation equipment (Figure 6.2-(b) and -(d)), the miniature size excitation equipment is also used, which is given in Figure 6.2-(a) and -(c).

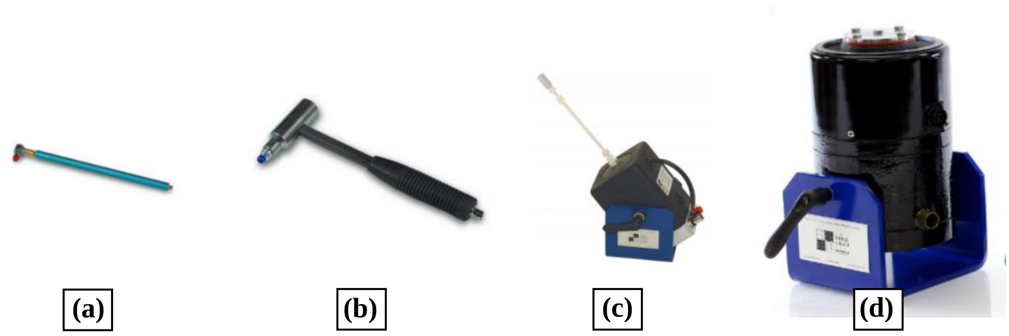

Figure 6.2: Excitation equipment used for modal testing: (a) impact hammer mini - PCB/086E80, (b) impact hammer - PCB/086D05, (c) mini modal shaker - MS/K2007E01, and (d) modal shaker - MS/2110E.

Two types of excitation methods, one for the pulse and the other for broadband loading, are used to excite the WRI system. Two different excitation methods are used in this study to examine the pros and cons of excitation methods for getting the best experimental results and supplying a wide range of loading excitation levels into the WRI system.

6.2.3 Data Acquisition and Signal Processing

To perform modal testing of the WRI system, LMS Scadas Recorder hardware and LMS Test.Lab software [56], [57] is used to implement the data acquisition and signal processing phase.

The following data acquisition and signal processing parameters [56] are utilized for the modal tests using the impact hammer excitation method: sampling frequency = 1024.0Hz, acquisition time = 8.0s, resolution = 0.125Hz, averages = 6, pretrigger time ≈ 0.01s, input window type = force-exponential 1.0%, and FRF estimator = H_v. Besides, “auto reject with overload” and “include hammer in autoranging” options are also activated for the measurement [56]. Moreover, autoranging is performed each time before the modal test is performed with a different excitation force amplitude.

For the modal tests with shaker excitation method, the following data acquisition and signal processing parameters [57] are used: signal type = burst random, noise type = white noise, burst time = 50%, sampling frequency = 1024.0Hz, acquisition time = 16.0s, resolution = 0.0625Hz, number of averages = 40, and FRF estimator = H_v. Similar to the impact hammer testing, autoranging is also performed each time before the shaker testing is performed with a different excitation force amplitude. In 8.0s of each 16.0s of data acquisition time, the burst random signal is applied by the shaker, and the WRI system is damped in the remaining 8.0s, as shown in Figure 6.8. Therefore, since both the force input signal and the acceleration response signals are periodic in themselves, no windowing function is used in the data acquisition and signal processing phase [59].

6.2.4 Modal Testing with Impact Hammer Excitation

A view from the modal testing of the WRI system showing the point where the hammer hits applied is given in Figure 6.3, including both mini and conventional size impact hammers. The WRI system shown in Figure 6.3 contains four pieces of WRI type-A. Impact hammer hits are applied to the centroid of the floating mass as close as possible and at a right angle to its top surface. Thus, by exciting the WRI system in this way, the WRI system can be forced to behave as an SDOF system making a translation motion as a whole only in the vertical direction.

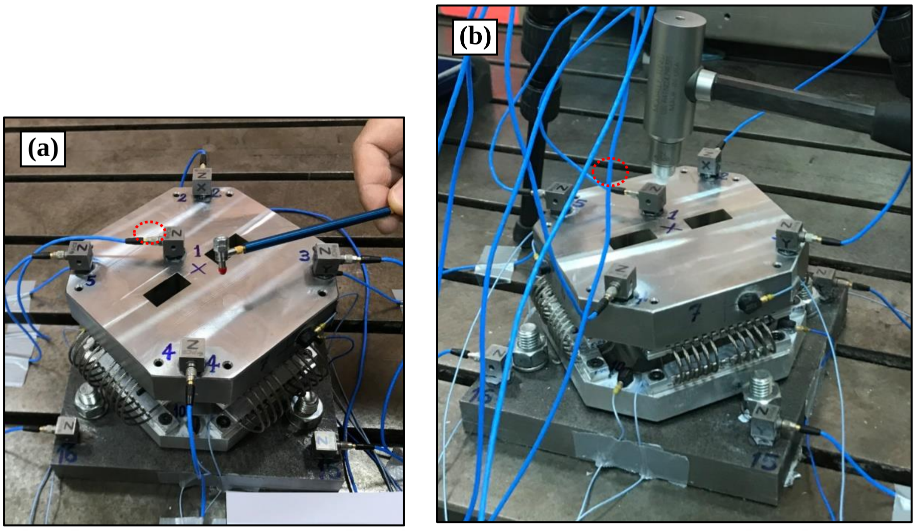

Figure 6.3: Modal testing of the WRI system with the mini (a) and medium (b) size impact hammers.

As mentioned above, six averages (impulses) are taken to measure the driving point FRF [60]. To this end, a trial-error approach is adopted to capture the best quality FRF data possible since it is impossible to apply precisely the same six impulses to the WRI system with a manually operated impact hammer. Thus, the approach adopted can be given as follows. Thus, the approach adopted is explained with an example as follows. For instance, the FRF curve entitled *"Avg imp force_5N"* in Figure 6.4 means that: if the peak of any one of the six measured impulse signals is not within the range of 4.5N and 5.5N, then that measured impulse signal is discarded from the FRF average calculation process.

The driving point FRF data obtained by the impact hammer testing are shown in Figure 6.4 and Figure 6.5. It can be seen that the FRF data given in both figures vary depending on the loading amplitude, which points out that the WRI system exhibits an amplitude-dependent non-linear behaviour. In other words, it can be said that with the increase in the amplitude of the impact force, the WRI system's resonance frequency decreases, whereas the damping level increases. However, this inference expires its validity when the loading amplitude applied with the impact hammer gets higher and higher, which is evident in Figure 6.5. Such that, when the amplitude of the impact force exceeds a specific value (in this case, roughly above the 60N), the measured FRF data becomes very distorted and misleading. As a result, the resonance frequency of the WRI system cannot be estimated from this erroneous FRF data.

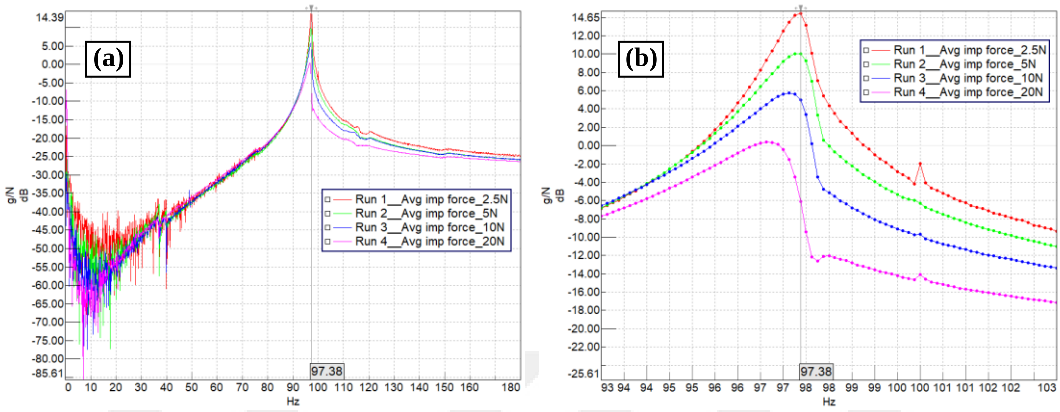

Figure 6.4: Driving point FRFs corresponding to varied loading levels applied with the mini hammer.

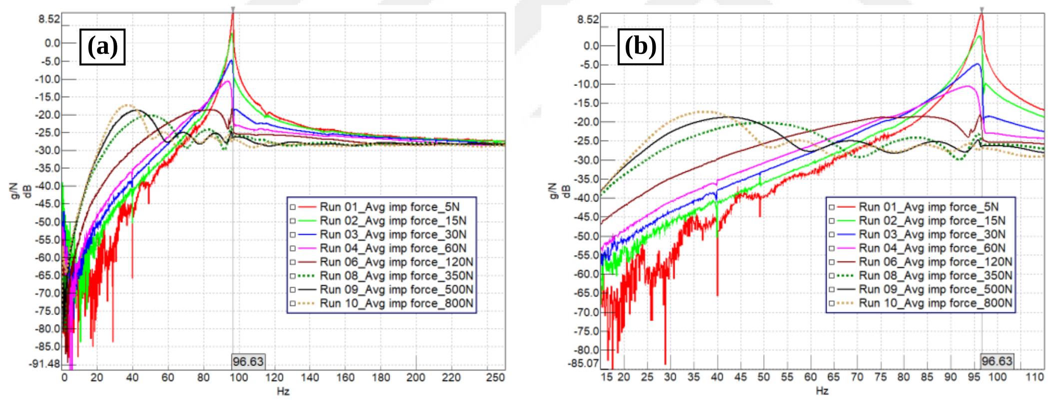

Figure 6.5: Driving point FRFs corresponding to varied loading levels applied with the medium hammer.

The following points should not be overlooked for the FRF data obtained by the impact testing of the WRI system (Figure 6.5). On the FRF curve, the amount of error increases for two reasons: one is due to the rise of the loading amplitude, and the other is due to moving away from the vicinity of the resonance frequency.

6.2.5 Modal Testing with Shaker Excitation

The WRI system to be excited with the shakers shown in Figure 6.6 and Figure 6.7 contains four pieces of WRI type B which is softer than WRI type-A. Here, the upside-down suspension of the mini and conventional size electrodynamic modal shakers over the WRI system is shown in Figure 6.6 and Figure 6.7, respectively. Suspension of the shakers is provided by using the elastic cords, which are connected with the turnbuckles serially, as shown in the corresponding figures.

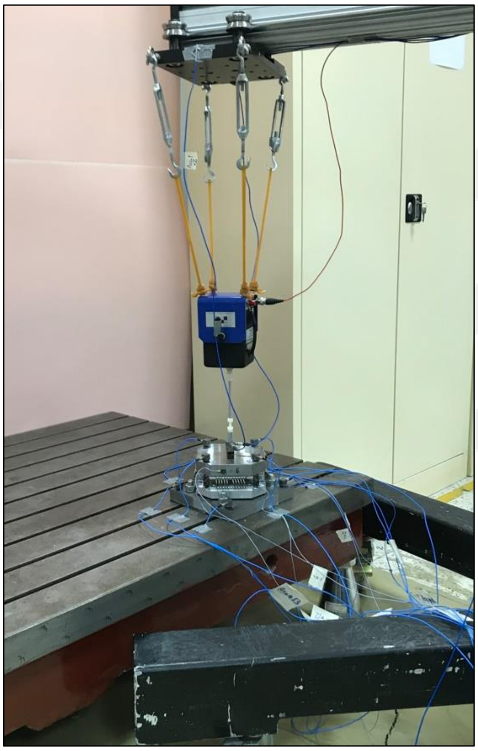

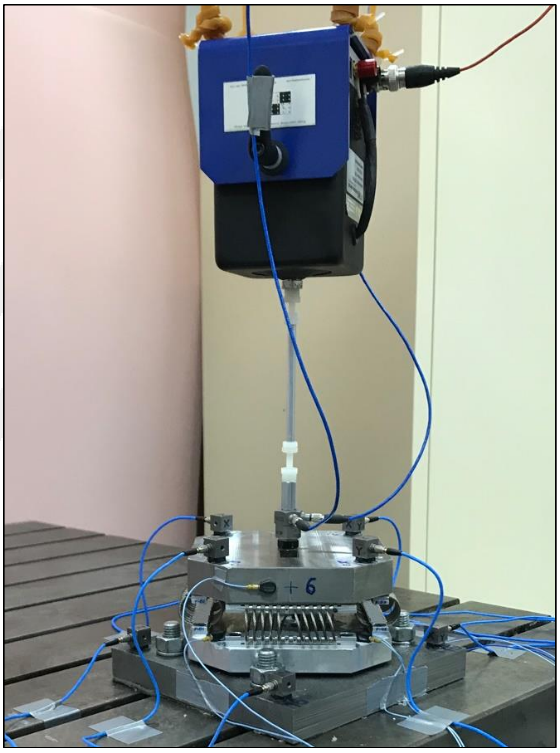

Figure 6.6: Modal testing with the mini modal shaker (MS/K2007E01) attached to the WRI system.

The excitation point by the shaker is aligned, passing through the centroid of the floating mass as close as possible to ensure that the WRI system responds only in the vertical direction as if it were an SDOF system. To this end, a remarkable amount of time is spent on the levelling of the shaker, the alignment of the stinger, and the attachment of the stinger to the top surface of the WRI system.

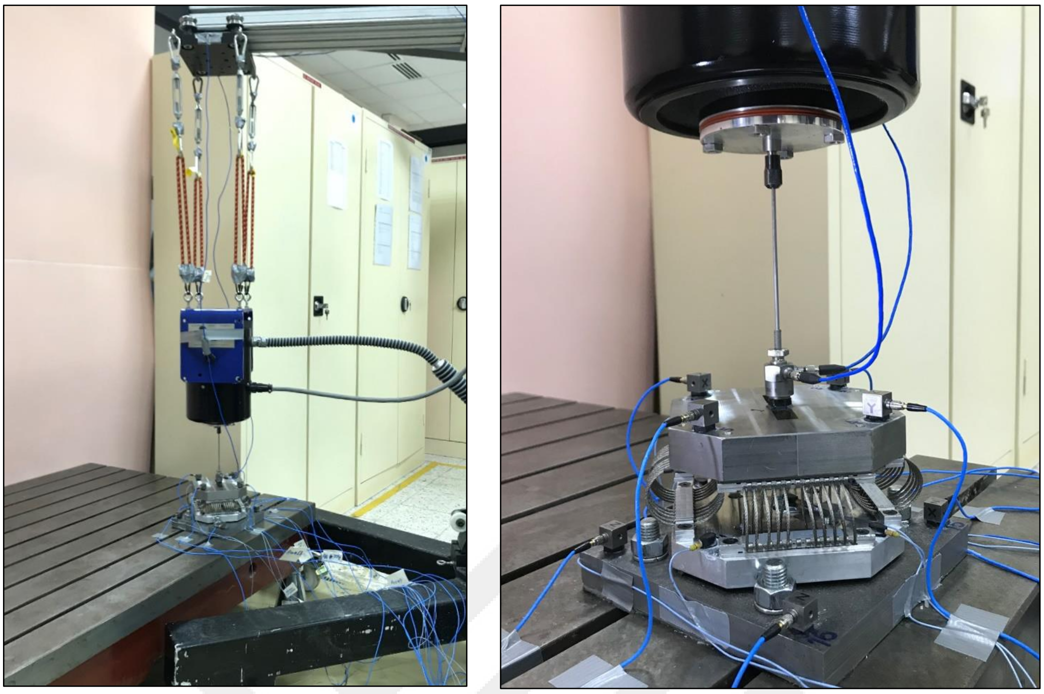

Figure 6.7: Modal testing with the modal shaker (MS/2110E) attached to the WRI system.

Levelling of the shakers and alignment of the stingers is provided with the adjustment of turnbuckles. Thus any mass loading effect (due to the mass of the suspended shaker body) can be introduced to the WRI system through the stinger attachment is tried to be minimised.

The modal test results obtained using the shaker are given in Figure 6.9 and Figure 6.10 in terms of driving point FRF data. The corresponding figures show that the loading amplitude is represented in units of “N-rms” since the nature of the excitation signal is random. At this point, modal tests are performed such that the loading amplitude in units of N-rms is swept from low-level to high-level. To this end, while the gain setting of the shaker amplifier is kept constant, the amplitude of the excitation signal is adjusted by altering the “voltage level” parameter within the software interface [57].

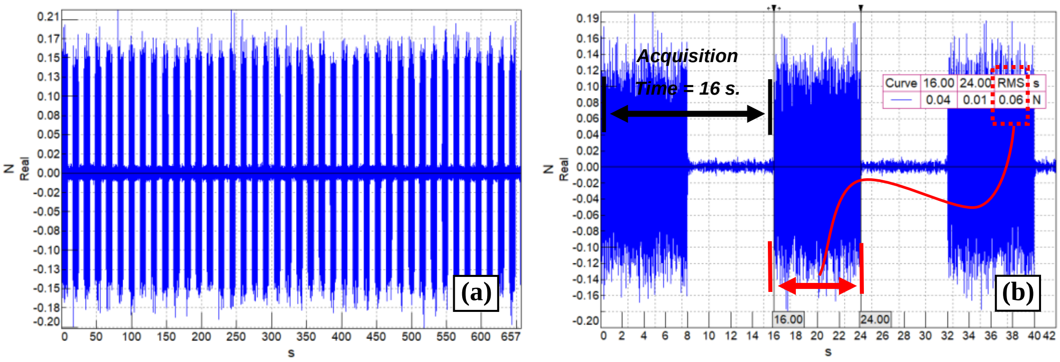

Figure 6.8: Burst random excitation signal (a) and specification of its rms value (= 0.06N-rms) (b).

An example of the burst random signal used to drive the WRI system via the shaker is shown in Figure 6.8. Here, it is also shown in Figure 6.8-(b) how the loading amplitude of 0.06N-rms is determined using which portion of the burst random excitation signal. And if the WRI system is excited by the burst random signal in Figure 6.8, then the specified driving point FRF data with the title *"Run_01__0.01V__0.06N-rms__40avg"* in Figure 6.9 is obtained.

The driving point FRF data of the WRI system, which was exposed to varying loading amplitudes in the range of 0.03N-rms to 22.7N-rms using the mini shaker, is given in Figure 6.9. Unfortunately, excitation forces higher than 22.7N-rms could not be applied since the maximum rms excitation force specified as 22N-rms in the performance limits of the mini-shaker was reached. Analogous to impact hammer testing, It can also be seen that the FRF data given in Figure 6.9 vary depending on the loading amplitude, which states that the WRI system exhibits an amplitude-dependent non-linear behaviour. Nevertheless, for relatively higher loading amplitudes, using a shaker for modal testing generates more error-free FRF data, contrary to the modal testing implemented by an impact hammer. This outcome can easily be observed by comparing the driving point FRF data found in Figure 6.5 and Figure 6.9, although their units of loading amplitudes are not consistent with each other.

To get the WRI system to be tested with higher loading amplitudes than with the mini shaker (22N-rms), it was preferred to use a high-capacity shaker (200N-rms). In this regard, the utilisation of the high-capacity shaker allowed us to excite the WRI system with varying loading amplitudes in the range of 0.13N-rms to 164N-rms, as shown in Figure 6.10. Although the shaker's capacity is 200N-rms, it was impossible to excite the WRI system above the 164N-rms level. Besides, similar to impact hammer and mini shaker testing, It can also be seen that the FRF data given in Figure 6.10 alter depending on the loading amplitude so that the WRI system exhibits an amplitude-dependent non-linear behaviour. However, this time unlike impact hammer and mini shaker testing, another interesting fact, revealing a complete picture of the amplitude-dependent non-linear dynamic behaviour of the WRI system, is detected. As shown in Figure 6.10, when the loading amplitude is swept upwards with sequential tests starting from a minimum level, what happens next can be described in three phases.

- Firstly, when the loading amplitude is very small, the WRI system's resonance frequency and dynamic stiffness are at their maximum value; contrary to this, damping (loss factor) is negligible.
- Secondly, as the loading amplitude reaches relatively moderate levels, the WRI system's damping passes through its maximum value during resonance frequency and dynamic stiffness decrease.
- Finally, as the loading amplitude gets larger, the WRI system's resonance frequency starts converging to a minimum value while damping continues to decrease towards a negligible value.

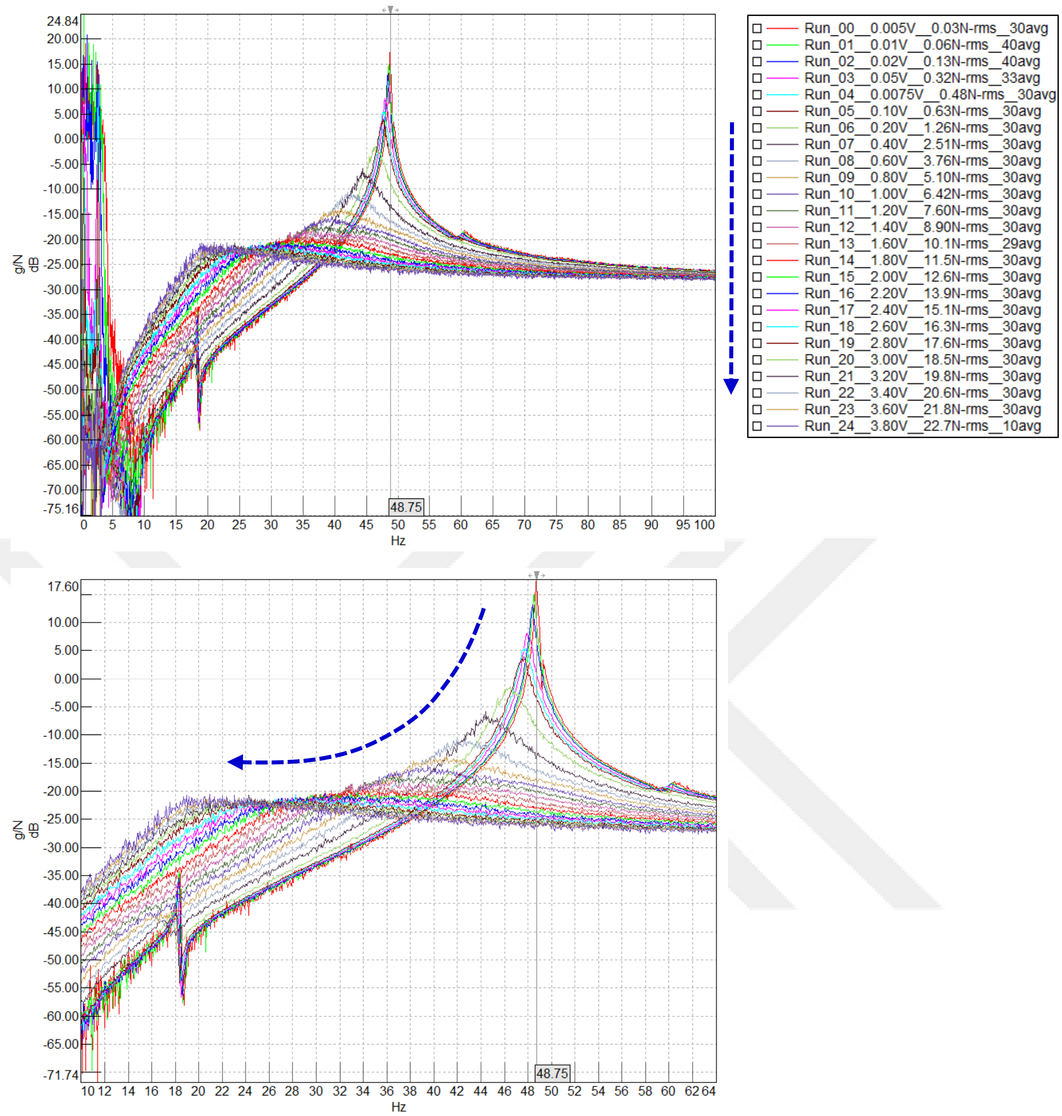

Figure 6.9: Driving point FRFs corresponding to varied loading levels applied with the mini modal shaker.

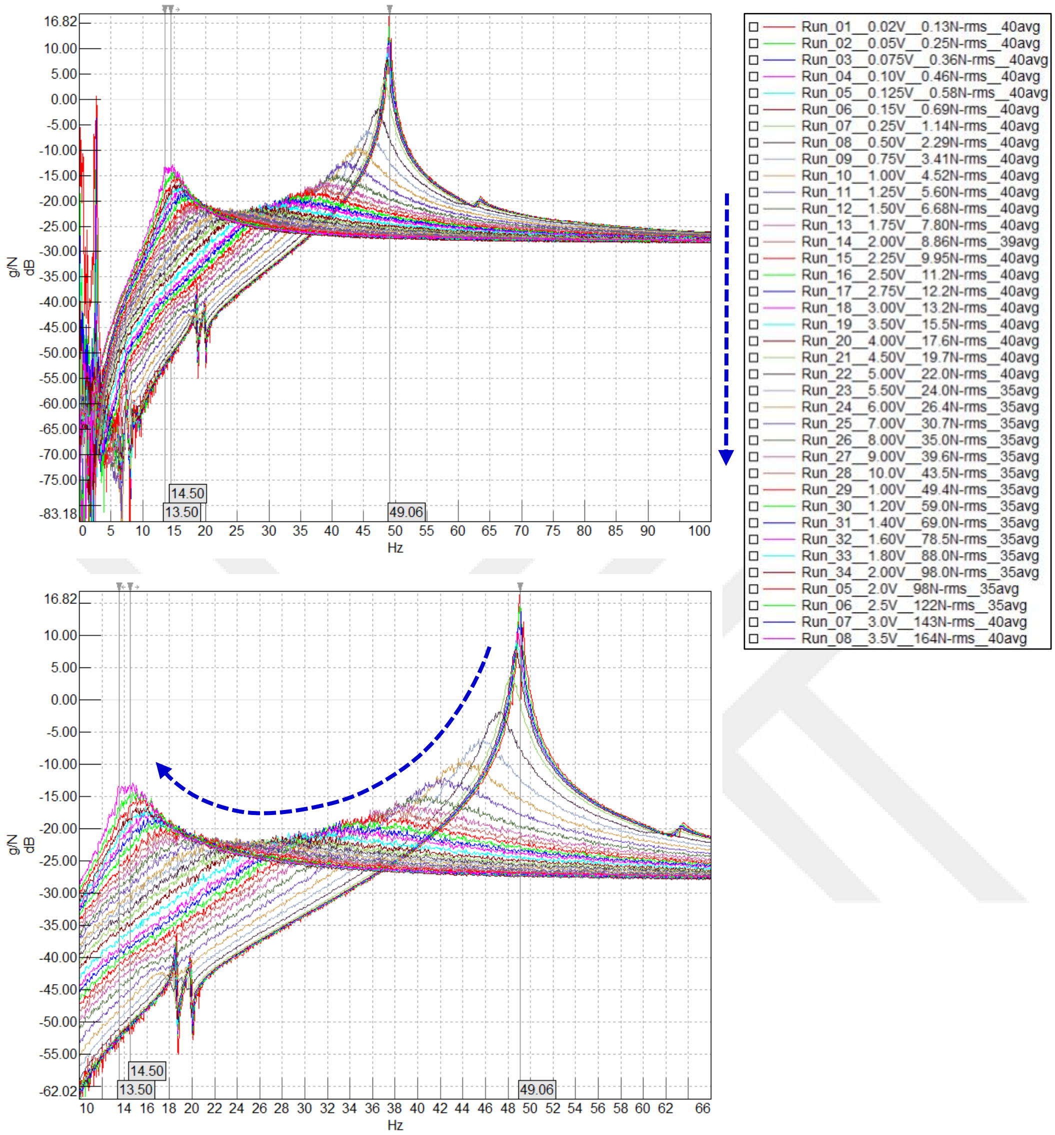

Figure 6.10: Driving point FRFs corresponding to varied loading levels applied with the modal shaker.

6.2.6 Discussion of the Modal Test Results

The results of modal tests of the WRI system, including both WRI type-A and type-B, are given in Table 6.1 and Table 6.2, respectively. The resonance frequency results shown in the tables are only provided for the smallest loading amplitudes as possible applied to the WRI system. That is to say, the resonance frequencies given in Table 6.1 and Table 6.2 represent the linear response of the WRI system since the loading amplitude is small.

The fact that the resonance frequencies are very close in the modal tests performed with the mini shaker and the mini impact hammer shows that the attachment of the mini shaker to the WRI system was made correctly. However, the WRI system's stiffness and mass properties can be modified due to the stinger connection of the shaker to the WRI system. Namely, stinger attachment might result in a structural coupling [59] between the shaker and the WRI system. When the loading is provided with an impact hammer, this coupling issue does not occur. Therefore, modal shaker testing can be calibrated with impact hammer testing only for small loading amplitudes. In this way, the reliability of the modal shaker test results can also be increased. Moreover, resonance frequency results state that the mini shaker is not coupled with the WRI system, as much as the high-capacity shaker is coupled.

Table 6.1 Modal test results of the WRI system with WRI type-A.

Excitation Method	***Resonance Freq. (Hz)***	***Δf (Hz)***	***Excitation Signal***	***Loading Amplitude***
Impact Hammer Mini. (PCB/086E80)	97.38	0.125	Impulse	2.5 N
Impact Hammer (PCB/086D05)	96.63	0.125	Impulse	5.0 N
Shaker Mini. (MS/K2007E01)	97.81	0.0625	Burst Random	0.06 N-rms

Table 6.2 Modal test results of the WRI system with WRI type-B.

Excitation Method	***Resonance Freq. (Hz)***	***Δf (Hz)***	***Excitation Signal***	***Loading Amplitude***
Impact Hammer Mini. (PCB/086E80)	48.38	0.125	Impulse	1.0 N
Shaker Mini. (MS/K2007E01)	48.75	0.0625	Burst Random	0.03 N-rms
Shaker Mini. (MS/K2007E01)	48.38	0.0625	Burst Random	0.13 N-rms
Shaker (MS/2110E)	49.06	0.0625	Burst Random	0.13 N-rms

It must be emphasised that when using the high-capacity shaker, as the loading amplitude increases (e.g., 122N-rms and above), the excitation of the other modes of the WRI system (i.e., lateral and torsional ones) becomes more pronounced, although not as much as the main vertical mode. The reason for this is considered to be the structural coupling effect.

If modal testing of a vibration/shock isolation system containing WRIs is intended to be performed by impact hammer, care should be taken in selecting the applied impact force amplitude. In other words, considering the system's mass and the stiffness of the WRIs, it should be preferred to perform modal tests by increasing the amplitude of the impact force to be applied, starting from a minimum value. As a result, modal testing of a WRI system using an impact hammer can only be implemented to determine the small amplitude dynamic behaviour. Nevertheless, using a modal shaker, modal tests could be performed to determine the relatively small and high amplitude dynamic behaviour of a WRI system.

In conclusion, the amplitude-dependent behaviour of a WRI system can be obtained using modal testing methods.

6.3 Dynamic Characterisation Testing of the WRI

WRI sample level characterisation tests are implemented using the dynamic (fatigue) test instrument shown in Figure 6.11-(a). The test instrument can perform dynamic tests via controlling the excitation frequency, dynamic loading amplitude, and static loading amplitude; besides, both static and dynamic loading amplitude can be defined in units of displacement or force. A specialized fixture shown in Figure 6.11-(b) was designed and manufactured to secure the WRI samples to the dynamic test instrument. The developed fixture ensures proper alignment of the WRI ends, enabling WRI sample tests to be performed in the tension-compression direction.

Before starting the characterisation test, suitable precycling is applied to the WRI samples at a small amplitude and low frequency. A static constant compression preload is then applied. The value of applied preload was selected to be equivalent to the static compressive preload per WRI sample in the WRI system in which modal tests were performed. Subsequently, dynamic testing was performed by step-by-step application of discrete sinusoidal displacement amplitudes u_0 $(u = u_0 \sin \omega t)$ superimposed on the preload with a constant excitation frequency of 1.0Hz.

When WRI samples are cycled with a constant displacement amplitude, they exhibit cyclic hardening behaviour [61]. Thus it is essential to get the stabilised hysteresis cycle by performing the necessary number of repetitions for a given excitation amplitude before stepping into the calculation phase of the hysteresis cycle metrics.

Dynamic characterisation test results of the WRI type-B sample are given in Figure 6.12 in terms of dynamic stiffness (a) and loss factor (b), which are clearly amplitude-dependent.

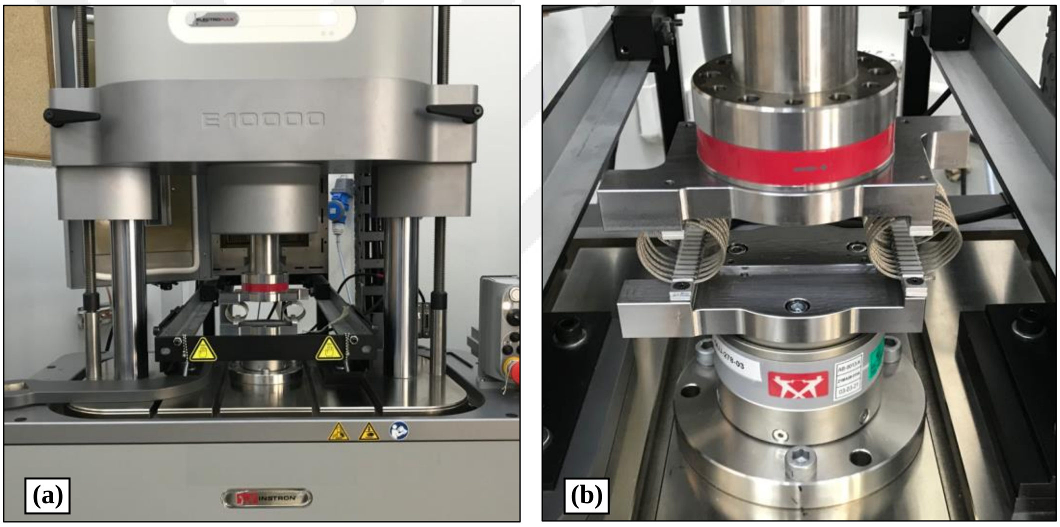

Figure 6.11 Instron ElectroPuls E10000 dynamic test instrument (a) and the specialized fixture for fastening WRI samples to the test instrument (b).

What has been observed in Figure 6.12 is that: (*i*) when the vibration amplitude is very small, the dynamic stiffness approaches a high-level asymptote while the loss factor is almost zero; (*ii*) as vibration amplitude gets increased, the stiffness keeps decreasing, and the loss factor passes through a maximum; and (*iii*) when the vibration amplitude is very large, then the dynamic stiffness approaches to a low-level asymptote while loss factor gets keeps decreasing. As a result, WRI exhibits the Payne effect or Fletcher-Gent effect, which is represented by the dependence of the dynamic stiffness and loss factor on the vibration amplitude.

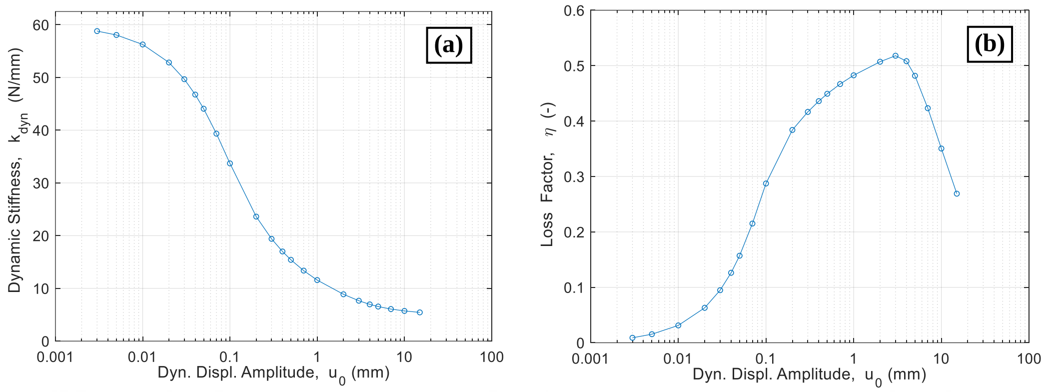

Figure 6.12 Amplitude-dependent dynamic stiffness (a) and loss factor (b) of the WRI type-B.

It must be emphasised that the term "dynamic" remarked in this section is used to refer to the type of loading that is oscillatory (sinusoidal), not to represent any inertial effects (i.e., $\omega^2 m$) or the resonance. Besides, the test instrument has an "inertia compensation" capability providing the inertial effects caused by the mass of the moving elements (fixtures, actuator, etc.) to be removed from the measurement data.

6.4 Theoretical Modelling of the WRI System

When searching for a theoretical model to represent the dynamic behaviour of the WRIs, it is reasonable to consider using theoretical models based on the dry friction mechanism. It is because the damping mechanism of a particular WRI system stems from the dry friction caused by relative motion between the individual wires and strands in the wire rope's cross-section [49], [50].

The simplest theoretical model to represent the steady-state dynamic behaviour of a dry friction-based unidirectional vibration isolation system is the *elastically coupled (or connected) Coulomb damper model* [62] shown in Figure 6.13-(a). Besides, the *bilinear hysteretic model* [63] is the most known of the many names attributed to this model in the literature. The elastically coupled Coulomb damper model consists of two branches connected in parallel. The first branch contains a linear spring, while the second includes a Coulomb damper and a linear spring connected in series, also named the elastoplastic [63], Jenkin [51] or Prandtl [54] element.

The claim that the *elastically coupled Coulomb damper model* is the simplest theoretical model to represent the dynamic behaviour of a vibration isolation system based on dry friction is supported by the following experimental facts: (a) As the loading amplitude gets increased from a minimum to a maximum value, the system's resonance frequency decreases (softening effect), as seen in Figure 6.10. (b) The amplitude of resonance frequency can increase or decrease by passing through a minimum value depending on loading amplitude, thereby indicating that for an optimum value of loading amplitude, the resonance frequency's amplitude can be found at a minimum, also shown in Figure 6.10.

The working principle of the *elastically coupled Coulomb damper model* can be described as follows [62]: (a) With the application of the load to the system, the isolator begins to deform. Since the value of the applied load is below the yield force of the Coulomb damper Y_1, the damper does not slip, and the system resists the applied load with the stiffness of $k_\infty + k_1$. (b) However, as soon as the load continues to increase and the damper reaches the yielding force, the damper starts to slide, and the stiffness of the k_1 spring is disabled. Thus, the stiffness of the isolator decreases to k_∞. (c) Subsequently, the applied load reaches its maximum value and then starts to decrease; since the load on the Coulomb damper will fall below Y_1, the slip on the damper stops and the stiffness of the k_1 spring is reactivated, and the stiffness of the isolator again becomes $k_\infty + k_1$. The same process mentioned above repeats as the direction of the applied load changes and eventually leads to a parallelogram-shaped (bilinear) hysteresis loop.

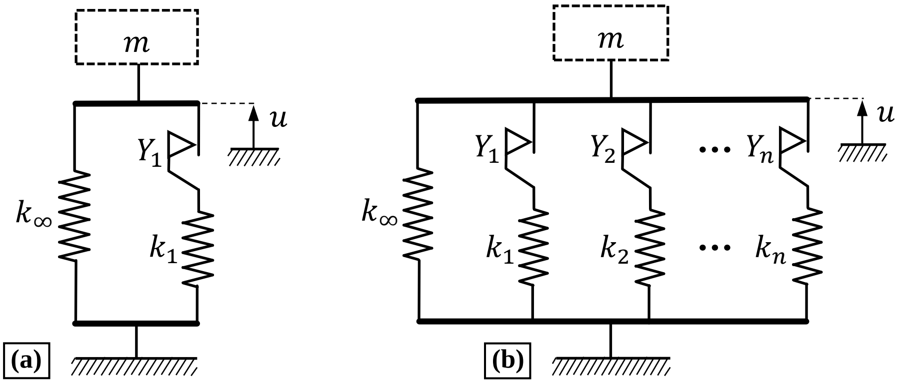

Figure 6.13 Elastically coupled Coulomb damper model (a) and Masing model (b).

However, as stated by Iwan [63], most real structures do not exhibit the bilinear type of hysteresis loop; hence, trying to fit this parallelogram-shaped (bilinear) hysteresis loop into real structures does not seem to be a rational approach. Therefore, to overcome this difficulty, more elaborate theoretical models are developed by Masing [58] and Iwan [63], [64] such that they can capture the curvilinear edges of the hysteresis loop.

For modelling the steady-state dynamic behaviour of the WRI, the Masing model, depicted in Figure 6.13-(b), looks promising considering the elastically coupled Coulomb damper model. The Masing model relies on the idea that a general hysteretic system may be represented by many ideal elastoplastic elements, each having different stiffness and yield force level [63]. The working principle of the Masing model resembles those of the elastically coupled Coulomb damper model, such that restoring force is distributed between many branches regarding their stiffness and yield force levels. The Masing model gives a sufficient phenomenological description of the Payne effect without considering any details of the processes that may occur due to the frictional contact effects between the tiny wires in the WRI's cross-section at the micron or sub-micron level. The term "phenomenological" is referred to the frictional contact model is based on experimental observations and describes the global relation between the tangential force and the relative displacement in the frictional interfaces [65] of the WRI.

When the loading amplitude applied to the Masing model is small, all dampers remain still since the yield force required for the dampers to slide cannot be reached, and the restoring force is only due to the deformation of the springs. Hence, the upper asymptote of the dynamic stiffness resulting from the Masing model can be given as:

$$k_{stick} = k_\infty + \sum_{i=1}^{n} k_i \tag{6.1}$$

In Equation (6.1), k_{stick} refers to the *sticking limit stiffness* of the model, describing an asymptote for small amplitude loading, depicted in Figure 6.14. On the other hand, when the loading amplitude applied to the Masing model is large, the yield force that will cause all dampers to slip is exceeded, and thus all springs are disabled except for the k_∞ spring. So, the lower asymptote of the dynamic stiffness resulting from the Masing model can be given as:

$$k_{slip} = k_\infty \tag{6.2}$$

In Equation (6.2), k_{slip} refers to the *slipping limit stiffness* of the model, defining an asymptote for large amplitude loading, shown in Figure 6.14. The sticking and slipping limit stiffness values are essential in calibrating the Masing model parameters.

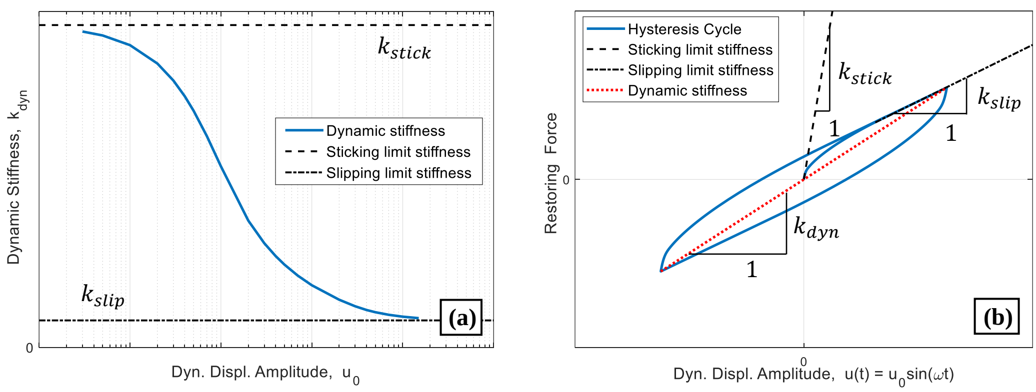

Figure 6.14 Asymptotes of the dynamic stiffness: sticking and slipping limit stiffnesses of a WRI.

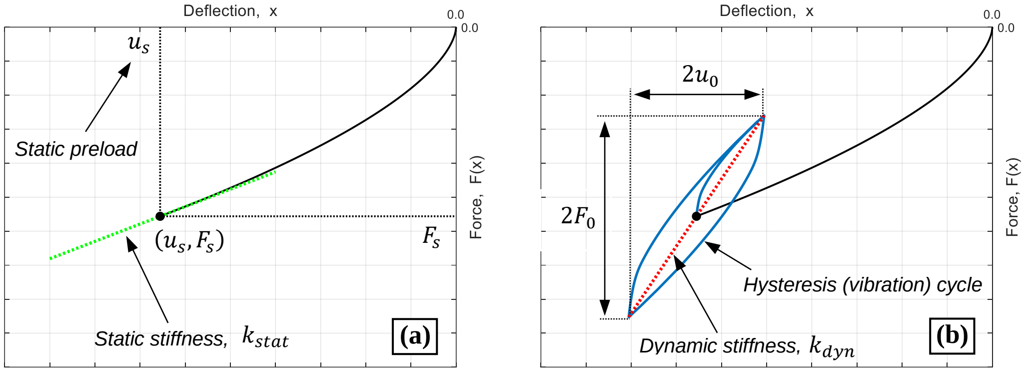

Figure 6.15 Representation of the static stiffness (a) and the dynamic stiffness (b) of a WRI.

As mentioned before, here again, it must be underlined that the term "dynamic" stated in this section refers to the type of loading which is oscillatory, and it has nothing to do with the inertial effects or the inverse FRF. In theoretical modelling, attention should be paid to the distinction between static and dynamic stiffness. In this context, the definition of these parameters is visualised in Figure 6.15. When a preload is applied to a WRI, it follows a monotonic loading curve, as it is shown in Figure 6.15-(a). Here a compression type of preload is applied (assumed to be slowly) to a WRI, causing the WRI to deflect to the operating point of (u_s, F_s), is illustrated. And the slope of that point defines the static stiffness of the WRI, as given in Equation (6.3).

$$k_{stat} = \left.\frac{dF(x)}{dx}\right|_{x=u_s} \tag{6.3}$$

Following the preloading step, the sinusoidal displacement loading $(u = u_0 \sin \omega t)$ is applied, as depicted in Figure 6.15-(b). When subjected to oscillatory loading, WRIs exhibit hysteresis loops with pointed ends rather than elliptical hysteresis loops; still, some definitions developed for the linear viscoelastic behaviour can be utilised. To this end, the dynamic stiffness or, more accurately, the storage stiffness can be given as:

$$k_{dyn}(u_0, F_0) = \frac{2F_0}{2u_0} \tag{6.4}$$

Storage stiffness is defined as the slope of the line aligned from the origin to the point of maximum displacement amplitude [66], which is depicted with a dashed red line in Figure 6.15-(b). It must also be noted that the hysteresis loop, shown in Figure 6.14-(b), is assumed to be symmetric about the origin.

6.5 Validation of the Theoretical Modelling

In this section, validation of the Masing model with the experimental results (both sample-level and system-level) is only given in terms of resonance frequency results. Previously, the dynamic stiffness data of the WRI type-B sample, obtained by dynamic characterisation testing, had been shown in Figure 6.12-(a).

In this context, to make a more appealing comparison between the modal test data (Figure 6.10) and the characterisation test data (Figure 6.12-(a)); the dynamic stiffness k_{dyn} of WRI type-B has been converted to frequency f_{res} data by using Equation (6.5):

$$f_{res} = \frac{1}{2\pi}\sqrt{\frac{N\,k_{dyn}}{m}} \tag{6.5}$$

Where N=4, is the number of WRIs found in the WRI system. Also, by switching the x- and y-axes of Figure 6.12-(a), the resulting data is presented in Figure 6.16-(b).

The sticking and slipping limit stiffness parameters of the Masing model were obtained from the dynamic characterisation test data given in Figure 6.12-(a), and the parameters of $k_{stick} \approx 60$ (N/mm) and $k_{slip} \approx 5$ (N/mm) were determined. By substituting these two parameters into the following Equation (6.6), the ratio between limiting resonance frequencies, which is shown in Figure 6.16-(a) and -(b), can be found as:

$$\frac{f_{stick}}{f_{slip}} = \sqrt{\frac{k_{stick}}{k_{slip}}} = \sqrt{\frac{k_\infty + \sum_{i=1}^{n} k_i}{k_\infty}} \approx \sqrt{\frac{60}{5}} \approx 3.5 \tag{6.6}$$

As seen in Figure 6.16, the results of the two different tests confirm each other in terms of resonance frequencies. All in all, limit stiffness values obtained from a system-level modal test or a sample-level characterisation test can be used to identify the limiting parameters of the Masing model. Besides, by correlating the outcomes of both the modal testing and characterisation testing, the confidence level in the test results can be increased, as was done here.

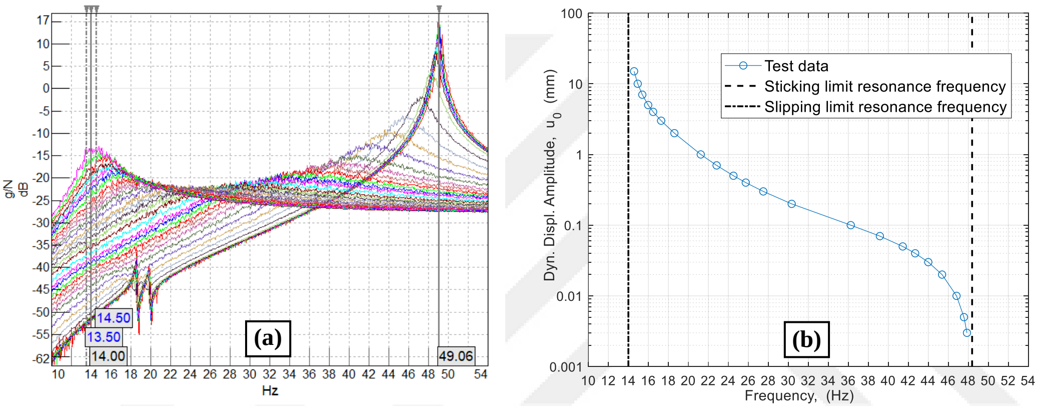

Figure 6.16 The resonance frequencies obtained from system-level modal testing (a) and sample-level dynamic characterisation testing (b).

6.6 Summary

This study has shown that the amplitude-dependent behaviour of a WRI system can be observed using modal testing methods such as an impact hammer or a modal shaker. Besides, amplitude-dependent behaviour, also known as the Payne effect, has also been observed through the WRI sample characterisation testing.

For modelling the steady-state dynamic behaviour of a WRI system, a phenomenological model known as the Masing model has been proposed that is used in various engineering fields to model hysteresis effects.

The two limit stiffness values, named sticking and slipping limit stiffness, needed to identify upper and lower asymptotes of the Masing model can be derived from both modal testing and characterisation testing results. However, choosing the characterisation test results for this purpose is wiser if available. Also, it must be noted that trying to implement characterisation testing could be a more expensive solution due to the need to prepare test fixtures and provide a suitable dynamic test instrument.

It is also observed that the type of non-linearity involved in the FRF data does not exhibit unstable jump phenomena [67]. This finding can also be confirmed by referring to the corresponding literature [68], which involves examples of the frequency response functions of friction-based non-linear mechanical systems.

The approach typically practised in the past was to derive the stiffness value to be used in the modal analysis from the slope of the monotonic static loading curve of the WRI; that is, the resonance frequency was tried to be calculated by taking into account the static stiffness value. However, in this study, it has been experimentally proven which type of stiffness and value of stiffness of a WRI should be used when implementing the modal analysis of a WRI isolation system, which can be considered a novelty concerning the studies in the literature. As a result, the resonance frequency of a WRI isolation system can be calculated more realistically in a finite element analysis (FEA) model corresponding to the small loading amplitude.

CHAPTER 7

MODELLING OF MECHANICAL SHOCK RESPONSE OF A WIRE ROPE ISOLATOR SYSTEM USING FINITE ELEMENT ANALYSIS

In this part of the thesis, the shock response of a wire rope isolator system is modeled using ABAQUS FEA software and the modeling approach used is validated by extensive system-level test studies. The wire rope isolator system is basically a canister transportation system consisting of WRIs to isolate the canister from incoming mechanical shock (transient) loading during its transportation phase of its life-cycle. That is why the canister containing ammunition represents a payload to be protected from the environmental loadings acting on it. To validate the developed FEA modeling approach, two types of tests are performed, one being the modal testing and the other the mechanical shock testing. Although both tests are carried out at the METU-BILTIR Center skid test facility, the primary target is naturally to perform a mechanical shock test. In the end, testing results have shown that the FEA modelling approach generates reasonably good results. As it can be understood from the extensive literature research, there is no detailed modelling approach of modelling WRIs in the FE environment, as was done in this study.

7.1 Introduction

The canister transportation system, whose mechanical shock analysis will be carried out by means of FEA, is shown in Figure 7.1. The system mainly consists of two main components: the two canisters that contain the ammunitions that is a kind of payload, and the outer transportation frame that also ensures the positioning of the

WRIs around these canisters. The transportation frame is formed by combining steel profiles and plates using welded manufacturing techniques.

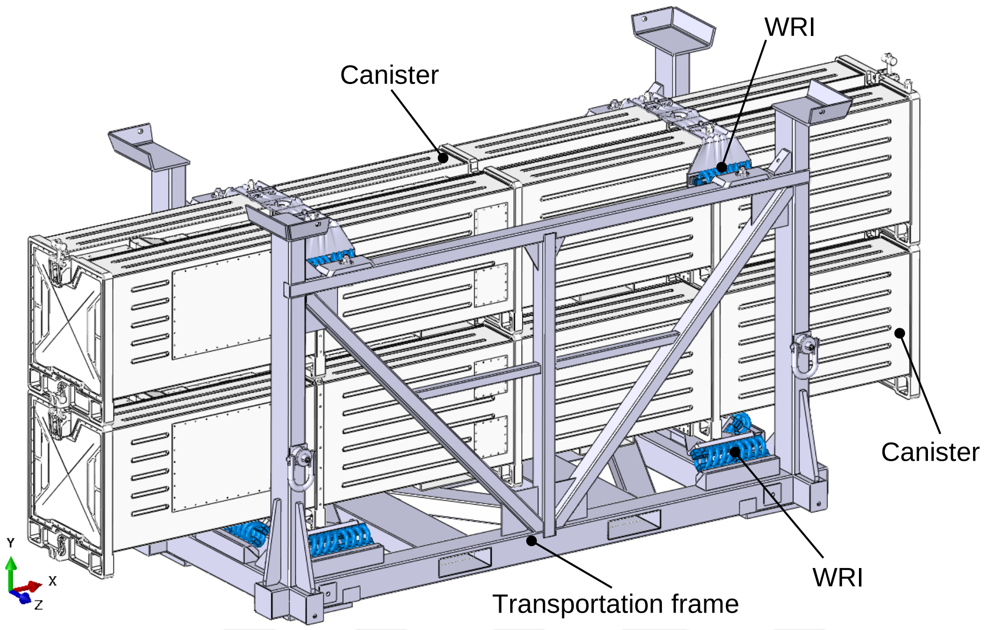

Figure 7.1: CAD model of a canister transportation system involving WRIs for the isolation of mechanical shock loading

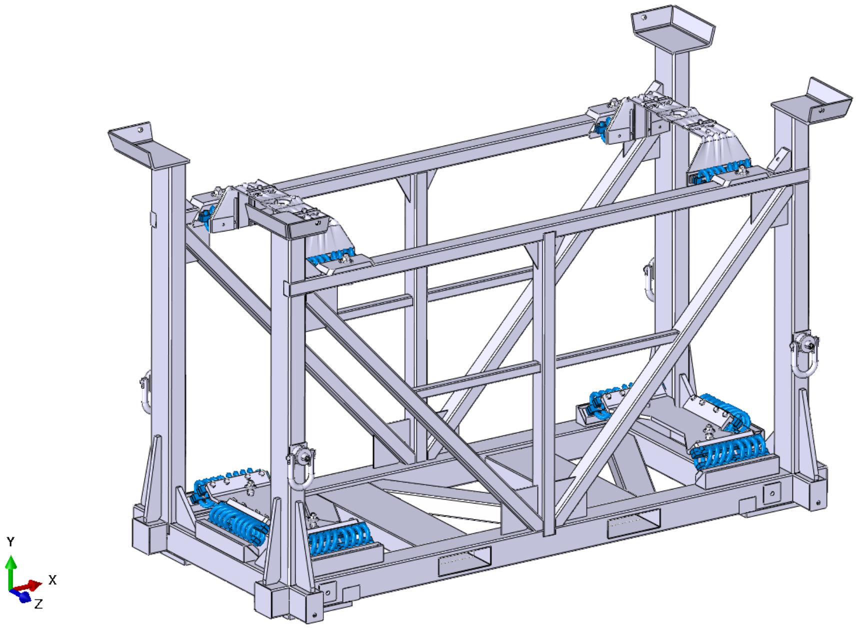

Figure 7.2: CAD model showing the placement and orientation of WRIs over the transportation system

Transportation of canisters by roadway, railway, airway and seaway can be provided by the base fixing interfaces of the transportation frame. It is possible for canisters to be exposed to mechanical shock loads during their transport with these various transport media throughout their life cycle. For this purpose, the canister transport system shown in Figure 7.1 and Figure 7.2 is designed in order to isolate the canisters and therefore the ammunition inside them from mechanical shock and vibration loads.

For confidentiality reasons, no images of the inside of the canisters are included in this study, and only the outer surfaces of the canisters are included in the relevant images.

The reason for choosing a WRI instead of a rubber-based isolator as an isolation member in the related canister transport system is that WRIs have some important features. These features are that WRIs have a very wide extreme operating temperature range and an almost infinite working life in environments with high corrosiveness, high solar radiation. Of course, the most important of these features is their superior shock isolation capability.

The canister transportation system shown in Figure 7.1 and Figure 7.2 contains a total of ten WRIs, six of which are located in the base area of the system and the other four are located in the ceiling area of the system. The tension-compression axes of the six WRIs in the base area are positioned inclined at an angle of 45° facing the center of mass of the double canister as much as possible. In addition, each WRI in the floor region has a volume of 300x100x120(mm^3) and a mass of 5(kg), while each WRI in the ceiling region has a volume of 260x90x100(mm^3) and a mass of 3(kg).

One of six WRIs positioned at an angle of 45° in the base region is given in Figure 7.3(b). In the remainder of this study, the details of the modeling of the WRI are explained through this WRI orientation and its local loading axis set, shown in Figure 7.4.

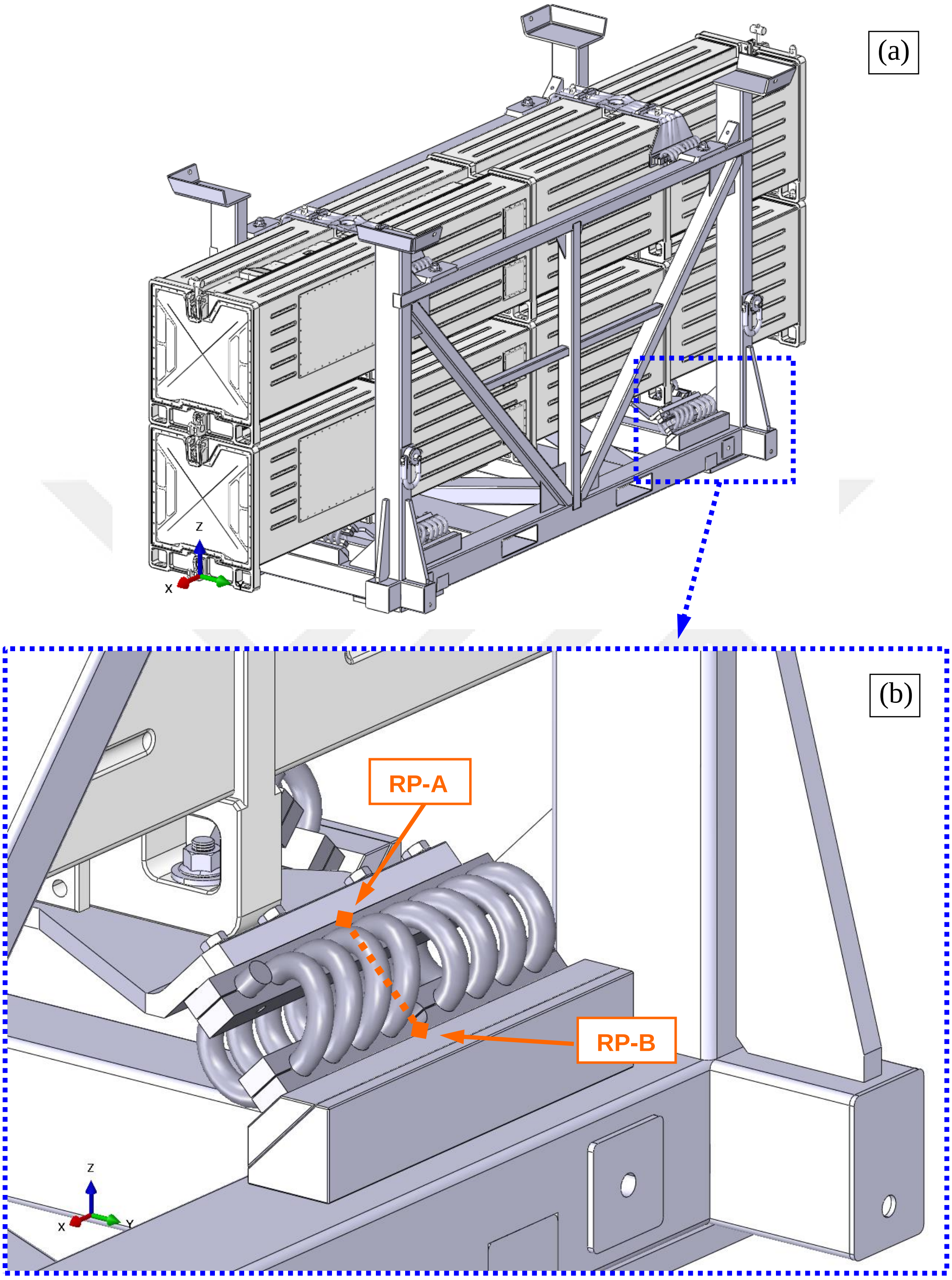

Figure 7.3: CAD model of a wire rope isolator system (a) and close view of a WRI with its connection end points (b)

The fictitious points A and B used to model the global mechanical behavior of the WRI is shown in Figure 7.3(b). These two points represent the end points on the upper and lower connection surface of the WRI, and it is assumed that there is a load transfer to the rest of the system through these two points in the three local loading axes direction. Essentially, in this study, it is aimed to model the restoring force-displacement relationship between these two points by means of Abaqus FE connector elements.

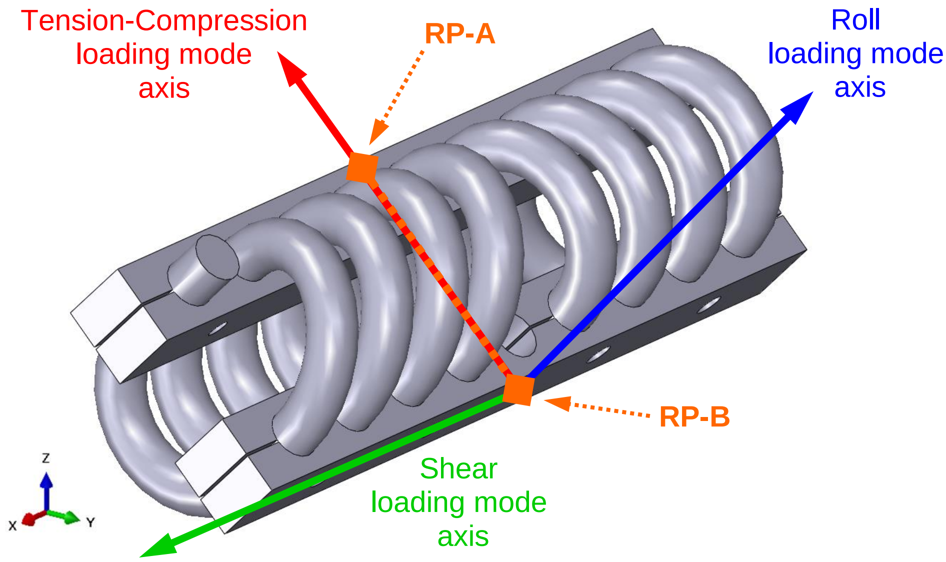

Figure 7.4: Connection end points and local loading axes of a WRI

Major companies producing WRIs can share the restoring force-displacement characteristics of the WRI with the users according to the local loading axis set shown in Figure 7.4, within the framework of certain assumptions. When a three-dimensional modeling is desired, the restoring force-displacement behavior of the WRI in each axis should be modelled simultaneously. However, in systems assumed to operate in one direction, modelling the restoring force-displacement behavior of the WRI in a single loading axis may also be sufficient.

In Figure 7.4, the end connection points of the WRI and the three local loading axes between these points are given as tension-compression, shear and roll axes, respectively.

7.2 Theoretical Modelling of Wire Rope Isolator

The Masing model shown in Figure 7.5 is formed by connecting one elastic linear element and N number of Jenkins elements in parallel, as stated in the previous sections.This model is suitable for representing relatively small amplitude loading cycles, and the symmetric hysteresis curves generated by this model are given in Figure 7.6 as an example.

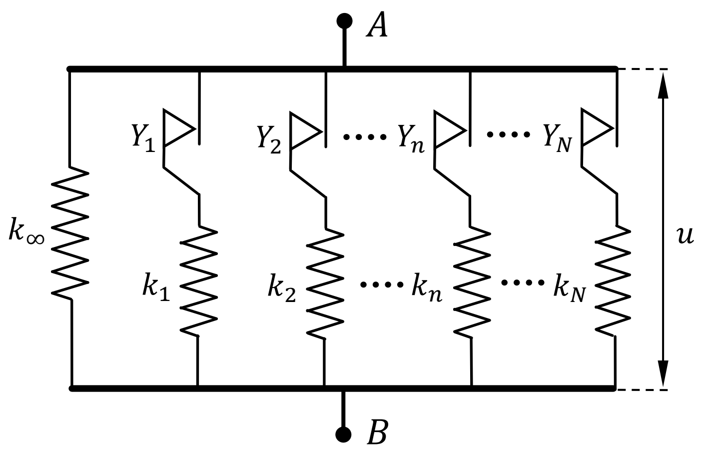

Figure 7.5: Masing's model

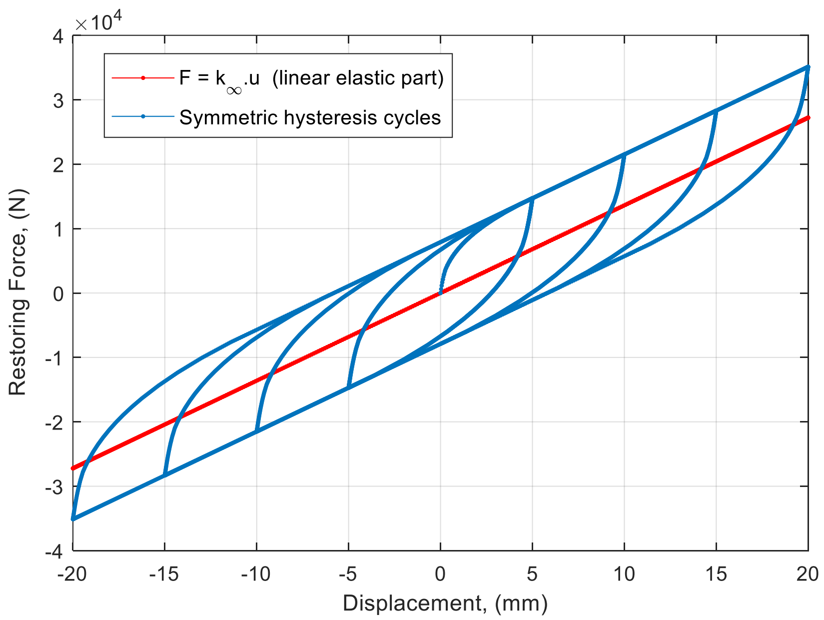

Figure 7.6: Symmetric hysteresis cycles generated by Masing's model

However, asymmetrical hysteresis curves occur due to excessive displacement of WRIs in mechanical shock loadings. As shown in Figure 7.7 as an example, the Masing model is insufficient in modeling the said asymmetric curves, and a modified Masing model should be used for this.

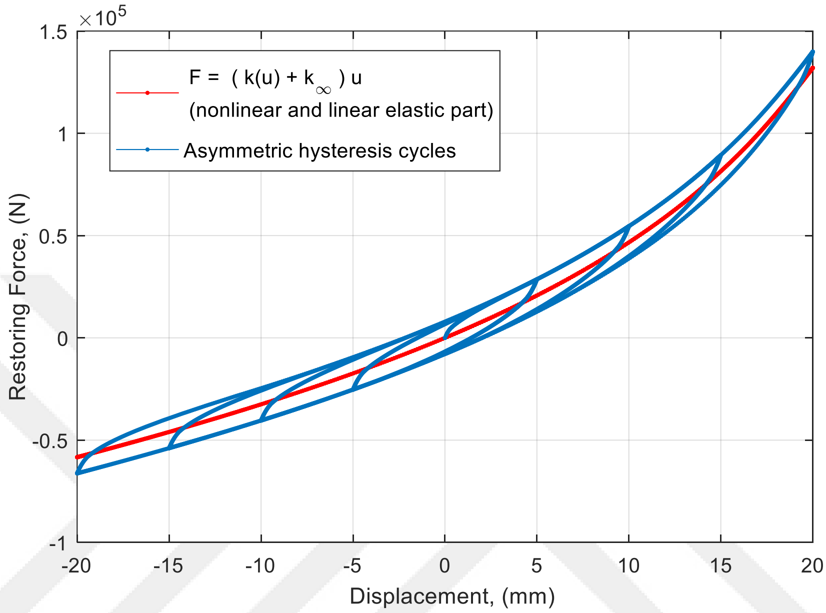

Figure 7.7: Asymmetric hysteresis cycles generated by modified Masing's model

The modified Masing's model shown in Figure 7.8 and Figure 7.9 is formed by connecting one linear elastic element, one nonlinear elastic element and N number of Jenkins elements in parallel, as stated in the previous sections. By means of the nonlinear elastic element $k(u)$, the asymmetric behavior required for the hysteresis cycle can be modeled.

In this study, the corresponding modified Masing model was used for each direction from the three local loading axes of the WRI. While the modified Masing model representation shown in Figure 7.8 is used for the loads in the tension-compression axis direction between the two end points of the WRI, the modified Masing model representation shown in Figure 7.9 is used for the loads in the shear and roll axes direction between the two end points of the WRI.

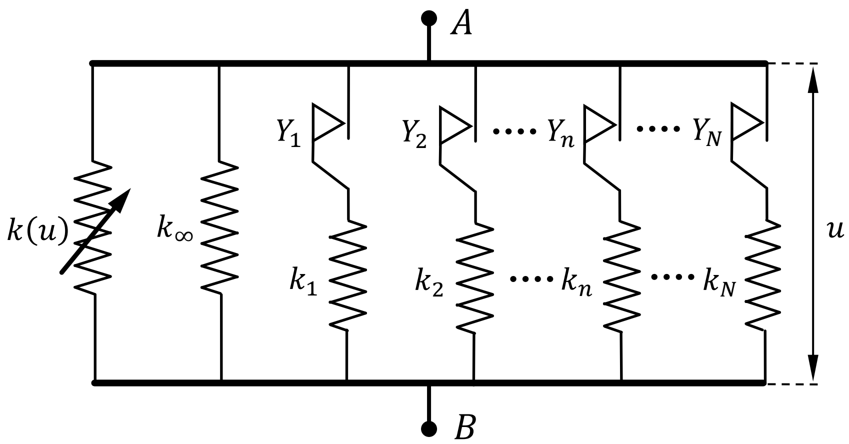

Figure 7.8: Modified Masing's model for Tension-Compression loading mode of a WRI

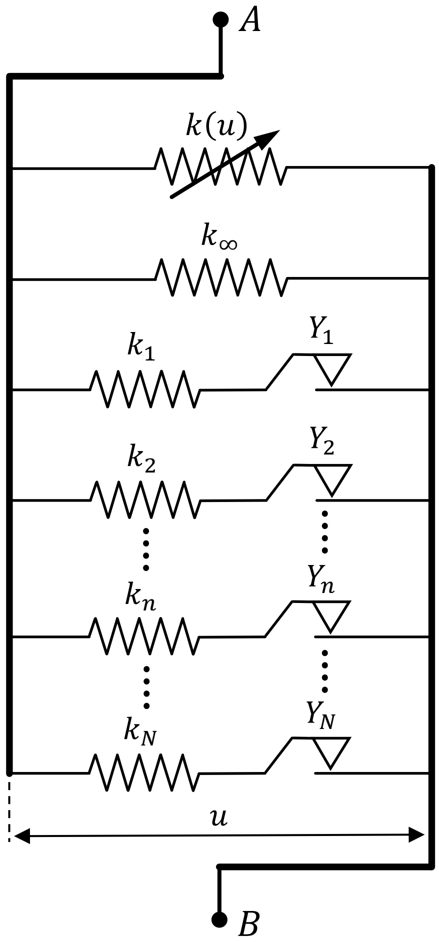

Figure 7.9: Modified Masing's model for Shear or Roll loading mode of a WRI

7.3 Identification of Theoretical Model

Two types of data representing the force-displacement characteristic of the WRI are shared by the WRI manufacturer. The first of these is the nonlinear elastic curve, which represents the large amplitude displacements of the WRI, and the corresponding data are shown in Figure 7.10, which corresponds to the tension-compression, shear and rolling axes of the WRI. The second is the dynamic stiffness curves representing the relatively small amplitude steady-state oscillations of the WRI given in Figure 7.11.

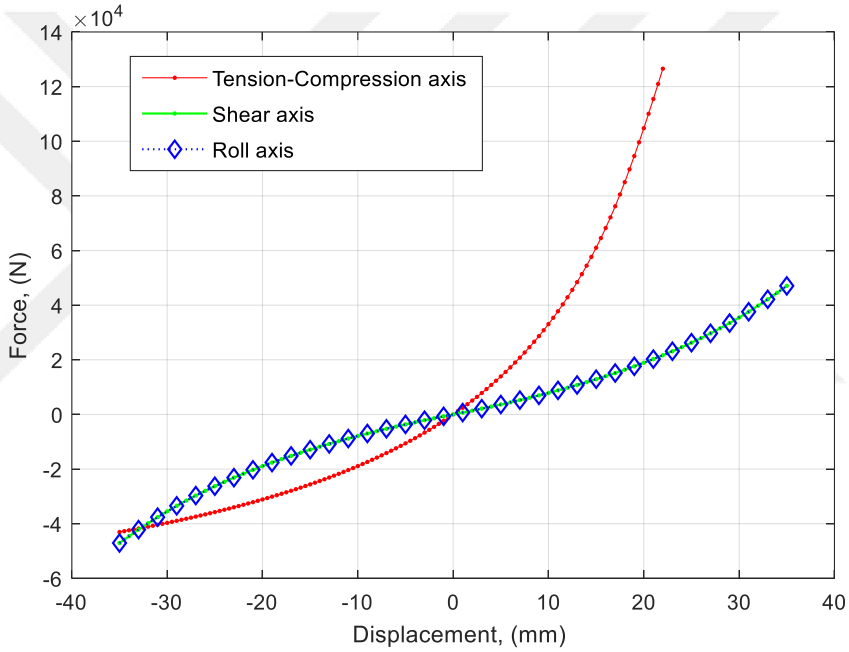

Figure 7.10: Dynamic load-displacement curves of WRI (data supplied by manufacturer)

Both Figure 7.10 and Figure 7.11 show that the shear and roll axis data overlap. The reason for this is that the WRI manufacturer accepts the two data as equal on the grounds that the data of the WRI in the shear and rolling axis directions are very close to each other.

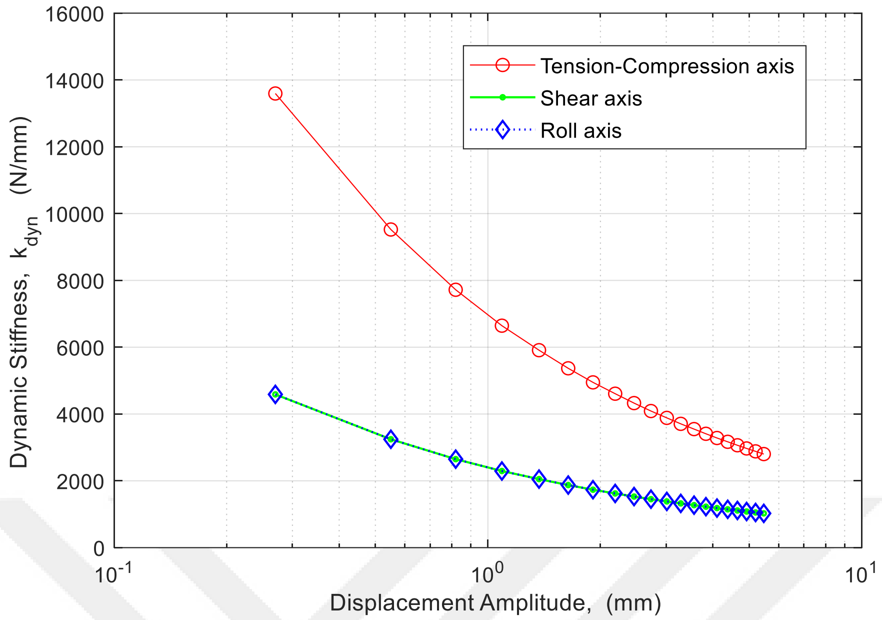

Figure 7.11: Dynamic stiffness curves of WRI as a fuction of its displacement amplitude (data supplied by manufacturer)

In order to obtain the Masing model parameters, in the first stage, the dynamic stiffness values provided by the manufacturer are converted into the dynamic force amplitude parameter by the relationship given below.

$$k_{dyn}^{i} = \frac{F_i}{u_i} \tag{7.1}$$

When the dynamic force amplitude (F_i) and dynamic displacement amplitude (u_i) data are plotted, a discrete curve called the initial loading curve is obtained and it is given in Figure 7.12. The u_i and F_i pairs that make up this curve are called breakpoints. In other words, it should be said that any point on the initial loading curve corresponds to the point where the displacement changes direction in the hysteresis loop (the sharp corner in the loop).

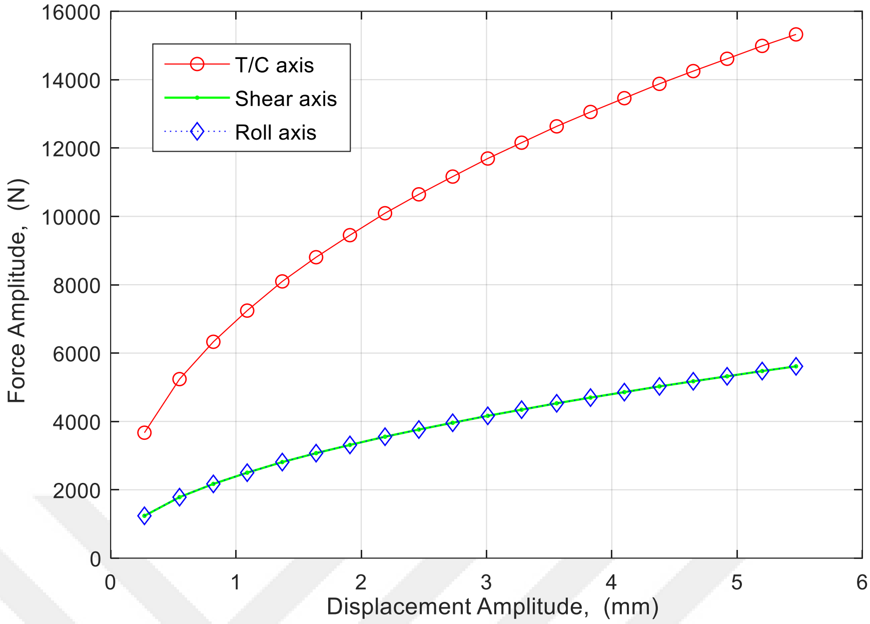

Figure 7.12: Initial loading curve (backbone or skeleton curve)

In the second stage, curve fitting is performed. For this, both curve fitting between breakpoints by interpolation method and also curve fitting between the first breakpoint and origin point by extrapolation method are performed.

In the trials done by using Matlab (R2018a) software, satisfactory results were obtained with $f(x) = ax^b + c$ function in curve fitting with interpolation, whereas good results were obtained with Matlab's PCHIP function in curve fitting with extrapolation as shown in Figure 7.13(a) and (b).

In the third stage, manual selection of breakpoints as shown in Figure 7.13, is performed over the initial loading curve reconstructed by curve fitting method. At this stage, the user should manually select breakpoints more densely when approaching to the origin point in order to be able to construct high quality and smooth hysteresis cycles in the end. After this manual selection process, the final breakpoints obtained is depicted in Figure 7.14

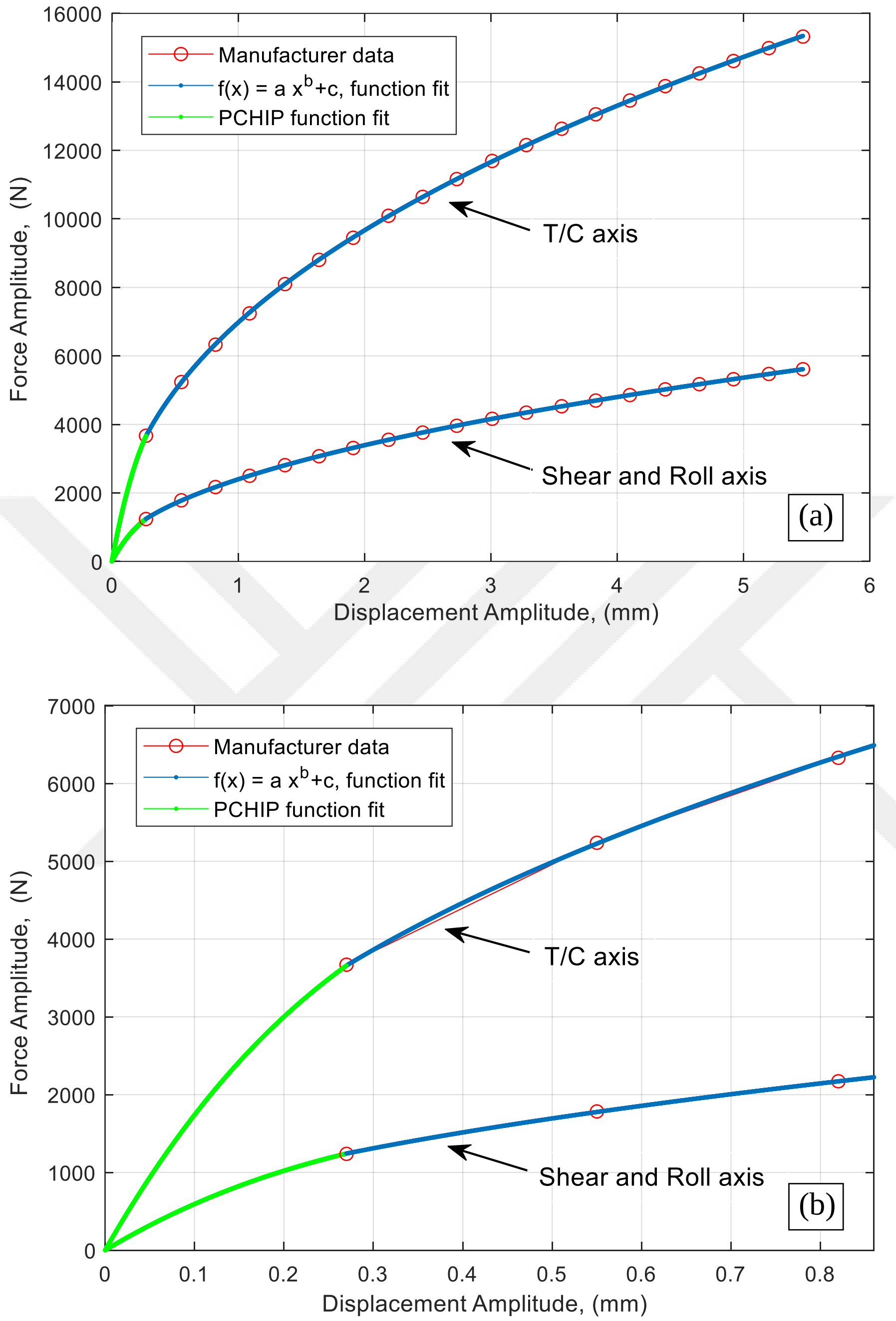

Figure 7.13: Initial loading curves revised after curve fitting stage (a) and a close view around the origin point (b)

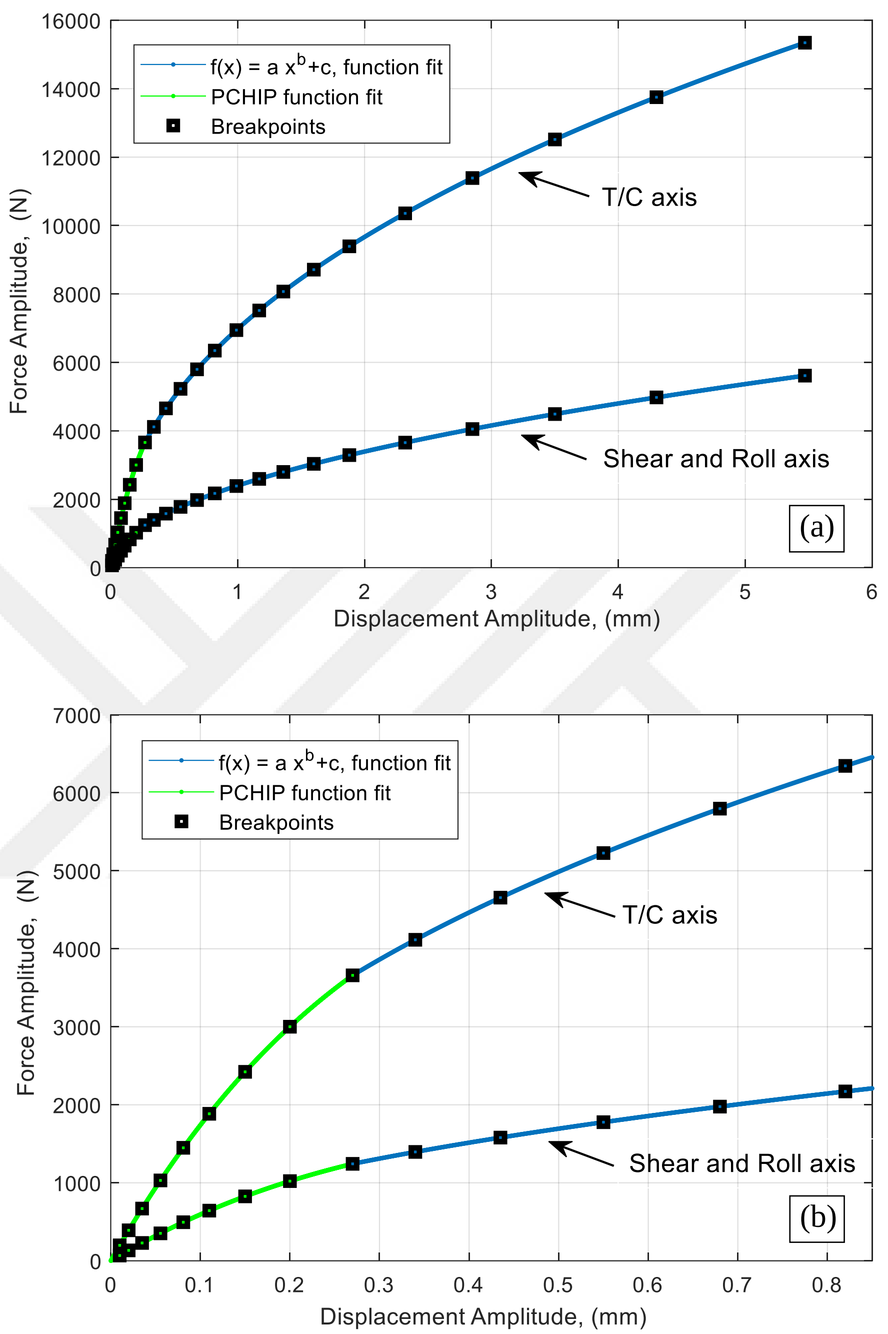

Figure 7.14: Final breakpoints created from the curve fitted initial loading curve (a), and a close view around orijin point (b)

In the end, Masing's model parameters k_∞, k_n, Y_n where $n = 1, 2, \ldots\ N$, depicted in Figure 7.8 and Figure 7.9 can be identified from utilizing those lastly created breakpoints as shown in Figure 7.14. To this end, using the following equations [11], one can identify the Masing's model parameters

$$k_n = \frac{F_n - F_{n-1}}{u_n - u_{n-1}} - \frac{F_{n+1} - F_n}{u_{n+1} - u_n} \qquad and \qquad Y_n = k_n u_n \tag{7.2}$$

where $n = 1, 2, \ldots, N$. It must be noted that number of total breakpoints which is N is equal to the total number of Jenkin's elements whose parameters to be identified.

Finally, using the identified Masing's model parameters, the dynamic stiffness and loss factor of the WRI can be calculated for a wide range of displacement amplitudes and compared with the dynamic stiffness data provided by the manufacturer, as shown in Figure 7.15. The calculated dynamic stiffness and loss factor curves given in Figure 7.15 and Figure 7.16, respectively, belong to the 23rd order (N=23) Masing model. As a result, there is a satisfactory agreement between the dynamic stiffness data provided by the manufacturer and the dynamic stiffness curve calculated over the identified Masing model.

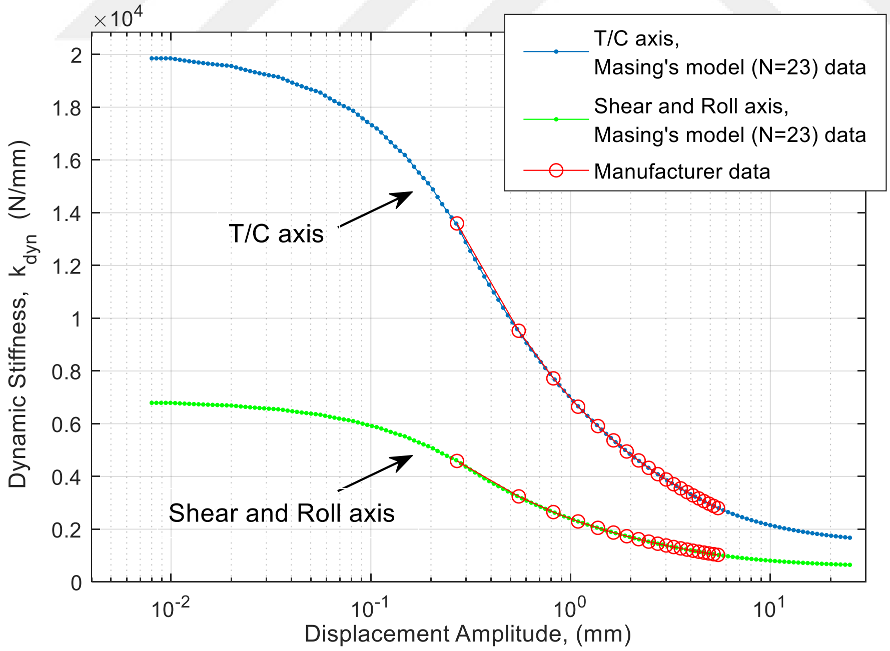

Figure 7.15: Dynamic stiffness curves calculated from the identified Masing's model

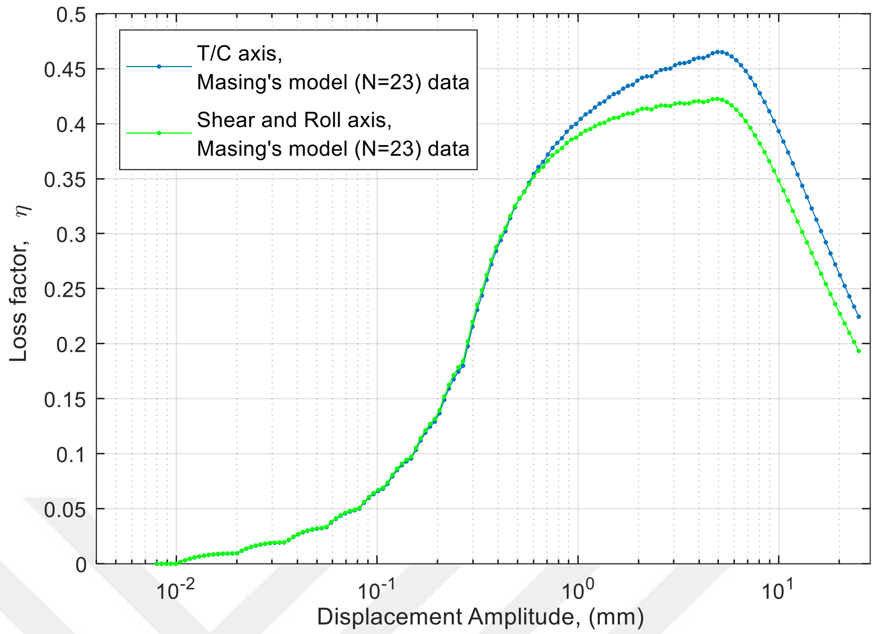

Figure 7.16: Loss factor curves calculated from the identified Masing's model

Dynamic stiffness curves shown in Figure 7.15 can be easily calculated from initial loading curve using the equation (7.1). On the other hand, loss factor is obtained by constructing hysteresis curves geometrically (via Matlab scripting) for each displacement amplitude value and calculating the enclosed dissipated energy in the hysteresis cycle.

7.4 FE Modelling of Wire Rope Isolators for Mechanical Shock Analysis

7.4.1 FE Modelling Approach

WRIs are normally three-dimensional solid bodies and are made of steel wire rope shaped in a helical form with a very complex geometry. If the Insulators are attempted to be modeled as 3D solids in the FE environment, it becomes impossible to solve the related problem in the FE environment, since they will require both very long solution times and high disk storage. Therefore, in this study it is aimed to model the global behaviour of WRIs in terms of its restoring force-displacement relationship between their connection end points. These two points represent the end points on the upper and lower connection surface of the WRI, and it is assumed that there is a load transfer to the rest of the system through these two points in the three local loading axes direction. Essentially, in this study, it is aimed to model the restoring force-displacement relationship between these two reference points (RP-A and RP-B shown in Figure 7.18(b)) in three local loading axes simultaneously by means of Abaqus FE connector elements.

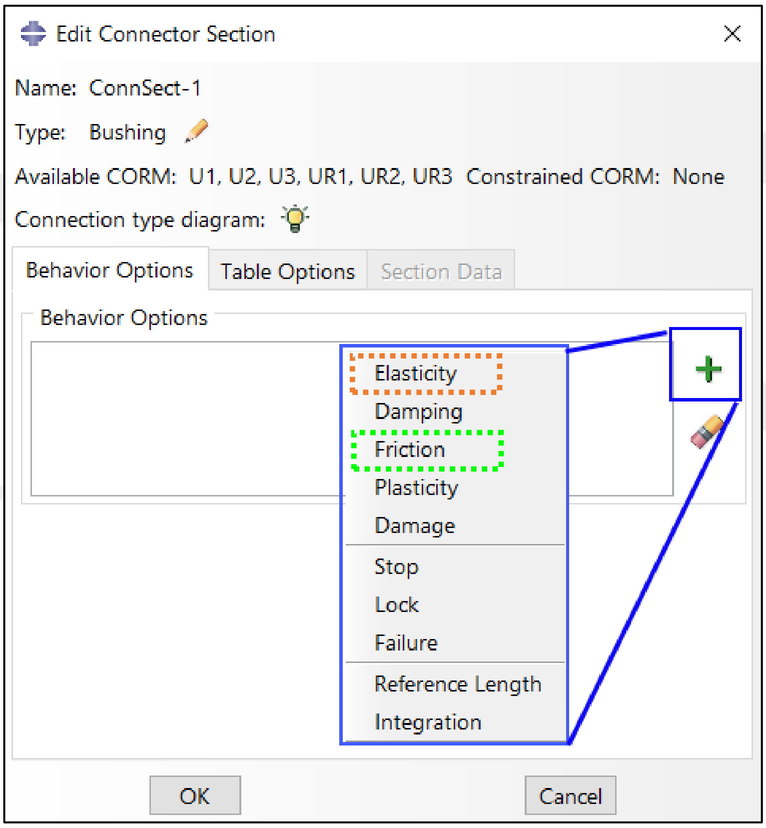

Figure 7.17: Abaqus FE model bushing connector element behaviour options [70]

As it is known, bushing type connector elements with six degrees of freedom provide an idealized load transfer between two points in a mechanical system through defined degrees of freedom. By means of bushing type connector elements, the idealized mechanical behavior of a roller bearing or a rubber isolator can be represented when appropriate. Figure 7.17 shows the “Elasticity” and “Friction” connector element behavior properties (options) used in the WRI modelling of the Abaqus FE bushing connector. In WRI modelling, angular degrees of freedom of bushing connector elements are released and only translational degrees of freedom are utilized for tranferring of the loads.

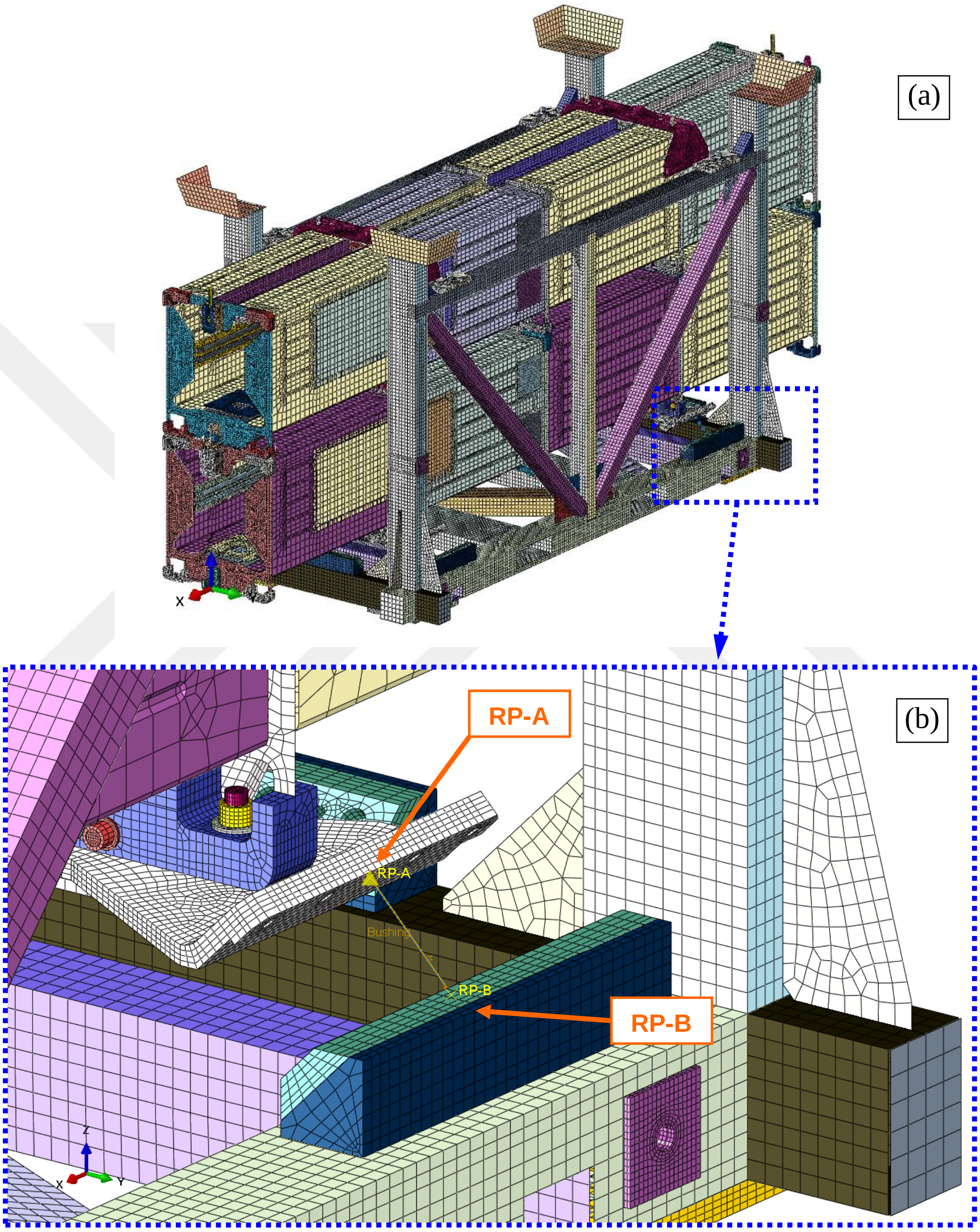

Figure 7.18: ABAQUS FE model of a wire rope isolator system (a) and a close view of WRI idealized by bushing connector elements (b)

The bushing connector model defined between the RP-A and RP-B reference points belonging to only one of the ten insulators in the FE model is shown in Figure 7.18(b).

Although one bushing connector element appears to be defined between RP-A and RP-B reference points in Figure 7.18(b), there are actually 25 bushing connector elements representing the modified Masing model. In summary, 1 nonlinear elastic element, 1 linear elastic and 23 Jenkins elements are represented by a total of 25 bushing connector elements located between RP-A and RP-B points. The behavior of the isolator in three axes is represented simultaneously by means of 25 bushing connector elements.

Details on defining the bushing connector element so that the parameters of the Modified Masing model represent the tension-compression axis behavior of the related WRI are shown in Figure 7.19, Figure 7.20 and Figure 7.21.

Similarly, details on defining the bushing connector element so that the parameters of the Modified Masing model represent the shear axis behavior of the related WRI are shown in Figure 7.22, Figure 7.23 and Figure 7.24.

Likewise, details on defining the bushing connector element so that the parameters of the Modified Masing model represent the shear axis behavior of the related WRI are shown in Figure 7.25, Figure 7.26 and Figure 7.27.

It must be noted that PYTHON scripting can be utilized for bushing connector element section creation and section assignment processes. In this way the preparation and assignment of bushing connector elements for large quantities can be automatized and preparation of the complex FE model could be done in a more error-free manner.

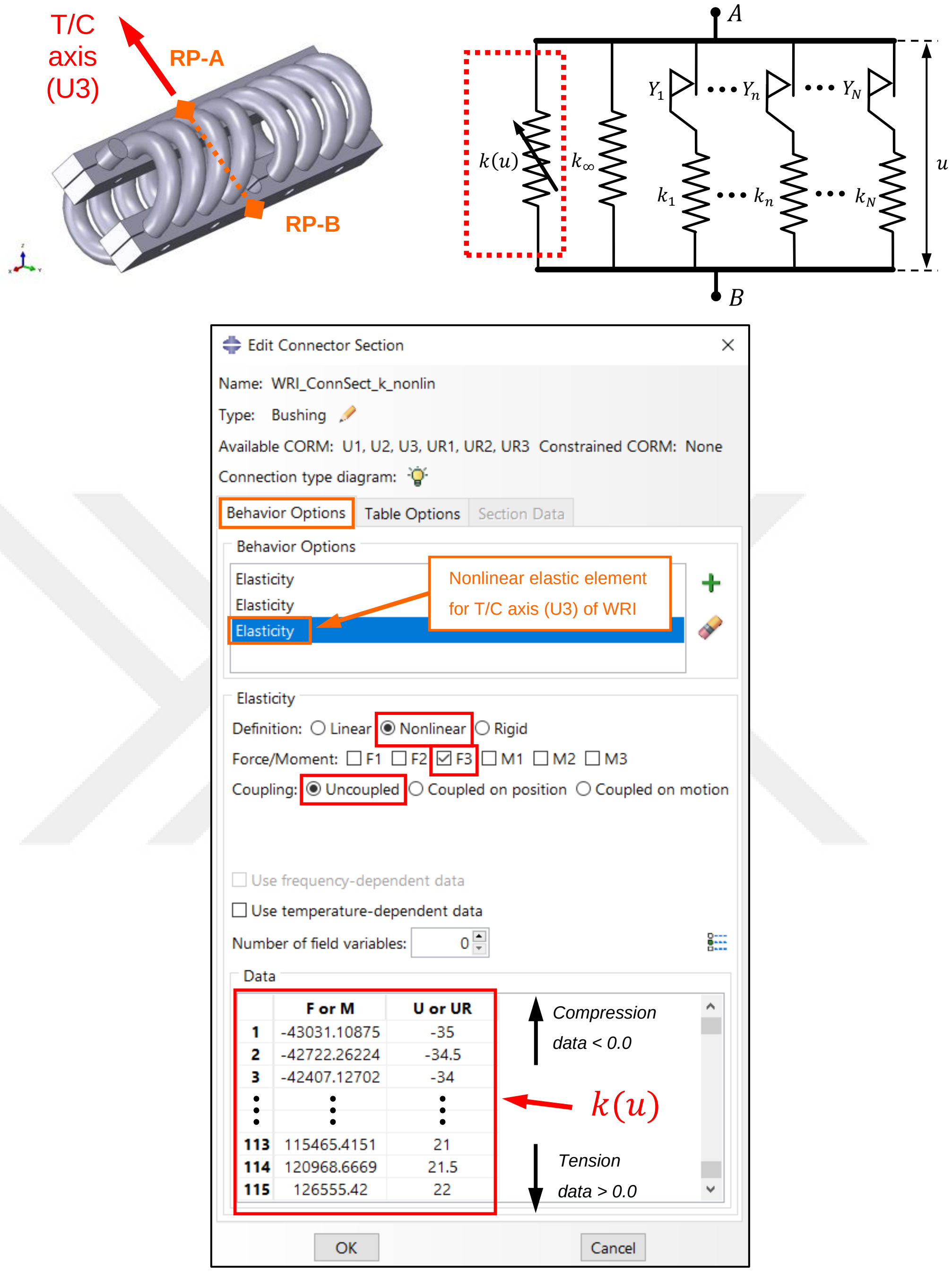

Figure 7.19: ABAQUS FE model bushing connector element properties representing the nonlinear elastic element for T/C axis of WRI

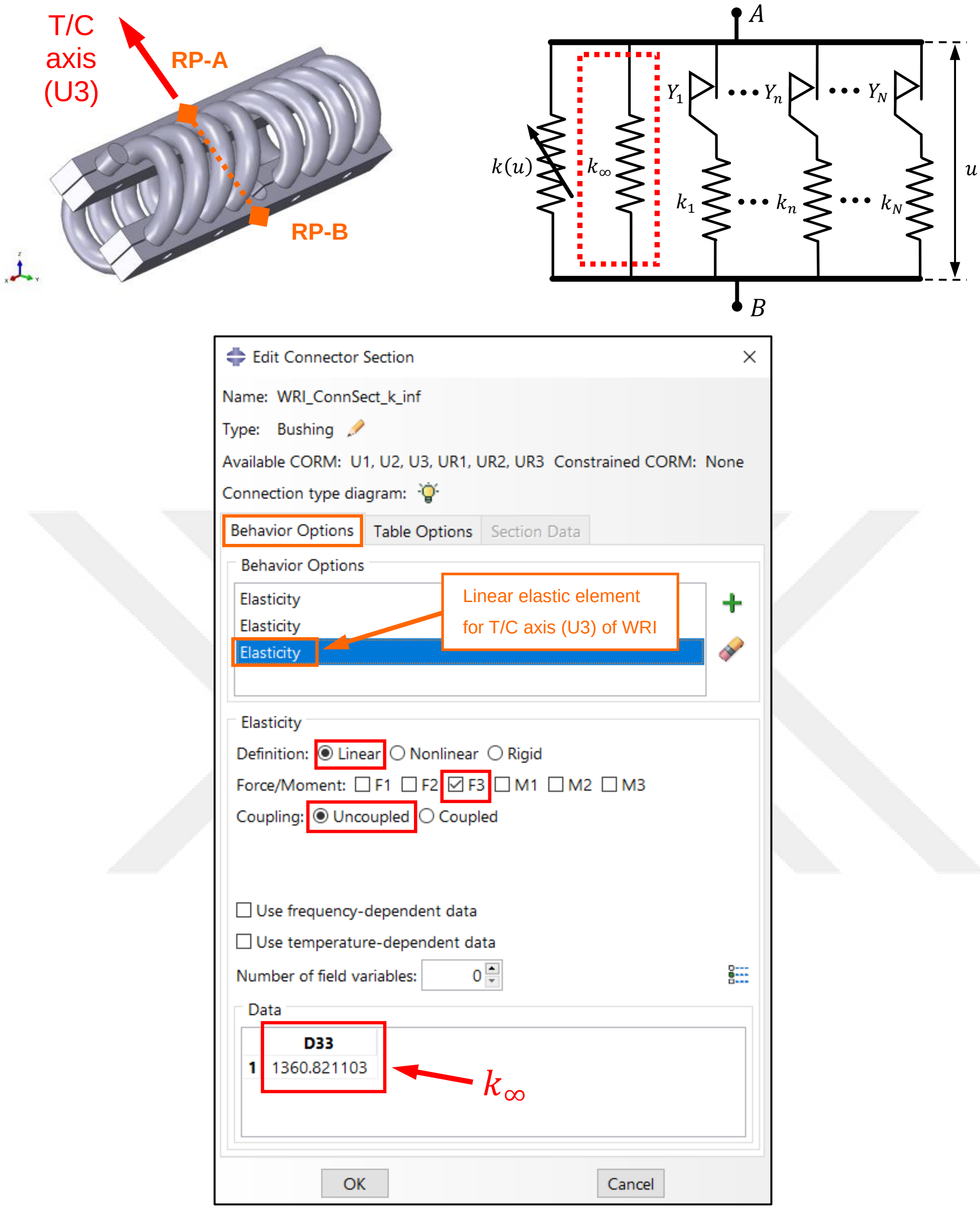

Figure 7.20: ABAQUS FE model bushing connector element properties representing the linear elastic element for T/C axis of WRI

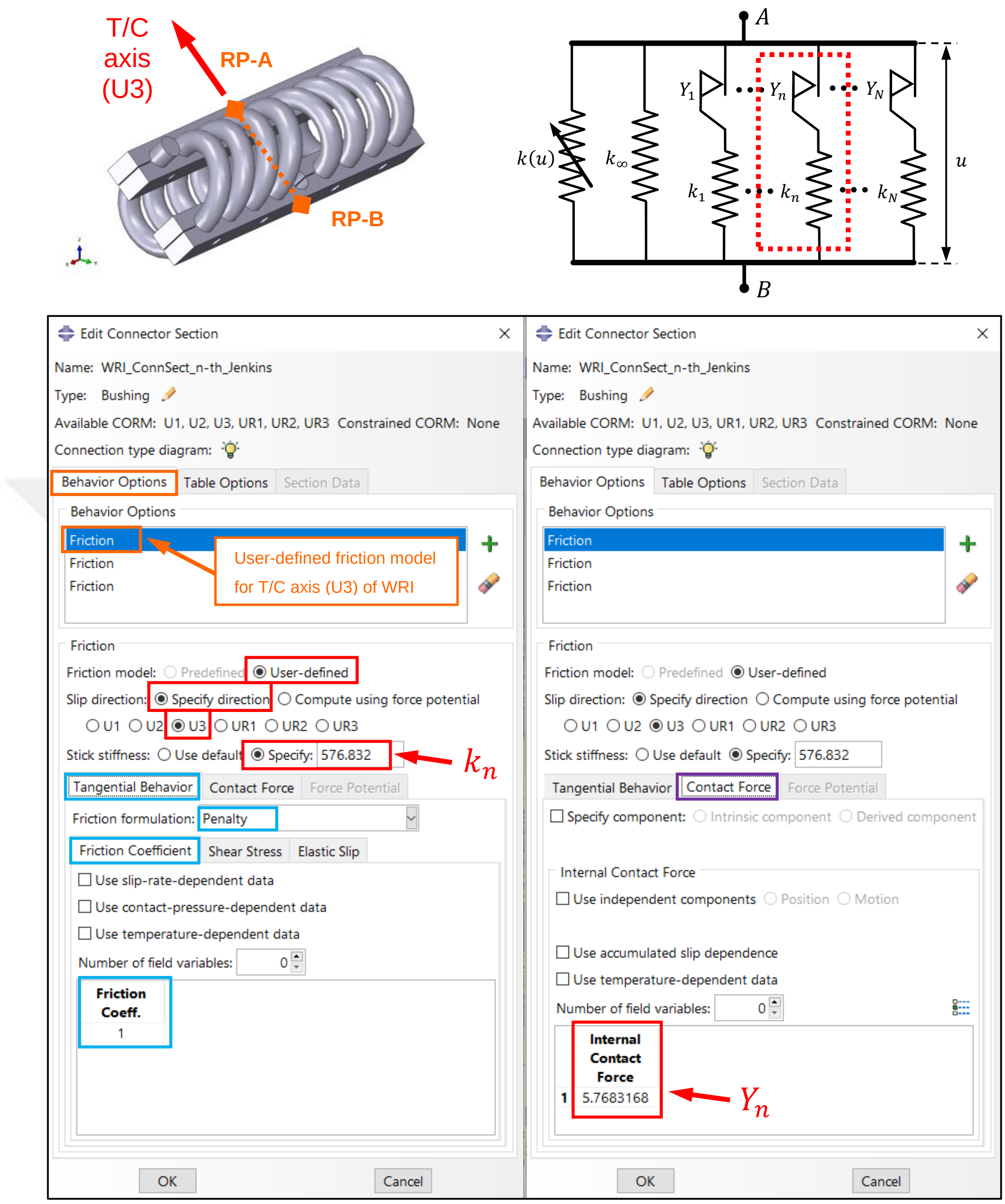

Figure 7.21: ABAQUS FE model bushing connector element properties representing the n[th] Jenkin's element for T/C axis of WRI

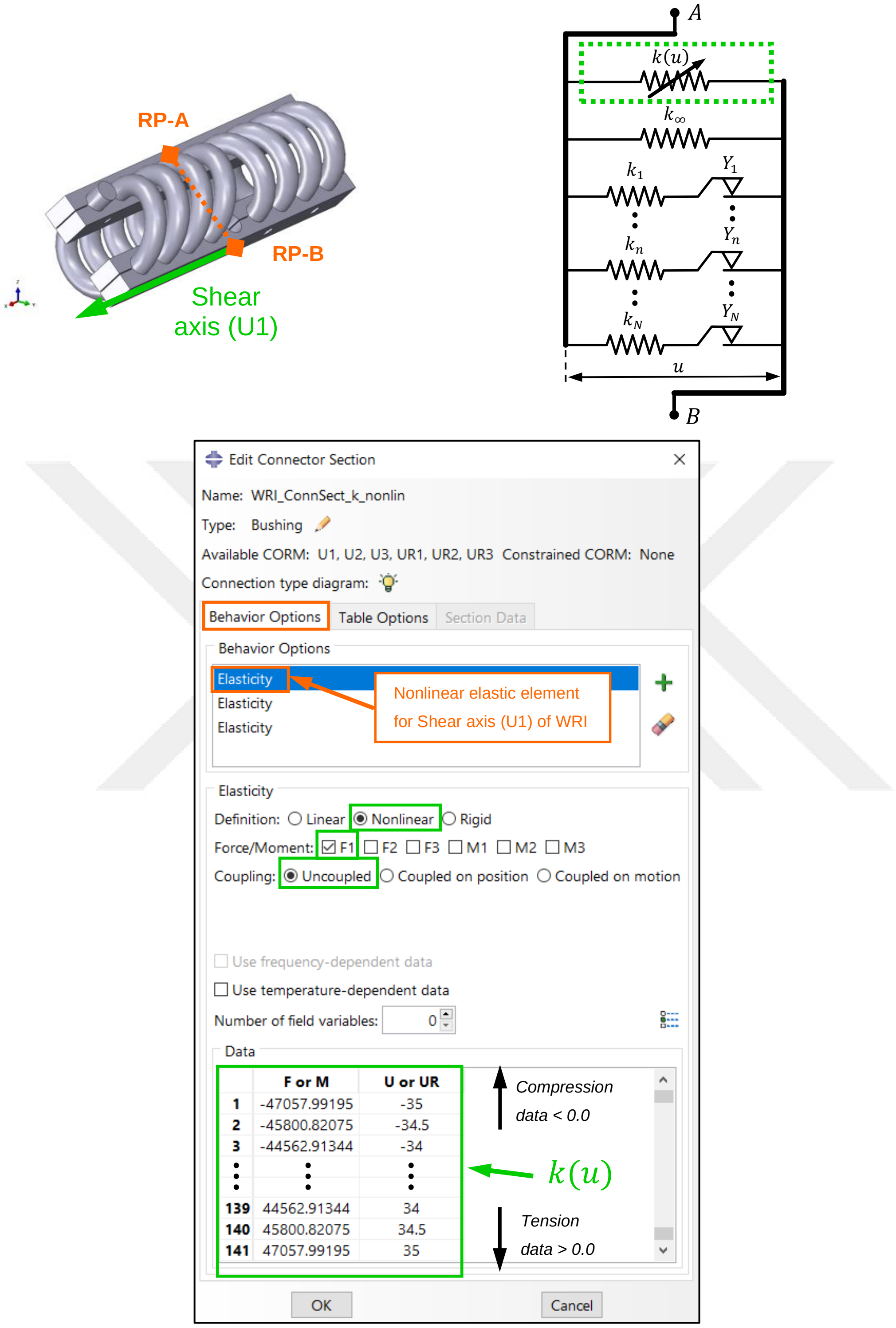

Figure 7.22: ABAQUS FE model bushing connector element properties representing the nonlinear elastic element for Shear axis of WRI

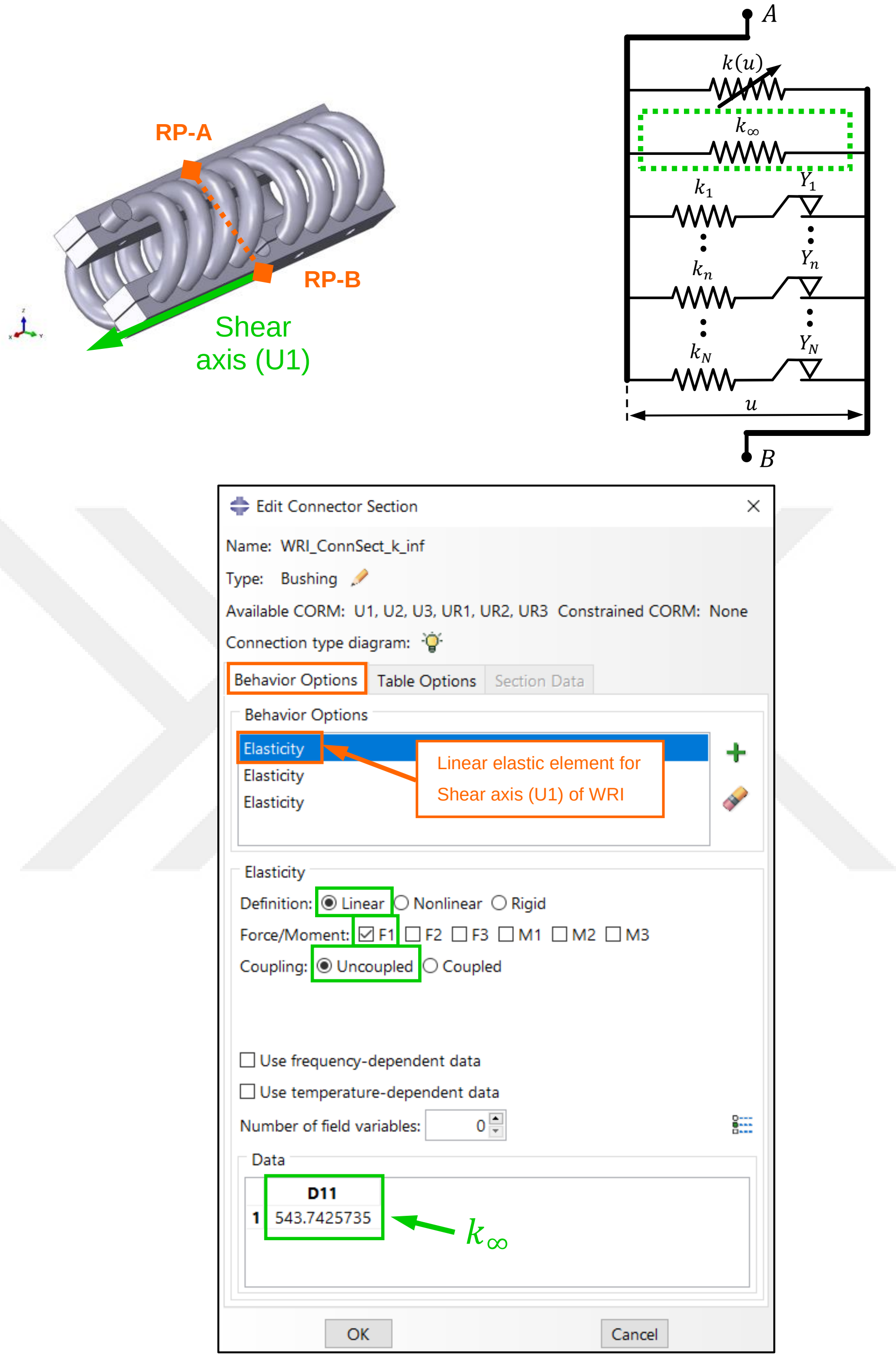

Figure 7.23: ABAQUS FE model bushing connector element properties representing the linear elastic element for Shear axis of WRI

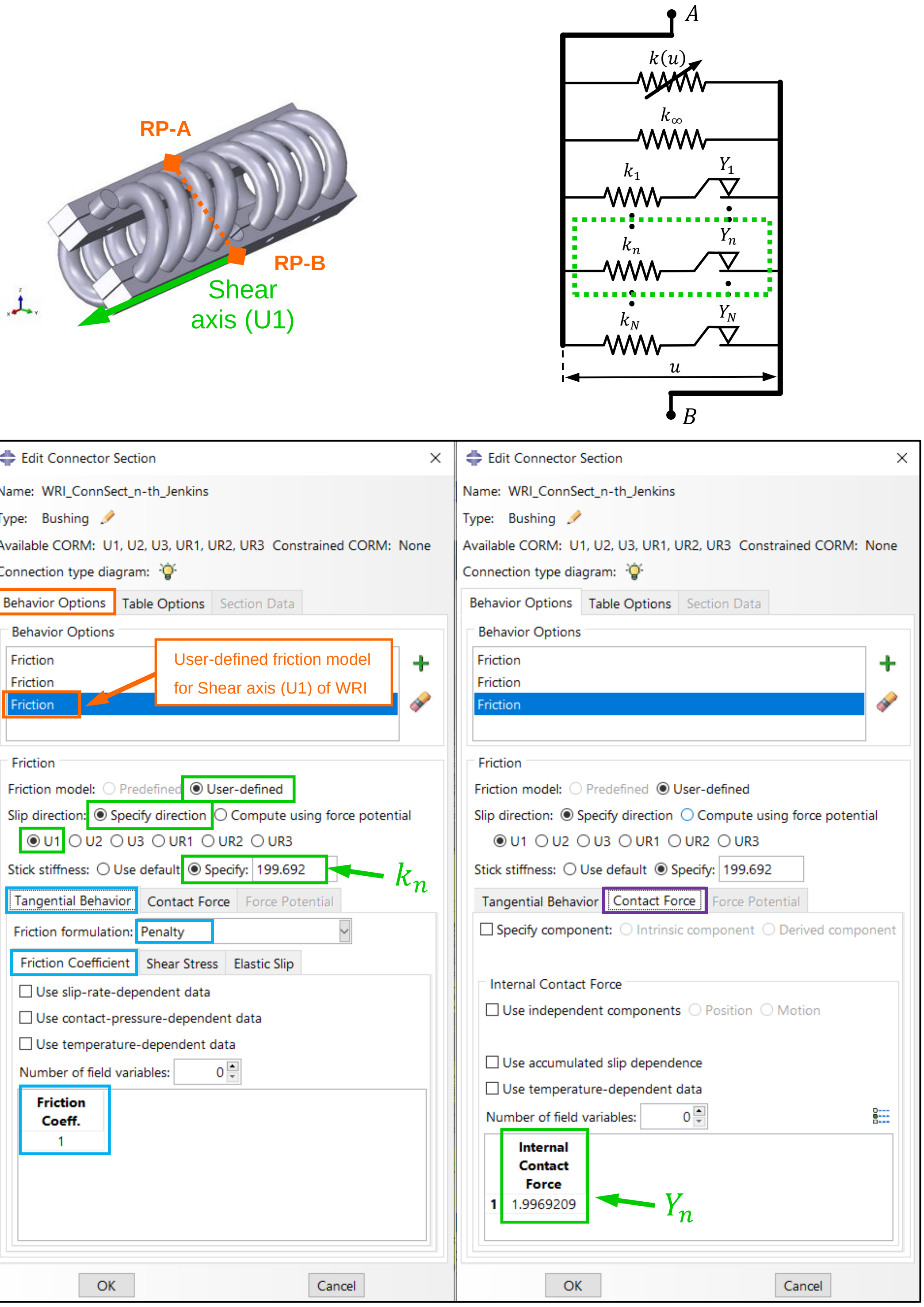

Figure 7.24: ABAQUS FE model bushing connector element properties representing the nth Jenkin's element for Shear axis of WRI

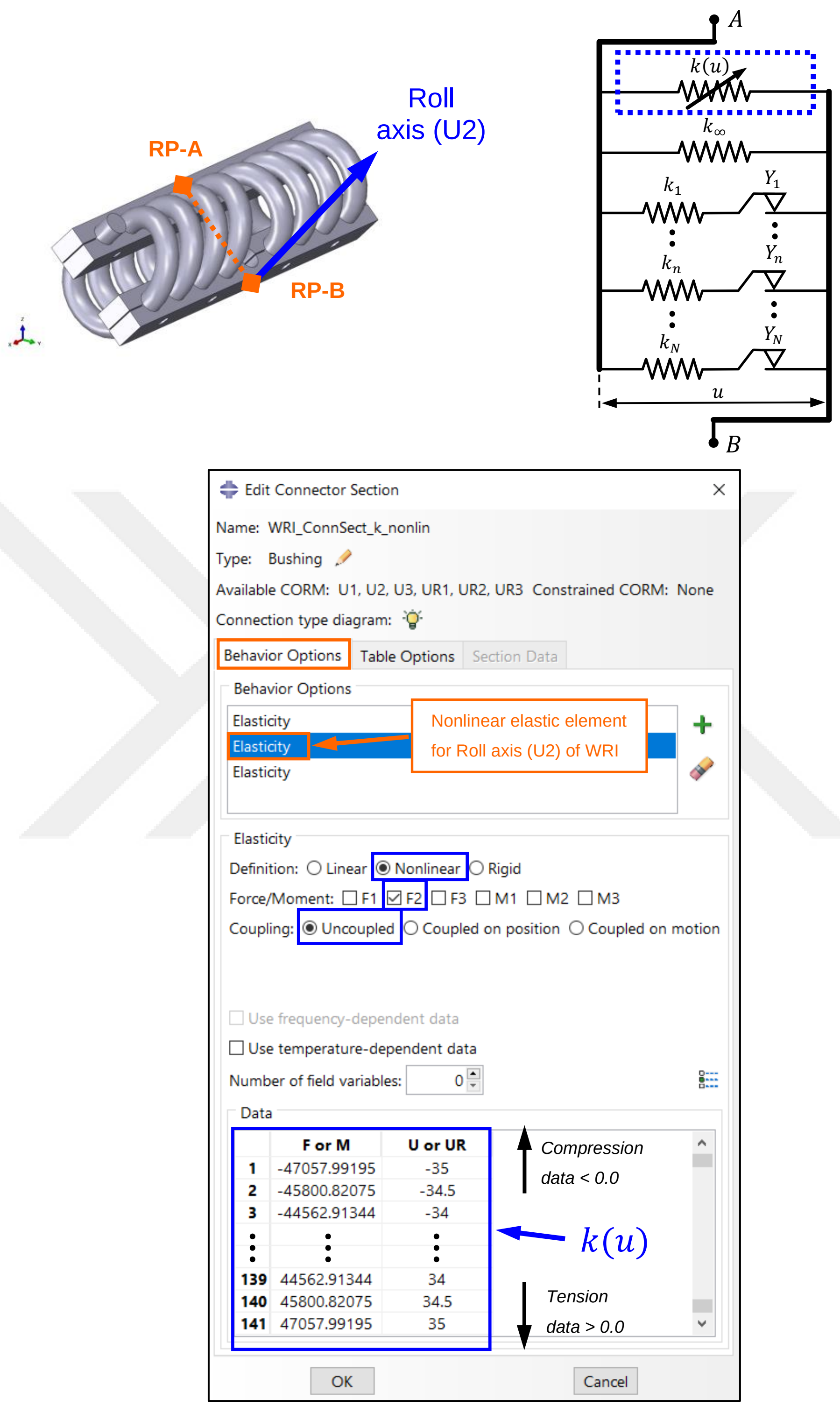

Figure 7.25: ABAQUS FE model bushing connector element properties representing the nonlinear elastic element for Roll axis of WRI

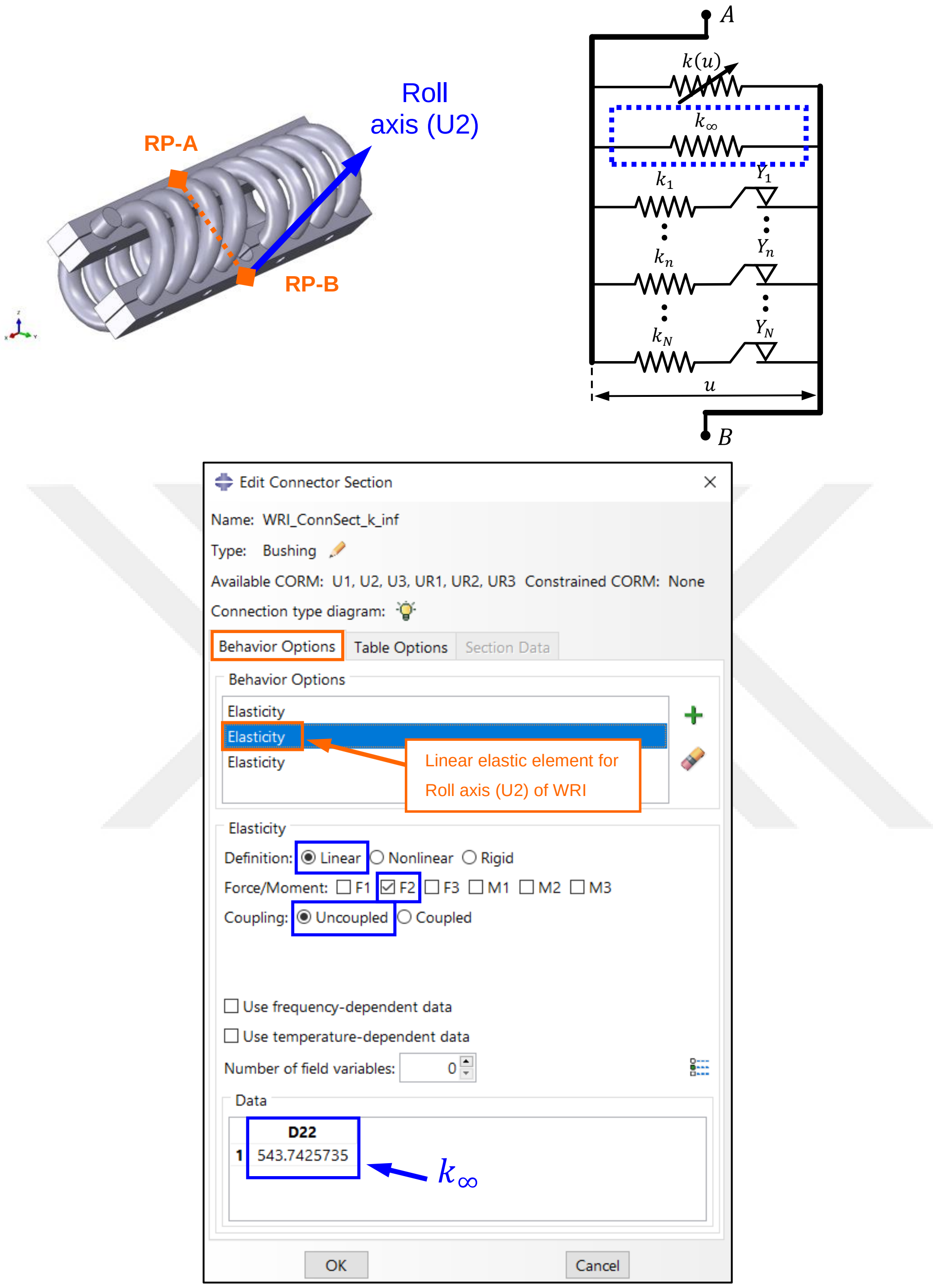

Figure 7.26: ABAQUS FE model bushing connector element properties representing the linear elastic element for Roll axis of WRI

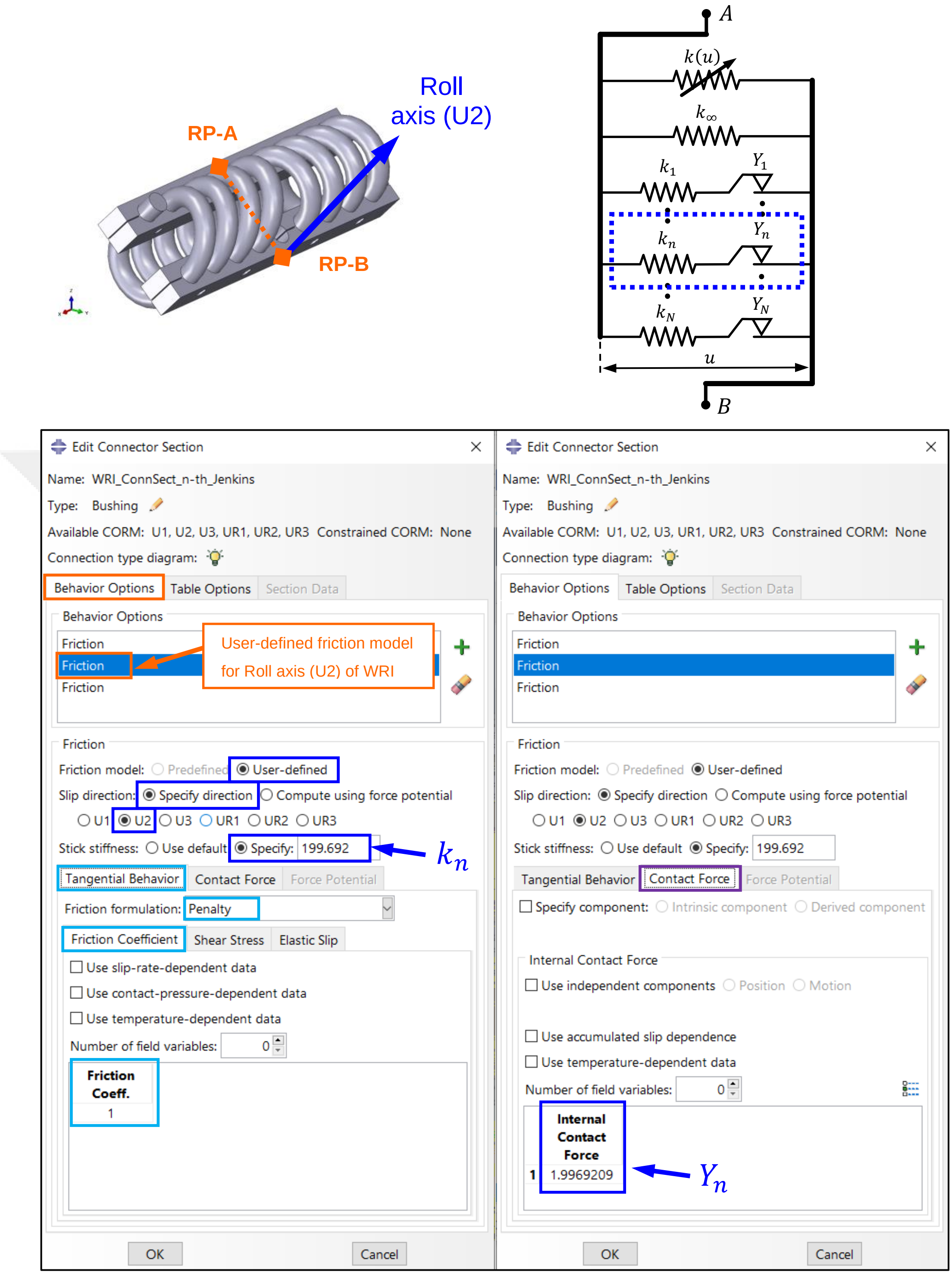

Figure 7.27: ABAQUS FE model bushing connector element properties representing the n[th] Jenkin's element for Roll axis of WRI

7.4.2 FE Model Loading and Boundary Conditions

First, assembly loads and then mechanical shock loads are applied to the canister transport system. Here, mounting loads mean preloading the various number of bolts found in the system and applying a gravity load to the entire canister transport system. Thus, the WRIs reach a static equilibrium position by stretching. The mechanical shock loading applied afterwards occurs as the WRIs are exposed to the mechanical shock load from this static equilibrium position.

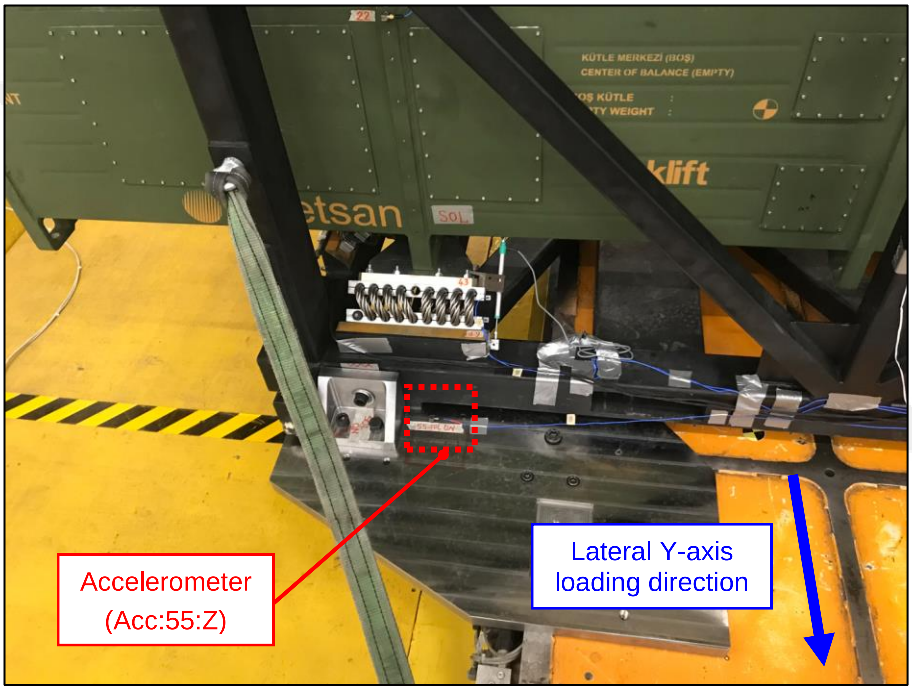

Figure 7.28: Location of accelerometer (Acc:55:Z) used to measure acceleration loading data to be applied to the FEA model

Figure 7.28 shows the accelerometer mounted to measure the shock load acting on the skid structure in terms of acceleration during the mechanical shock test. The acceleration data measured during the mechanical shock test is shown in Figure 7.29. This measured acceleration data shown in Figure 7.29 is used to apply mechanical shock loading to the canister transportation system, and the mechanical shock load is applied to the FE model as a boundary condition in terms of acceleration loading.

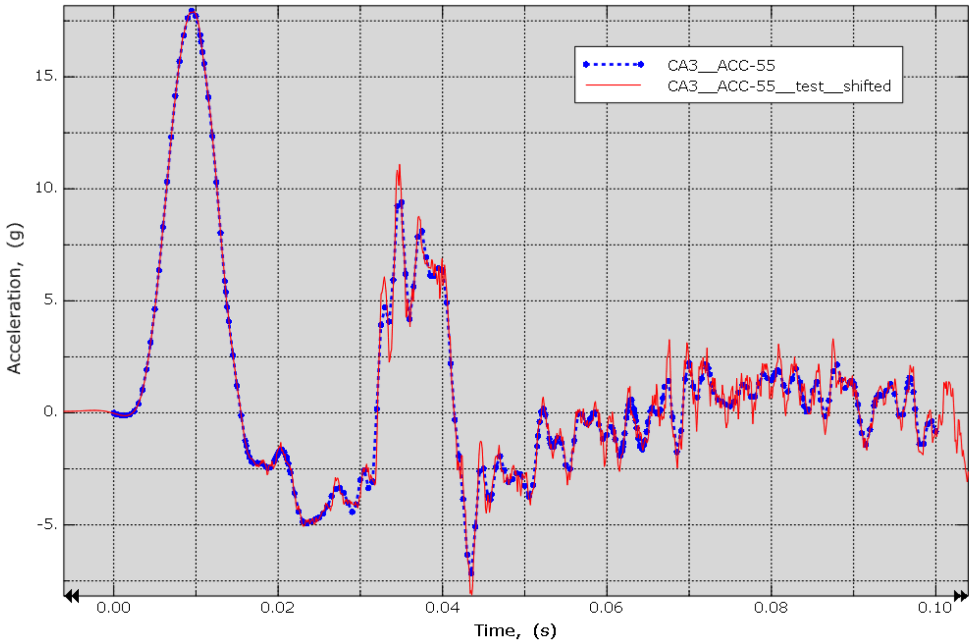

Figure 7.29: Acceleration (Acc:55:Z) loading data applied to the FEA model

7.4.3 FE Model Solver Settings

Abaqus FEA software has mainly two solvers known as Abaqus/Standard and Abaqus/Explicit for modeling solid mechanics problems [70]. In this study, Abaqus/Standard solver is used since FE model containts many elements in non uniform size, then solution with Abaqus/Explicit solver would be too expension because of the critical stable time incerement parameter. Furthermore, mechanical shock loading is solved by utilizing Abaqus FE "Dynamic-Implicit" solution procedure with "moderate dissipation" parameter is activated.

7.5 Test Setup and Instrumentation

Mechanical shock tests and modal tests of the canister transportation system were carried out at the METU-BILTIR test center. In order to carry out the mentioned tests, the canister transportationt system has been integrated on the skid structure (shown in orange color in Figure 7.30) by designing suitable fixture interfaces.

During the mechanical shock testing, 55 accelerometers and 5 LPTs were mounted in order to measure the acceleration and displacement data at various critical locations on the system.

Figure 7.30: A general view of test setup for lateral Y-axis loading

The general view of the system, whose sensor assembly has been completed, before the Y-axis mechanical shock test is given in Figure 7.30. The LMS Scadas Mobile data collection system, shown in Figure 7.31, was used to collect accelerometer data in the mechanical shock test. Accelerometer data were collected at a sampling rate of 10000 Hz. The same data acquisition system and accelerometer layout were also used for the execution of the modal tests.

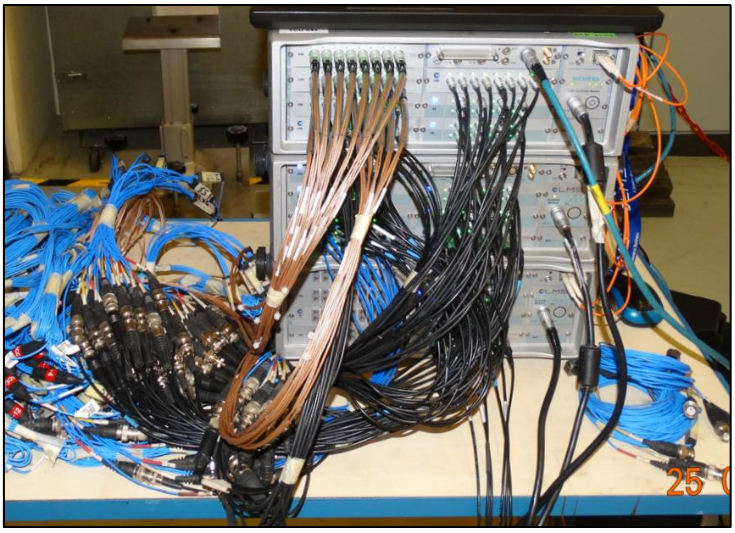

Figure 7.31: Data acquisiton and signal processing system (LMS SCADAS Mobile)

In addition, LPT displacement data were collected with the ESAM Traveler CF data collection system with a sampling rate of 1000 Hz.

7.6 Validation of Finite Element Analysis Model with Testing

7.6.1 Validation with Modal Testing

The modal test run was performed under the boundary condition shown in Figure 7.32 for a very limited time. Modal tests were performed using the LMS Test.LAB Impact testing software. The trigger point and impact hammer selected for performing the modal test are shown in Figure 7.33. Then, LMS Test.LAB PolyMAX Plus software (shown in Figure 7.34) was used to calculate resonance frequencies and experimental mode shapes by processing the modal test data (FRFs).

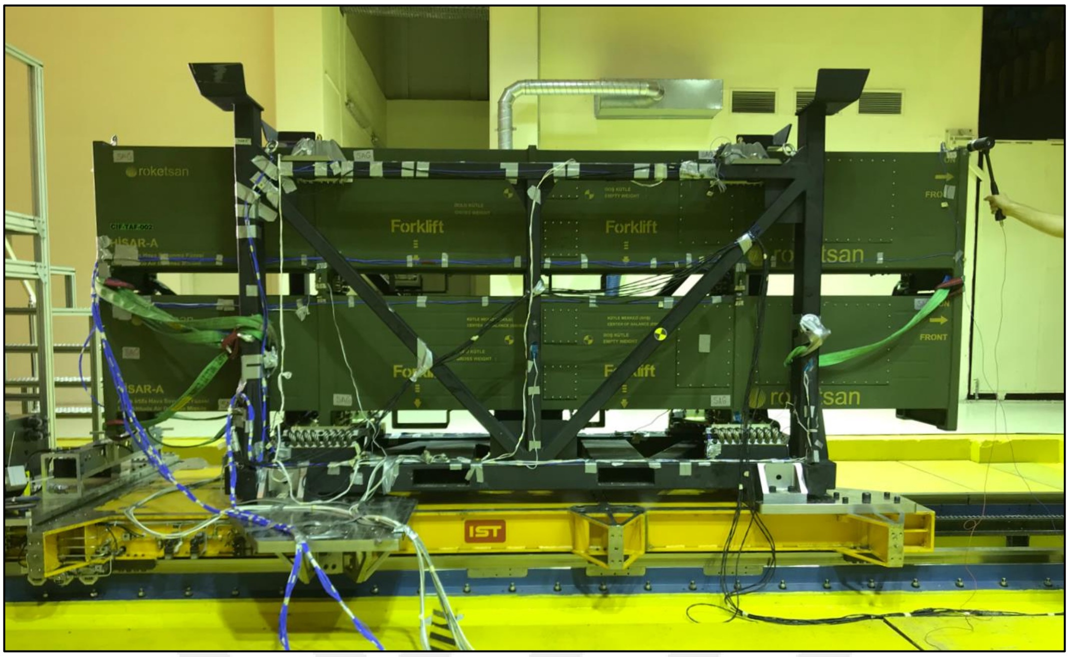

Figure 7.32: Test setup configuration for modal testing

Figure 7.33: Modal impact hammer excitation point for modal testing

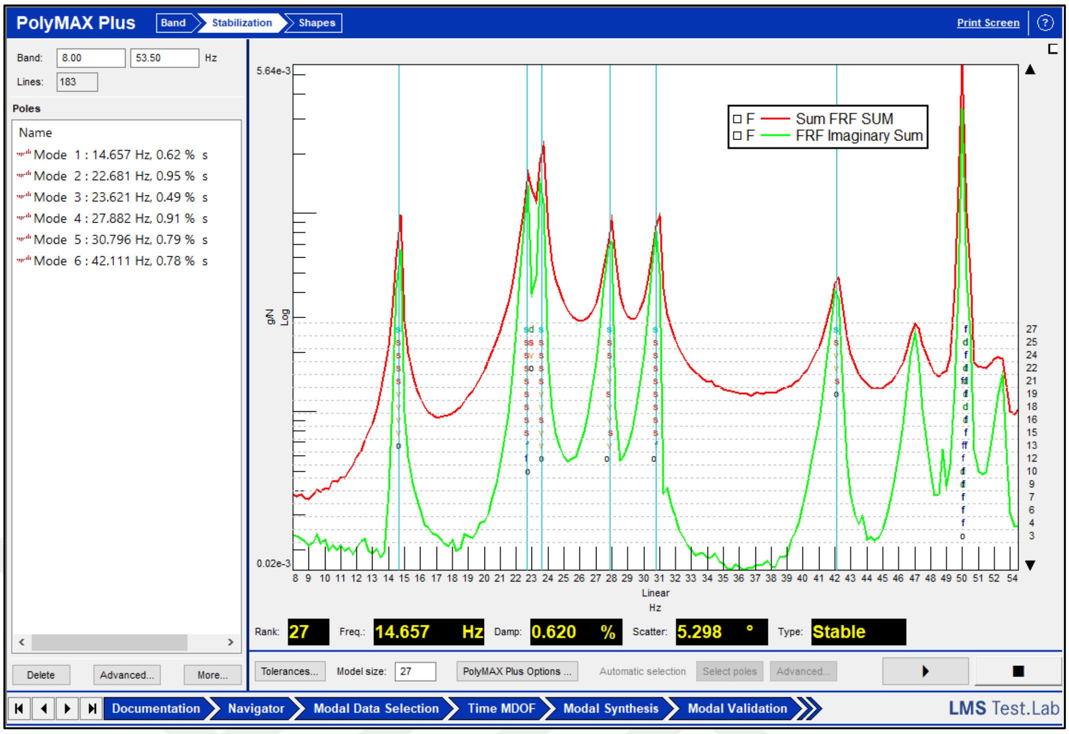

Figure 7.34: Implementation of experimental modal analysis using LMS Test.Lab / PolyMAX Plus solver

In Table 7.1, the comparison of the FE model modal analysis results and the modal test results is given. According to the results given in the Table 7.1, it can be said that the FE model predicts the frequency of the first 5 modes very well.

Table 7.1: Comparison of mode frequencies of modal test and FE model

Mode No.	Test Freqs (Hz)	FEA Freqs (Hz)	Difference (Hz)	Rel. Err. (%)
1	14.66	15.69	1.04	7.07
2	22.68	20.91	1.77	7.8
3	23.62	23.9	0.28	1.18
4	27.89	26.43	1.46	5.23
5	30.8	30.96	0.16	0.52
6	42.05	35.87	6.18	14.7

In addition, the MAC matrix can be calculated according to the equation below to compare the FE model mode shapes and the modal test mode shapes. Figure 7.35

$$MAC(A,X) = \frac{|\{\psi_X\}^T\{\psi_A\}|^2}{(\{\psi_X\}^T\{\psi_X\})\,(\{\psi_A\}^T\{\psi_A\})} \tag{7.3}$$

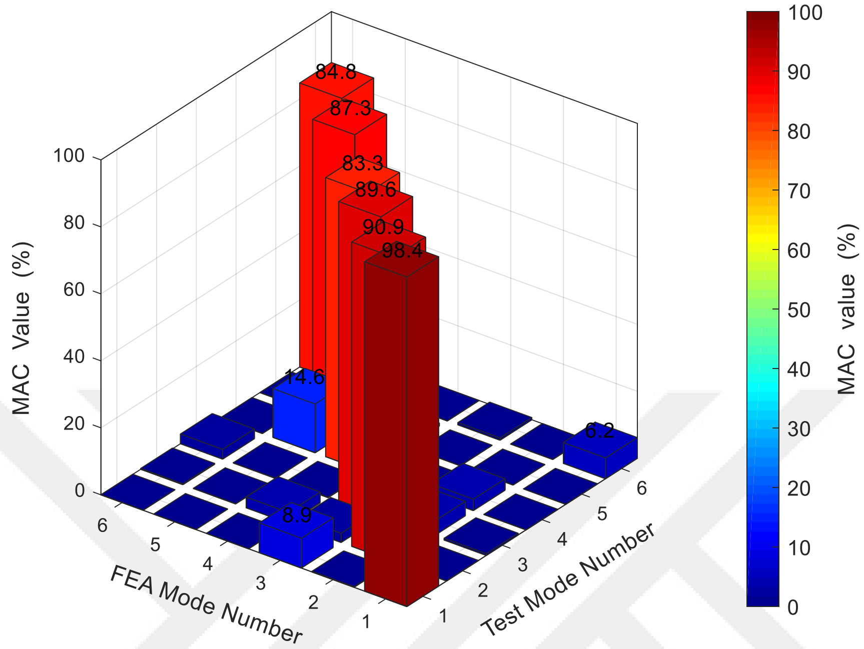

Figure 7.35: MAC matrix correlation for mode shapes in 3D representation

Figure 7.35 shows the calculated MAC matrix results for the first six mode shapes. Accordingly, it can be said that the mode shapes obtained with the FE model are confirmed by the modal test mode shapes since the diagonal terms of MAC matrix is mostly above 85% and off diagonal terms is mostly below 10%.

7.6.2 Validation with Mechanical Shock Testing

Mechanical shock analysis was performed for the Y-axis shock loading configuration of the FE model shown in Figure 7.36, and the analysis and test results were compared. As mentioned before, the acceleration data shown in Figure 7.29. is applied to the FE model shown in Figure 7.36 from the base of skid structure and the mechanical shock analysis is solved.

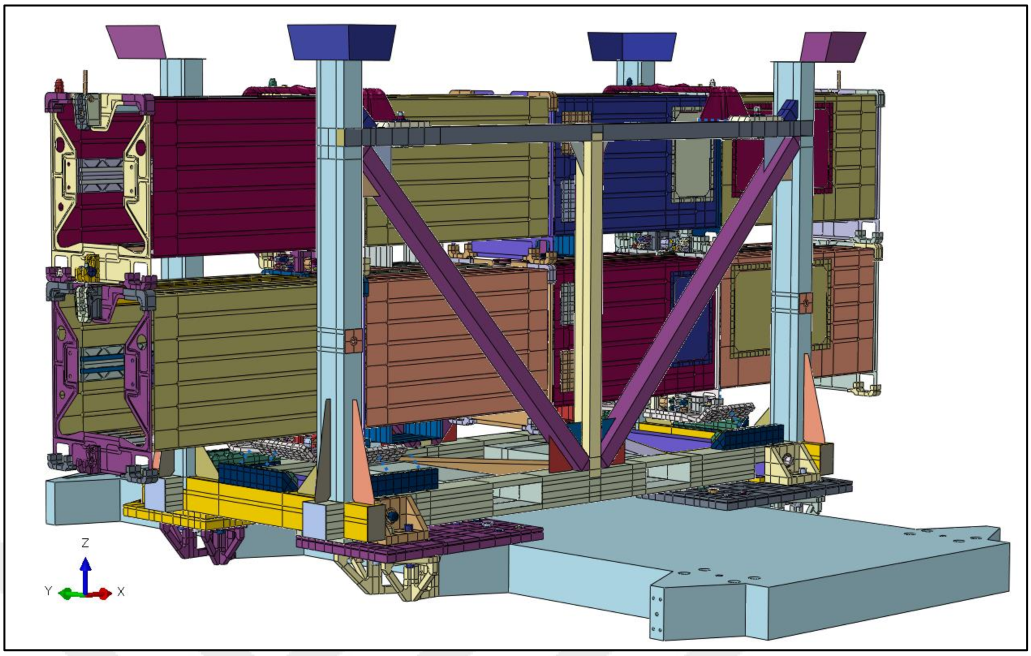

Figure 7.36: FEA model corresponding to lateral Y-axis mechanical shock loading

Comparison of LPT displacement sensor results and FE model results are given in Figure 7.37, Figure 7.38, Figure 7.39, Figure 7.40, and Figure 7.41. Additionally, comparison of some accelerometer sensor results with FE model results are given in Figure 7.42, Figure 7.43, Figure 7.44, Figure 7.45. Although the noise of the acceleration data is higher than the displacement data, it can be said that the acceleration data of the FE model are in good agreement with the test acceleration data. However, it is seen that the FE model displacement data are in good agreement with the LPT displacement sensor data.

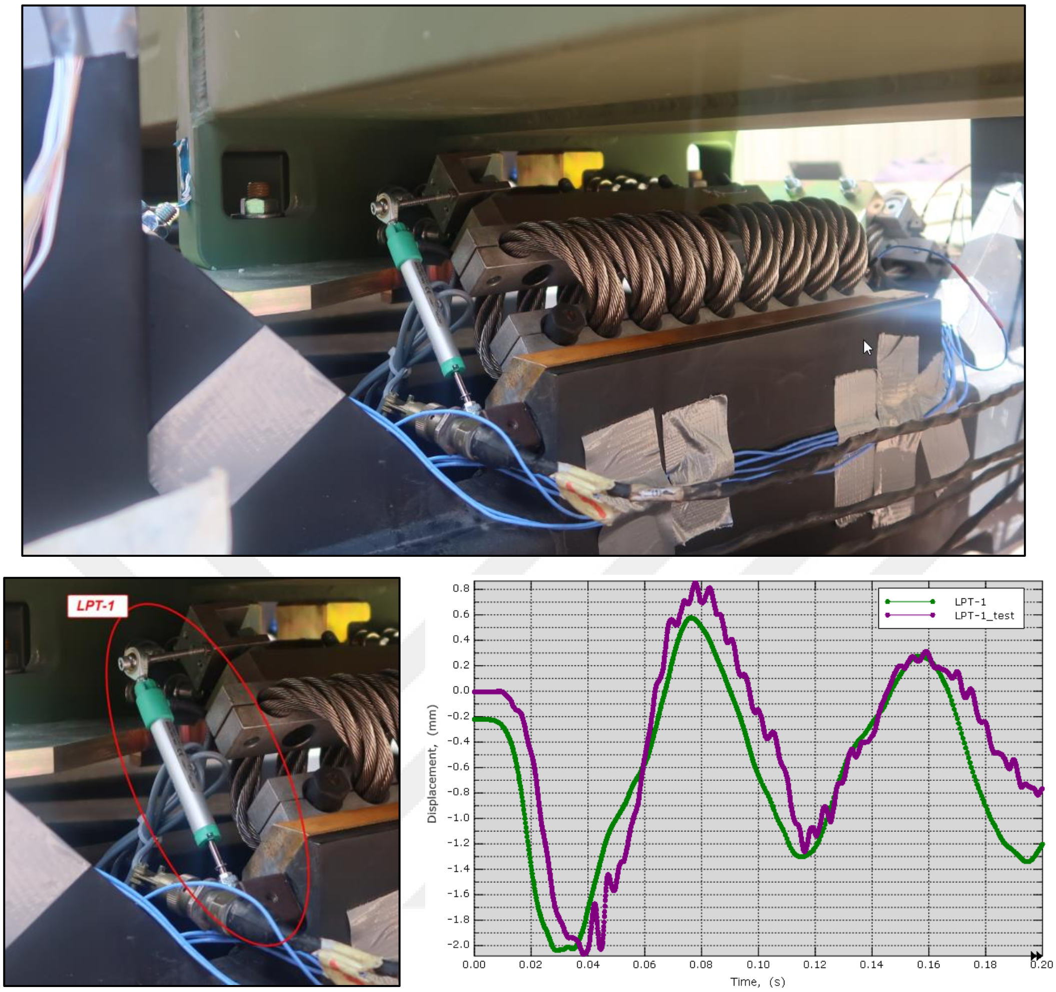

Figure 7.37: Comparison of shock testing and FEA model results of LPT-1

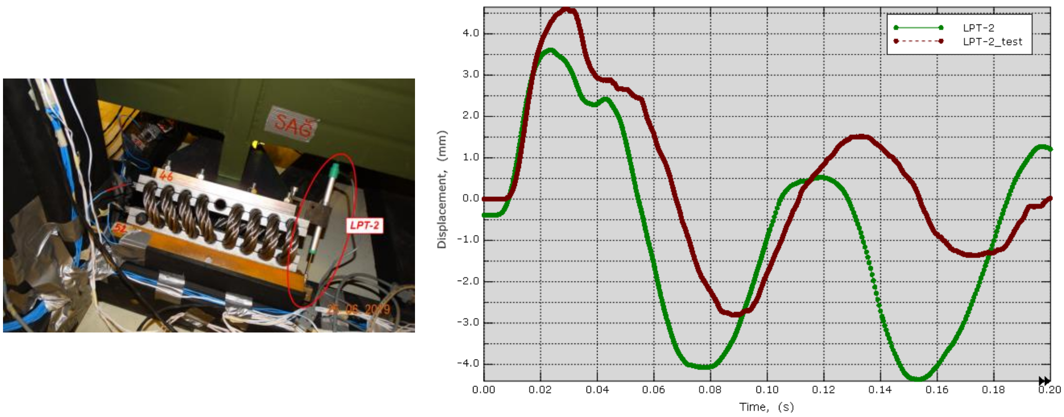

Figure 7.38: Comparison of shock testing and FEA model results of LPT-2

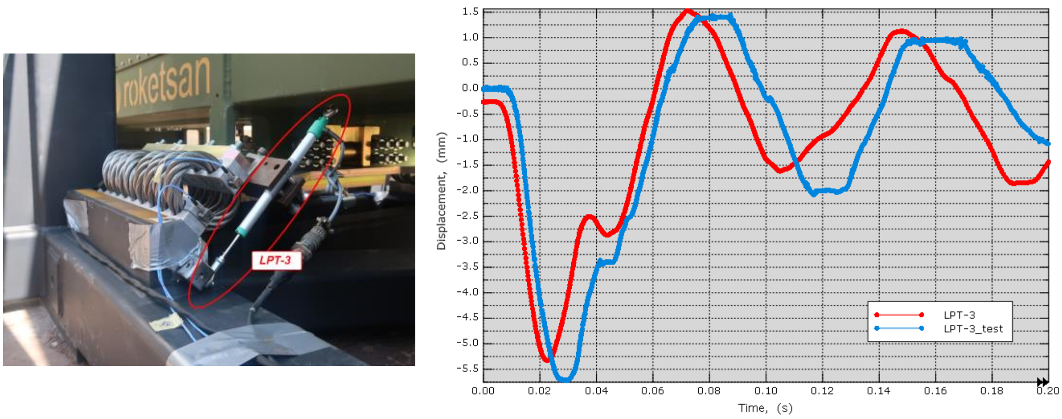

Figure 7.39: Comparison of shock testing and FEA model results of LPT-3

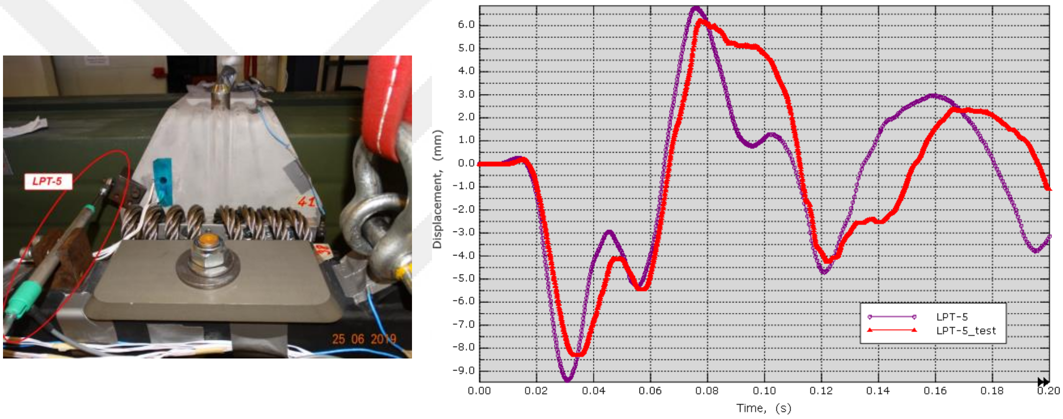

Figure 7.40: Comparison of shock testing and FEA model results of LPT-5

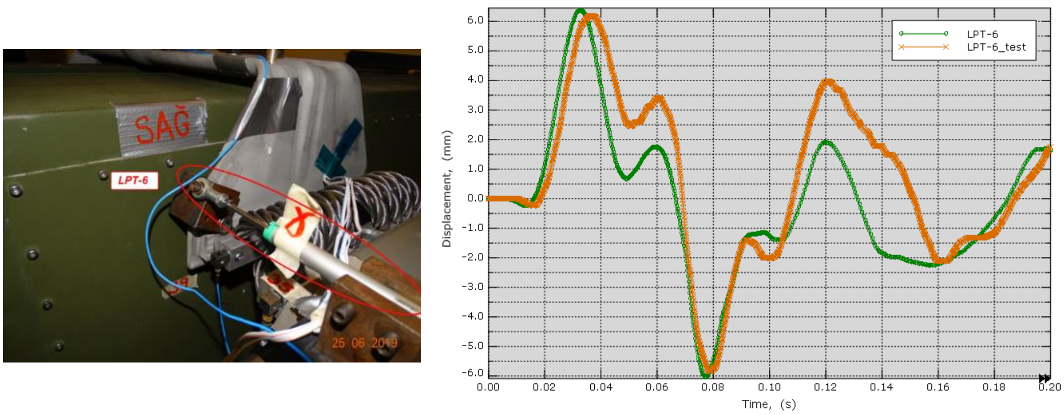

Figure 7.41: Comparison of shock testing and FEA model results of LPT-6

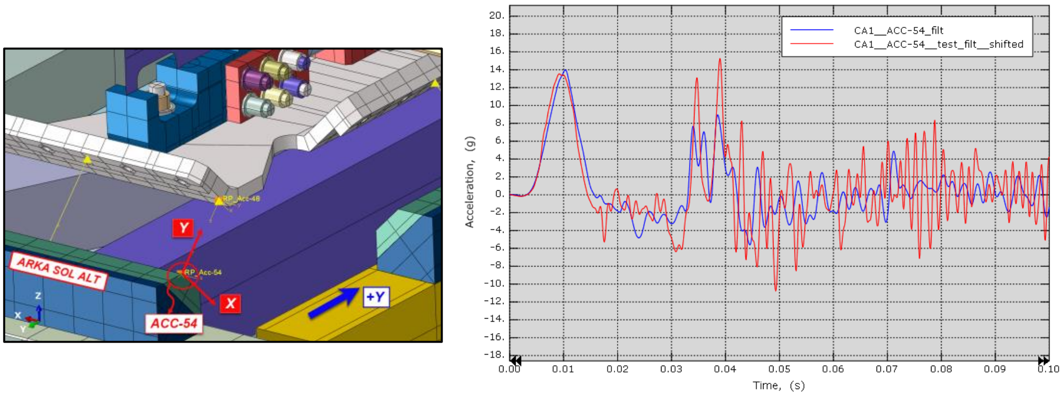

Figure 7.42: Comparison of shock testing and FEA model results of ACC No.54

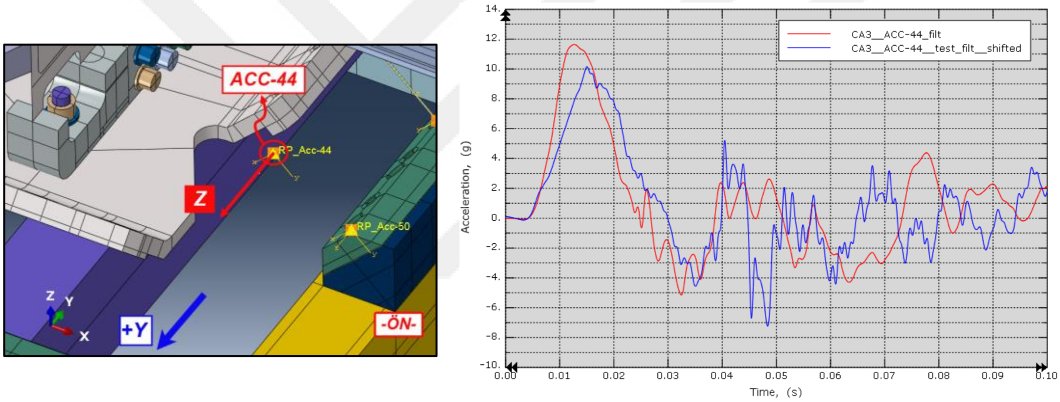

Figure 7.43: Comparison of shock testing and FEA model results of ACC No.44

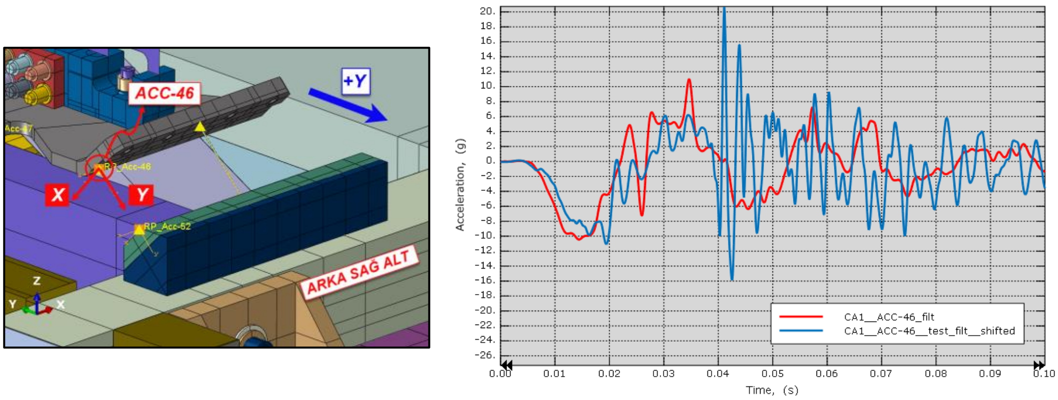

Figure 7.44: Comparison of shock testing and FEA model results of ACC No.46

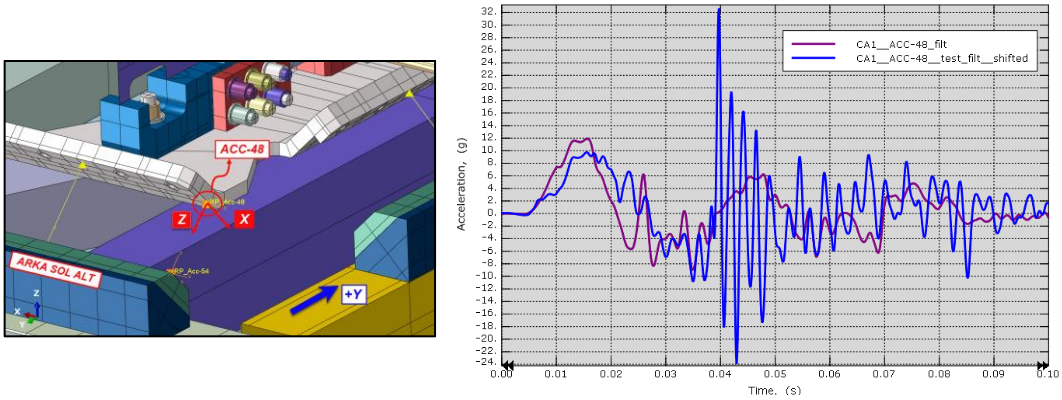

Figure 7.45: Comparison of shock testing and FEA model results of ACC No.48

7.7 Patent Application for Canister Transportation System

Within the scope of this thesis and The Researcher Training Program for Defense Industry (SAYP) project, the application for the patent titled "A canister transportation system involving wire rope isolators as damping elements" shown in Figure 7.46 with the application number TR 2023/003739 has been made.

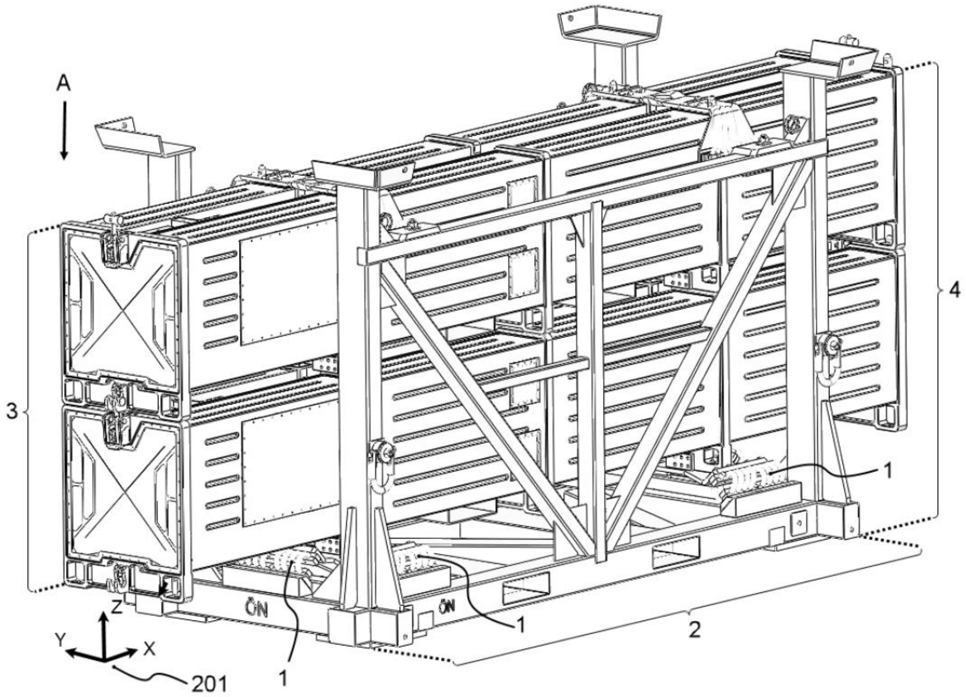

Figure 7.46: A canister transportation system involving wire rope isolators as damping elements [72]

Briefly, the invention is made of steel, which provides a significant isolation from the mechanical shock and vibration loads that an ammunition stored in the canister will be exposed to during transportation by land/air/sea during its life cycle from its manufacture to the stage of integration with the launch vehicle where it will be fired in the field. The whole of the dual canister transport system, which is the subject of the invention; basically, it consists of a canister transport system assembly involving WRI type of damping elements and the dual canister assembly integrating with each other via interconnecting elements over the carrier plate and clamp interfaces. The whole canister transport system is a portable mechanical shock and vibration isolation system that stands out with its ability to be mounted (assembled) and disassembled (disassembled) in a short time as a double canister as a whole or as a single canister as a whole.

In this patent application, a canister transportation system involving WRIs for the isolation of mechanical shock and vibration loading is a novelty when available literature is taken into consideration.

7.8 Concluding Remarks

In this chapter, a methodology for modelling of shock response of a wire rope isolator system using ABAQUS FEA software was developed. This methodology is basically relies on the adaptation of Masing’s model to the FEA software. An extensive experimental studies including both modal testing and mechanical shock testing for validation of FEA model were done. The results have indicated that a good correlation between FEA modelling and testing was obtained even though such a large and complex FEA model was taken into consideration.

CHAPTER 8

CONCLUSIONS

8.1 Summary and Conclusions

In this thesis study, modellling of dynamic behaviour of wire rope isolators is implemented by utilizing various theoretical and experimental studies. Theoretical investigations have shown that a slight variation of Masing's model is very effective for modelling the amplitude-dependent hysteresis behaviour of WRIs using a FEA modelling software.

Sample-level characterisation tests of WRIs were carried out by utilising special designed characterisation test fixtures which enables the WRIs to be tested in tension/compression, shear and roll direction loading axes. Characterisation tests of WRI samples were implemented under cyclic loading by using an electromechanically excited dynamic (fatigue) test instrument. Characterisation tests have shown that hysteresis cycles experienced by WRIs under cyclic loading are nearly independent of loading frequency; however, they exhibit a preload-dependent behaviour.

An approach for modelling the nonlinear harmonic response of WRIs was developed and proposed. This appoach relies on the solving equation of motions iteratively in frequency domain while updating the dynamic stiffness and loss factor values of a given WRI repeatedly until a convergence criteria has reached.

A simple approach for identification of cofficients of Masing's model was utilized. In this approach, to be able to determine the coefficients of the Masing's model, dynamic stiffness captured from characterisation testing what is needed.

In the end, a methodology for modelling of shock response of a wire rope isolator system using ABAQUS FEA software was developed. This methodology is basically relies on the adaptation of Masing’s model to the FEA software. An extensive experimental studies including both modal testing and mechanical shock testing for validation of FEA model were done. The results have indicated that a good correlation between FEA modelling and testing was obtained even though such a large and complex FEA model was taken into consideration.

8.2 Future Work

The work planned for the future is to modelling the micromechanical behaviour of the WRI in ABAQUS FEA environment. The aim here is to simulate the characterization testing in the FEA environment instead of performing dynamic testing physically which is quite costly and time-consuming. To this end, dynamic stiffness as a function of dynamic amplitude can be used to identify the theoretical Masing's model as long as we validate the micromechanical FEA modelling approach with certain characterisation test results.

REFERENCES

[1]. Iwan, W. D., 1966, "A Distributed-Element Model for Hysteresis and Its Steady-State Dynamic Response", ASME. J. Appl. Mech., 33(4), p.893–900.

[2]. Ruzicka, J. E., 1967, “Resonance Characteristics of Unidirectional Viscous and Coulomb-Damped Vibration Isolation Systems”, Journal of Engineering for Industry, 89(4), p.729-740.

[3]. Cutchins, M. A., Cochran, J. E., Kumar, K., Fitz-Coy, N. G., Tinker, M. L., 1987, “Initial Investigations into The Damping Characteristics of Wire Rope Vibration Isolators”, Auburn University, Technical Report 87-1, NASA Research Grant NAG8-532.

[4]. Tinker, M. L., 1989, PhD Thesis, “Damping Phenomena in a Wire Rope Vibration Isolation System”, Auburn University.

[5]. Demetriades, G. F., Constantinou M. C., and Reinhorn, A. M., 1992, “Study of Wire Rope Systems for Seismic Protection of Equipment in Buildings”, Technical Report NCEER-92-0012, State University of New York

[6]. Ottl, D., “Modellierung der mechanischen Hysteresis”, (=Modeling of Mechanical Hysteresis), Naturwissenschaften, Vol. 80, No. 9, p. 391-396, 1993.

[7]. Kolsch, H., 1993, “Schwingungsdämpfung durch statische Hysterese”, (=Vibration Damping by Static Hysteresis), PhD Dissertation, Technical University Braunschweig.

[8]. Kolsch, H., 1994, “On the Identification of Parameters for Structural Members Exhibiting Static Hysteresis”, Mechanics Research Communications, 21(1), p.31-40.

[9]. Rassaian, M., 1994, “Power Spectral Density Conversions and Nonlinear Dynamics”, Shock and Vibration, Vol. 1, No. 4, pp. 349-356.

[10]. Sanliturk, K. Y., and Ewins, D. J., 1996, “Modelling Two-Dimensional Friction Contact and Its Application Using Harmonic Balance Method”, J. of Sound and Vibration, 193(2), p.511-523.

[11]. Austrell, P-E., 1997, PhD Thesis, "Modelling of elasticity and damping for filled elastomers", Lund University - Lund Institute of Technology, Report TVSM-1009, Sweden.

[12]. Van Aanhold, J. E., 1999, “A model for describing the damping behavior of wire rope springs with an application to small amplitude vibrations”, 70th Shock and Vibration Symposium, Albuquerque, USA.

[13]. Ni, Y. Q., Ko, J. M., Wong, C. W., and Zhan, S., 1999, “Modeling and identification of a wire-cable vibration isolator via a cyclic loading test Part 1: experiments and model development”, Proc Instn Mech Engrs Part I, Vol 213, Issue 3, p.163-171.

[14]. Ni, Y. Q., Ko, J. M., Wong, C. W., and Zhan, S., 1999, “Modeling and identification of a wire-cable vibration isolator via a cyclic loading test Part 2: identification and response prediction”, Proc Instn Mech Engrs Part I, Vol 213, Issue 3, p.173-182.

[15]. Leenen, R., 2002, “The Modelling and Identification of a Hysteretic System”, Technical Report DCT-2002/72, Eindhoven University of Technology.

[16]. Juntunen, M., and Linjama, J., 2003, “Presentation of the VTT Benchmark”, Mechanical Systems and Signal Processing, 17(1), pp. 179-182.

[17]. Sauter, D., 2003, PhD Thesis, “Modeling the Dynamic Characteristics of Slack Wire Cables in Stockbridge Dampers”, Darmstadt University of Technology.

[18]. Schwanen, W., 2004, MSc Thesis, “Modelling and Identification of the Dynamic Behavior of a Wire Rope Spring”, Technical Report DCT-2004/28, Eindhoven University of Technology.

[19]. Foss, G. C., 2006, “Modal Damping Estimates from Static Load-Deflection Curves”, IMAC XXIV, (24th International Modal Analysis Conference), St. Louis, USA.

[20]. Olsson, A. K., 2007, PhD Thesis, “Finite Element Procedures in Modelling the Dynamic Properties of Rubber”, Lund University - Lund Institute of Technology, Report TVSM-1021, Sweden.

[21]. Li, H., and Meng, G., 2007, “Non-linear dynamics of a SDOF oscillator with Bouc–Wen hysteresis”, Chaos, Solitons and Fractals 34, pp. 337-343.

[22]. Kari, L., and Hagerstrand, S., 2008, “Structure-Borne Sound Properties of Wire Rope Isolators”, Joint Baltic-Nordic Acoustics Meeting 2008, Reykjavik, Iceland.

[23]. Paolacci, F., and Giannini, R., 2008, “Study of the effectiveness of steel cable dampers for the seismic protection of electrical equipment”, The 14th World Conference on Earthquake Engineering, Beijing, China.

[24]. Petitjean, B., Jaumouille, V., and Saad, P., 2010, “Modeling non linear effects in elastomer components, including uncertainties”, International Conference on Noise and Vibration Engineering, (ISMA-2010), p.3237-3246., Leuven, Belgium.

[25]. Mangin, P. E., Faux, D., Cuvelier, P., and Tartary, J. P., 2012, “Modeling of the vibratory behavior of a wire rope spring by using the Dahl model with variable parameters”, XVIIIth Vibrations, Shocks & Noise Symposium, Clamart, France.

[26]. Ülker-Kaustell, M., 2013, PhD Thesis, “Essential modelling details in dynamic FE-analyses of railway bridges”, KTH School of ABE, Stockholm, Sweden.

[27]. Wang, H. X., Gong, X. S., Pan, F. Dang, X. J., 2015, “Experimental investigations on the dynamic behaviour of o-type wire-cable vibration isolators”, Shock and Vibration, Vol 2015, Article ID 869325.

[28]. Tax, J. C. A., 2016, MSc Thesis, “Modelling and Validation of a Hybrid Damper in a New Non-linear Shock and Vibration Isolation System”, Eindhoven University of Technology.

[29]. Tartary, J P., Maran, R., and Coquet, C., 2016, “Suspension par des amortisseurs à câble d’un groupe électrogène en condition de séisme”, (=Wire rope vibration isolation for a generating set subjected to seismic condition), AVE2016 – Analyse Vibratorie Experimentale, 15-17 Nov. 2016, Blois, France.

[30]. Smetryns, E., Tartary, J. P., and Courzereaux, J. M., 2018, “Suspension par des amortisseurs à câble d’un onduleur en condition de séisme”, (=Suspension by cable shock absorbers of an inverter in earthquake condition), Socitec Company.

[31]. Gaul, L., and Nitsche, R., 2001, “The role of friction in mechanical joints”, Appl Mech Rev, 54(2), pp. 93-105.

[32]. Oldfield, M., Ouyang, H., and Mottershead, J. E., 2005, “Simplified models of bolted joints under harmonic loading”, Computers and Structures 84, pp. 25-33.

[33]. Vibro/Dynamics LLC, a Socitec Group Company, Shock and Vibration Solutions, http://www.vibrodynamics.com/usa/pdf/literature/LIT-WRI.pdf, 2017.

[34]. Frampton, R. C., 2019, “The Dynamic Testing of Elastomers”, http://www.alphatestingsystems.com/RFdynamic-testingPaperWEB.pdf

[35]. Ardıç, H., 2013, MSc Thesis, "Design and Modeling Elastomeric Vibration Isolators Using Finite Element Method", METU, Ankara, Turkey.

[36]. Balaji, P. S., Rahman,M. E., et al., 2015, "Wire rope isolators for vibration isolation of equipment and structures – A review", IOP Conf. Series: Materials Science and Engineering (78).

[37]. Aeroflex International, Isolators for shock and vibration protection in all Environments - Selection Guide, www.thevmcgroup.com, 2001.

[38]. Wire Rope Isolator Technologies, ITT Enidine Inc., https://www.enidine.com/, 2012.

[39]. Isolation News, 1984 13, Aeroflex Corporation, Long Island, New York. USA.

[40]. Davis, L. P., et al., 1986, "Hubble Space telescope Reaction Wheel Assembly Vibration Isolation System", Proceedings AFWAL-TR-86-3059, Las Vegas, Nevada, USA.

[41]. Kircher, C. A., 2012, "*FEMA P-751, 2009 NEHRP Recommended Provisions: Design Examples*", Chapter-12, https://www.fema.gov/media-library-data/1393877415270-d563663961c9f40e88ce3ad673377362/FEMA_P-751.pdf

[42]. Tyan, F., Tu, S. H., and Wu, J., "An Investigation on Mathematical Models of Wire Rope Isolators", The 30th National Conference on Theoretical and Applied Mechanics, 2006.

[43]. Visitin, A., 1994, "Differential Models of Hysteresis", Applied Mathematical Sciences, Vol.111, Springer-Verlag, Berlin.

[44]. Dowling, N. E., Kampe, S. L., and Kral, M. V., (2019), *"Mechanical Behavior of Materials: Engineering Methods for Deformation, Fracture, and Fatigue"*, 5th Ed., Pearson Education Limited.

[45]. Suresh, S., (1998), Fatigue of Materials, 2nd Ed., Cambridge University Press.

[46]. Christ, H. J., (1991), *"Wechselverformung von Metallen: Zyklisches Spannungs-Dehnungs-Verhalten und Mikrostruktur"*, Springer-Verlag Berlin Heidelberg GmbH.

[47]. INSTRON® ElectroPuls® E10000 All-Electric Dynamic and Fatigue Test System, ElectroPuls® | E10000 All-Electric Dynamic Test Instrument (instron.com)

[48]. Tinker, M. L., “A NASA/industry/university partnership for development of dual-use vibration isolation technology,” in *TABES 1994: 10th Annu. Tech. Bus. Exhib. Symp.*, Huntsville, AL, USA, May 10-11, 1994, Paper 94-613.

[49]. Cochran, J. E., Fitz-Coy, N. G., and Cutchins, M. A., “Finite element models of wire rope for vibration analysis,” in *Proc. Struct. Dyn. Control Interact. Flexible Struct. (a workshop held at Marshall Space Flight Center)*, Huntsville, AL, USA, Apr. 22-24, 1986, pp. 1251-1270.

[50]. Cutchins, M. A., Cochran J. E., Kumar, K., Fitz-Coy, N. G., and Tinker, M. L., “Initial investigations into the damping characteristics of wire rope vibration isolators,” Auburn University, Auburn, AL, USA, Aerosp. Eng. Tech. Rep. 87-1, NASA Res. Grant NAG8-532, 1987.

[51]. Sauter, D., “Modeling the dynamic characteristics of slack wire cables in Stockbridge dampers,” Ph.D. dissertation, Dept. Mechanics, TU Darmstadt, Darmstadt, Germany, 2003.

[52]. Payne, A. R., “The dynamic properties of carbon black-loaded natural rubber vulcanizates. Part I,” Journal of Applied Polymer Science, vol. 6, no. 19, pp. 57-63, 1962.

[53]. Fletcher, W. P., and Gent, A. N., “Non-linearity in the dynamic properties of vulcanised rubber compounds,” Trans. Inst. Rubber Ind., vol.29, pp. 266–280, 1953.

[54]. *Marc 2019, Volume A: Theory and User Information*, MSC Software Corp., Irvine, CA, USA, 2019.

[55]. Juntunen, M., and Linjama, J., “Presentation of the VTT benchmark,” Mechanical Systems and Signal Processing, vol. 17, no. 1, pp. 179-182, 2003.

[56]. LMS Test.Lab Release 17, Impact Testing User Manual, Siemens Industry Software NV, Leuven, Belgium, 2017.

[57]. LMS Test.Lab Release 17, MIMO FRF Testing User Manual, Siemens Industry Software NV, Leuven, Belgium, 2017.

[58]. Masing, G., “Eigenspannungen and verfestigung beim messing,” in Proc. 2nd Int. Congr. Appl. Mech., Zurich, Switzerland, 1926, pp. 332-335.

[59]. Ewins, D. J., *Modal Testing: Theory, Practice and Application*. 2nd ed. Baldock, England: Research Studies Press Ltd., 2009.

[60]. Avitabile, P., *Modal Testing: A Practitioner’s Guide*. Hoboken, NJ, USA: John Wiley & Sons Ltd and The Society for Experimental Mechanics, 2017.

[61]. Dowling, N. E., *Mechanical Behavior of Materials.* 3rd ed. New Jersey, NJ, USA: Pearson Education Int., 2007.

[62]. Crede C. E., and Ruzicka, J. E., "Theory of Vibration Isolation," in *Harris' Shock and Vibration Handbook*, C. M. Harris and A. G. Piersol, Eds., 5th ed. New York, NY, USA: McGraw-Hill, 2002.

[63]. Iwan, W. D., "A distributed-element model for hysteresis and its steady-state dynamic response," ASME Journal of Applied Mechanics, vol. 33, no. 4, pp. 893-900, 1966.

[64]. Iwan, W. D., "On a class of models for the yielding behavior of continuous and composite systems," ASME Journal of Applied Mechanics, vol. 34, no. 3, pp. 612-617, 1967.

[65]. Gaul, L., and Nitsche, R., "The role of friction in mechanical joints," Applied Mechanics Reviews, vol. 54, no. 2, pp. 93-106, 2001.

[66]. Lakes, R., *Viscoelastic Materials*. Cambridge, England: Cambridge University Press, 2009.

[67]. Den Hartog, J. P., *Mechanical Vibrations*. New York, NY, USA: Dover Publications, 1985.

[68]. Brake, M. R. W., Ed., *The Mechanics of Jointed Structures*. Cham, Switzerland: Springer Int. Publishing, 2018.

[69]. Carella, A., Ewins, D. J., and Harper, L., "Using Transmissibility Measurements for Nonlinear Identification", Modal Analysis Topics, Volume 3: Proceedings of the 29th IMAC, A Conference on Structural Dynamics, 2011.

[70]. ABAQUS 2020 Documentation manual.

[71]. Gürses, K. and Özgen, G. O. "Çelik Sarmal Halat Tipi Sönümleme Elemanlarının Karakterizasyonu İçin Ayarlanabilir Bir Test Tertibatı", Turkish Patent and Trademark Office Application No.: TR 2023/004708, Applicant: Roketsan Inc.

[72]. Gürses, K., Uzun, C., and Özgen, G. O., "Çelik Sarmal Halat Tipi Sönümleme Elemanlarına Sahip Bir Kanister Taşıma Sistemi", Turkish Patent and Trademark Office Application No.: TR 2023/003739, Applicant: Roketsan Inc.

CURRICULUM VITAE

Surname, Name: Gürses, Kenan

EDUCATION

Degree	Institution	Year of Graduation
PhD	METU Mechanical Engineering	2023
MSc	ITU Mechanical Engineering	2009
BSc	ITU Mechanical Engineering	2006

WORK EXPERIENCE

Year	Place	Enrollment
2009-Present	Roketsan Inc.	Senior Lead Engineer
2006-2009	FİGES Inc.	R&D Engineer

FOREIGN LANGUAGES

Advanced English

PUBLICATIONS

1. K. Gürses, G. O. Özgen, and B. Acar, "Experimental Investigation of Amplitude-Dependent Behaviour of a Wire Rope Isolator System Using Modal Testing methods," in *Proceedings of ISMA2022 International Conference on Noise and Vibration Engineering*, Leuven, Belgium, Sept. 12-14, 2022, pp. 2454-2468.

2. D. Bahan, M. T. Akpolat, C. Çitak, Ö. Harputlu, K. Gürses, and B. Acar, "Experimental Evaluation of Aerodynamic Performance and Structural Excitation Characteristics of a Supersonic Air Inlet," in *AIAA Aviation 2021 Forum*, Virtual Event, Aug. 2-6, 2021, https://doi.org/10.2514/6.2021-2494.

3. K. Gürses and B. Acar, "Modeling Dynamic Behavior of a Safety and Arming Mechanism," in *Proceedings of Science in The Age of Experience*, Chicago, IL, USA, May 15-18, 2017, pp. 138-149.

4. K. Gürses, B. Kuran, and C. Gençoğlu, "Identification of Material Properties of Composite Plates Utilizing Model Updating and Response Surface Techniques.," in *Proceedings of the 29th IMAC, A Conference on Structural Dynamics*,

Jacksonville, FL, USA, Jan 31 - Feb 3, 2011, https://doi.org/10.1007/978-1-4419-9305-2_18.

5. K. Gürses, K. Y. Şanlıtürk, “Helikopter Yer Rezonansı: Modelleme ve Analiz”, UMTS 2009 - 14. Ulusal Makina Teorisi Sempozyumu Bildiri Kitabı, Sayfa 47-58, ODTÜ Kuzey Kıbrıs Kampusu, 2-4 Temmuz 2009.

PATENTS

1. K. Gürses, C. Uzun, and G. O. Özgen, “Çelik Sarmal Halat Tipi Sönümleme Elemanlarına Sahip Bir Kanister Taşıma Sistemi”, Turkish Patent and Trademark Office Application No.: TR 2023/003739, Applicant: Roketsan Inc.
2. K. Gürses and G. O. Özgen, “Çelik Sarmal Halat Tipi Sönümleme Elemanlarının Karakterizasyonu İçin Ayarlanabilir Bir Test Tertibatı”, Turkish Patent and Trademark Office Application No.: TR 2023/004708, Applicant: Roketsan Inc.
3. B. Altıntaş, H. Ardıç, and K. Gürses, “Erişim Kısıtı Bulunan Kanister-Platform Arayüz Bağlantıları İçin Cıvatalı Bir Kilit Mekanizması”, Turkish Patent and Trademark Office Application No.: TR 2023/006127, Applicant: Roketsan Inc.
4. K. Gürses, N. Bilgili, B. Acar, Y. Demirci, “Bolt Apparatus With A Spherical Seating Surface For Canister-Ammunition Interface”, WIPO-PCT, International Application No.: PCT/TR 2020/051337, International Publication No.: WO 2021/133338 A1, Applicant: Roketsan Inc.
5. K. Gürses, N. Bilgili, B. Acar, Y. Demirci, “Kanister-Mühimmat Arayüzü İçin Küresel Basma Yüzeyine Sahip Bir Cıvata Tertibatı”, Turkish Patent and Trademark Office Application No.: TR 2019/21792, Publication No.: TR 2019 21792 B, Applicant: Roketsan Inc.